In presenting the dissertation as a partial fulfillment of the requirements for an advanced degree from the Georgia Institute of Technology, I agree that the Library of the Institute shall make it available for inspection and circulation in accordance with its regulations governing materials of this type. I agree that permission to copy from, or to publish from, this dissertation may be granted by the professor under whose direction it was written, or, in his absence, by the Dean of the Graduate Division when such copying or publication is solely for scholarly purposes and does not involve potential financial gain. It is understood that any copying from, or publication of, this dissertation which involves potential financial gain will not be allowed without written permission.

3/17/65
b

STUDIES OF MAGNETIC EFFECTS OF ICℓ

A THESIS

Presented to

The Faculty of the Graduate Division

by

Arnold Frederick Stalder

In Partial Fulfillment

of the Requirements for the Degree

Doctor of Philosophy in the School of Chemistry

Georgia Institute of Technology

January, 1967

STUDIES OF MAGNETIC EFFECTS OF ICℓ

Approved:

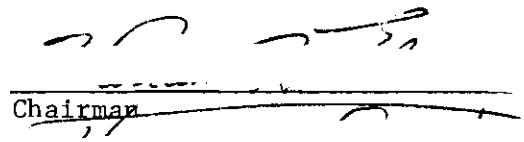

Chairman

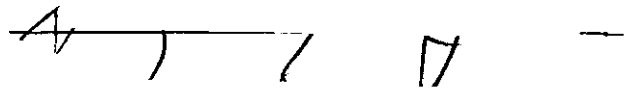

Date approved by Chairman: February 6, 1967

ACKNOWLEDGMENTS

The author wishes to thank all of those on the faculty and staff of the School of Chemistry, Georgia Institute of Technology, for their advice and assistance during the course of this work.

In addition, he wishes to thank the National Aeronautics and Space Administration for fellowships and research grants which he received through the course of this work, and the National Science Foundation for grants which helped to finance his experimental work.

TABLE OF CONTENTS

LIST OF TABLES

LIST OF ILLUSTRATIONS

LIST OF ILLUSTRATIONS (Continued)

LIST OF ILLUSTRATIONS (Continued)

SUMMARY

Magnetically induced optical phenomena have been of interest for many years. Effects such as those found by Faraday, Zeeman, and Kerr were observed experimentally long before any satisfactory theoretical explanation based on wave mechanics was available. The work in this thesis was directed toward the observation and explanation of the magneto-optic effects associated with single lines in the spectra of diatomic molecules. These effects are classified in terms of two closely related phenomena, the rotation of the plane of plane polarized radiation, and magnetically induced circular dichroism.

Serber presented one of the first wave mechanical treatments of the Verdet constant, which related the angle of rotation to molecular properties. This treatment was subsequently extended and specialized to diatomic molecules by Carroll, and these treatments have served as guides for the interpretation of many experiments. Unfortunately, this theory was valid only far from regions of absorption, and hence not applicable to magneto-optic phenomena occurring near individual spectral lines. More recent theories have been presented, some of which are claimed to be valid within regions of absorption. However, none of these theories can be used without modification to analyze magneto-optic effects associated with sharp spectral lines, since the assumptions critical to their development are not suitable for the consideration of sharp but finite spectral features.

In this work, a theoretical development concerned with the calculation of the Faraday rotation and circular dichroism is presented, making no assumptions which invalidate its application to sharp transition lines. The derivation starts from formulas for the index of refraction and absorption coefficient for a classical oscillator using the Van Vleck-Weisskopf line shape. Wave mechanical substitutions are made and the magnetic field effects taken into account to deduce formulas for the magnetically induced circular dichroism and Faraday rotation.

The $^3\pi_1 \leftarrow {}^1\Sigma^+$ transition in the ICℓ molecule was chosen to test the formulas because much of the fine structure is easily resolved and has been identified, and the transition occurs in an easily accessible region of the visible spectrum.

An attempt was made to study magneto-optic effects in six ICℓ lines using as a source isolated Zeeman components of atomic lines emitted by a Ne discharge in a longitudinal magnetic field. The frequency of the Zeeman components was varied over a narrow range by changing the intensity of the magnetic field inducing the Zeeman effect, and hence these components provided a nearly monochromatic source which could be swept over nearby ICℓ lines. This attempt proved unsuccessful due to fluctuations of the Ne discharge intensity caused by the magnetic field.

An apparatus was designed and constructed to make semi-quantitative measurements of the Faraday rotation and circular dichroism using a D.C. radiation source and the Jarrell-Ash Mark IV Ebert Spectrograph as a monochromator. Both effects appeared as time dependent signals induced by the continuous rotation of a polarizing device in the optical path and were studied by phase sensitive detection. It was possible to make measurements on several vibrational bands, and where the resolution was

sufficient the frequency dependence of the magneto-optic phenomena near individual rotational lines was studied.

These data were used to test the formulas developed in this thesis. A Hund's case (a) model was chosen for the $^3\pi_1$ state of the molecule, with a magnetic moment of one Bohr magneton lying along the internuclear axis. Nuclear hyperfine structure was ignored, but the slit function and line width, Zeeman splitting, and intensity perturbations caused by the field were all considered explicitly. The Faraday rotation and magnetically induced circular dichroism were calculated for each line of the P, Q, and R branches in the $V'' = 1 \rightarrow V' = 12$ vibrational band. The results of the calculations compared well with the experimental data on the same band, and demonstrate clearly that all of the effects mentioned must be considered to interpret the data properly.

The formulas developed in this thesis proved adequate to explain the extensive data obtained on the ICℓ $^3\pi_1 \leftarrow {}^1\Sigma^+$ transition. These formulas should be generally applicable to any transition in which only the excited state exhibits a magnetic moment, and a suitable model exists to describe this magnetic state. It appears that a complete interpretation of the magneto-optic phenomena associated with individual spectral lines can only be obtained through very detailed calculations. These calculations must involve a valid model for the molecule, and include experimental parameters such as the pressure, slit width, and absorption line width.

Cases in which the ground state of a transition also exhibits a magnetic moment require that the formulas be modified to include ground state magnetic effects. The modifications must be added in the theoretical development, and will increase the complexity of the formulas.

CHAPTER I

INTRODUCTION

Magnetically induced optical phenomena have been of scientific interest for many years. These phenomena appear in several ways; all of which are in some way related to each other. One of the earliest was observed by Faraday, who found that a piece of lead borate glass, placed between crossed polarizers, allowed light to pass through the polarizers if a magnetic field was imposed upon the glass in such a way that the field axis coincided with the direction of light propagation. The Faraday effect was explained as a rotation, by the magnetically perturbed sample, of the plane of polarization of the incident light. The quantitative aspects of this phenomenon were first studied by Verdet, who found that the amount of rotation, ϕ, induced by a particular sample in a magnetizing field was expressable in terms of the field intensity, H, and sample length, ℓ. This relation took the form $\phi = VH\ell$, where V, the Verdet constant, was a frequency dependent function characteristic of the sample.

If a molecule in the gas state replaces the glass mentioned in Faraday's experiment, the light which passes through the polarizer is sometimes in the form of a discrete spectrum, called the magnetic rotation spectrum (MRS). Should a molecule exhibit such an MRS, the spectral features will occur near molecular absorption transitions. The existence of an MRS in a molecule seems to have the following requirements: 1. The gas must exhibit a transition in which at least one of the states in-

volved has a magnetic moment coupled to the nuclear framework. 2. The gas must be at a pressure allowing sharp absorption lines to appear. 3. The gas molecules must be symmetric or nearly symmetric rotors. Among the many molecules which have exhibited an MRS are ICℓ, IBr, I_2, SO_2, CS_2, and NO (1-6).

Two types of magnetically induced optical phenomena which have received attention recently are magnetic circular dichroism (MCD) and magnetic optical rotatory dispersion (MORD). The former is a measure of the difference between the absorption coefficients for right and left circularly polarized light, and the latter a measure of the difference between the indices of refraction for right and left circularly polarized light. The two are not independent, for they are related theoretically by the Kramers-Kronig relations. Both MCD and MORD are related to MRS, as will be more clearly seen when the physical aspects of MRS are developed later in this thesis.

During the past several years the MRS phenomenon has been of primary interest in this laboratory, and a great amount of data have been collected on various molecular systems. Among the molecules studied are ICℓ, IBr, $CSCℓ_2$, SO_2, CS_2, and pyrazine. As the available instrumentation improved, however, it became apparent that a thorough understanding of the phenomenon being measured was necessary. Even though theories had been available for many years, no really well-defined high resolution data were available to test the theories. One of the objectives of this work was to obtain high resolution data on a simple system which could be used to test the available theories.

The measurement of MRS has been considered to be a sensitive device for the study of magnetically active states in a molecule, partic-

ularly triplet states. It was hoped that magnetic rotation could be used to study photolytically produced transient species, many of which are free radicals and hence magnetically active. The experimental work described in this thesis was originally designed to culminate in the study of such transient species. The experiments completed were to provide the technological background for the experiment involving free radicals.

The stable species ICℓ was chosen for study because of the large amount of data available for the system and the high intensity of the MRS. Some of the work was done with pulsed energy discharges. The energy, stored in capacitor banks, was used to produce pulsed magnetic fields or a Lyman discharge.

The initial experiment involved two pulses; both being used to produce magnetic fields. One of the fields was used to induce the Zeeman effect on a Ne discharge. One of the Zeeman components of an emission line was isolated and used as a source to observe magneto-optic effects in the ICℓ sample, which was placed within the second magnetic field. Such a Zeeman component provided a nearly monochromatic light source with its frequency variable over a narrow range. Both MRS and absorption were studied by varying the optical system to suit the desired experiment.

Another two-pulse experiment was performed, but this time one of the discharges was into a Lyman source lamp. This Lyman source was used to observe the ICℓ sample, which was placed within a pulsed magnetic field. A suitable choice of optical elements allowed the study of MRS or absorption. The purpose of this experiment, in addition to study MRS in high fields, was to observe the Zeeman effect in ICℓ. Unfortunately, when the instrumental resolution necessary to observe the Zeeman effect was used, the intensity was too low for observation. MRS, which is at

least 1000 times less intense than absorption was also impossible to observe. Because of the low intensity exhibited in this stable system, a three-pulse system using the third pulse to photolytically produce free radicals was not attempted. The concentration of free radicals would be expected to be much less than the concentration of magnetically active molecules in ICℓ, and the experiment was abandoned.

Neither of the experiments previously described provided data useful to test the theories, so another method was designed to obtain information. An apparatus was devised to measure MORD and MCD by phase sensitive detection. This experiment was successful, and data were obtained to compare with the theories.

Most of the early work on magneto-optics was summarized by Wood (7). Experimental and theoretical work was discussed, even though the theoretical discussion was limited by classical optics. After the advent of wave mechanics, Rosenfeld presented a theoretical treatment concerned with magnetic rotation in atoms. Serber's theory, applicable to molecules in general, was developed shortly after Rosenfeld's, and was designed to calculate the Verdet constant far from any absorption in the molecular system (8). Carroll specialized Serber's theory to the case of diatomic molecules (9). The theoretical presentations by Rosenfeld, Serber and Carroll were all concerned with the calculation of the Verdet constant. Recently, several theories of magnetically induced optical activity have been presented, and are included in a review by Buckingham and Stephens (10). In this review the authors have included their own development of magnetic optical activity, which includes MCD and MORD.

All of the theories include assumptions which make them inapplicable under the conditions favorable for the observation of MRS. The

early theories are useful only in regions of the spectrum far from absorption. More recent theories include regions of absorption, but only if the absorption line width is much greater than the Zeeman splitting or vice versa. The MRS seen in this laboratory were observed when the absorption line width and Zeeman splitting were on the same order of magnitude. It was necessary, then, to develop a theoretical presentation applicable to the conditions observed in this laboratory, and to test this theory against the data that were obtained.

CHAPTER II

THEORETICAL DEVELOPMENT

Definitions and Sign Conventions

There exists some confusion in the literature regarding the definitions and sign conventions associated with magnetic optical activity. To avoid such confusion, the definitions and sign conventions used in this thesis will be given in this section.

The direction of the vector representing the magnetic field in a coil is important in all of the experiments discussed under the topic of magneto-optics. The direction of the magnetic field vector in the center of a loop of wire of radius r is defined by the vector produce $\vec{r} \times \vec{i}$, where i is the positive current flowing in the loop.

When light is viewed along the axis of a homogeneous longitudinal magnetic field, the only indices of refraction that remain constant throughout the field are those for circularly polarized light. If an observer is looking toward the light source, and the axis of the magnetic field coincides with the direction of light propagation, then the electric vector representing right circularly polarized light will rotate clockwise when seen in a plane fixed in space, and perpendicular to the optical axis.

The angle of rotation of the plane of polarization of a polarized light beam is positive if the rotation is counterclockwise when viewed looking toward the light source; positive rotation is in the same sense as the direction of positive current in a coil generating the field.

In a magnetic field the degeneracy of the quantum number M is removed for atomic and molecular states which possess a magnetic moment. Transitions in which $\Delta M = \pm 1$ will be circularly polarized when viewed along the field axis, but transitions for which $\Delta M = 0$ will be polarized parallel to the field direction and thus be invisible when viewed along the field axis. If the direction of the magnetic field vector coincides with the direction of light propagation and both point toward the observer, absorption transitions involving $\Delta M = \pm 1$ will be left circularly polarized and transitions with $\Delta M = -1$ will be right circularly polarized. The polarization will be reversed if emission rather than absorption is observed. This is shown in the diagram in Figure 1, where the circular arrows represent the motion of the electric field vector viewed in a plane perpendicular to the direction of light propagation.

Physical Aspects of MRS

Consider the magnetic rotation experiment described in the coordinate system shown in Figure 2. The direction of light propagation and that of the magnetic field vector were chosen to coincide with the positive z direction. The electric vector of radiation transmitted by the polarizer nearest the source is parallel to the x-axis. The second polarizer, usually denoted the analyzer, has its axis oriented relative to the y-axis. The angle ϕ, defining the rotation of the analyzer axis relative to the positive y direction, is positive if the rotation is counterclockwise looking toward the light source. The magnetic rotation experiment involves the measurement of the light intensity passing through the analyzer. This intensity is a function of both the angle ϕ and the frequency of the radiation observed, and is the time average of the square of the amplitude of the electric vector passed by the analyzer.

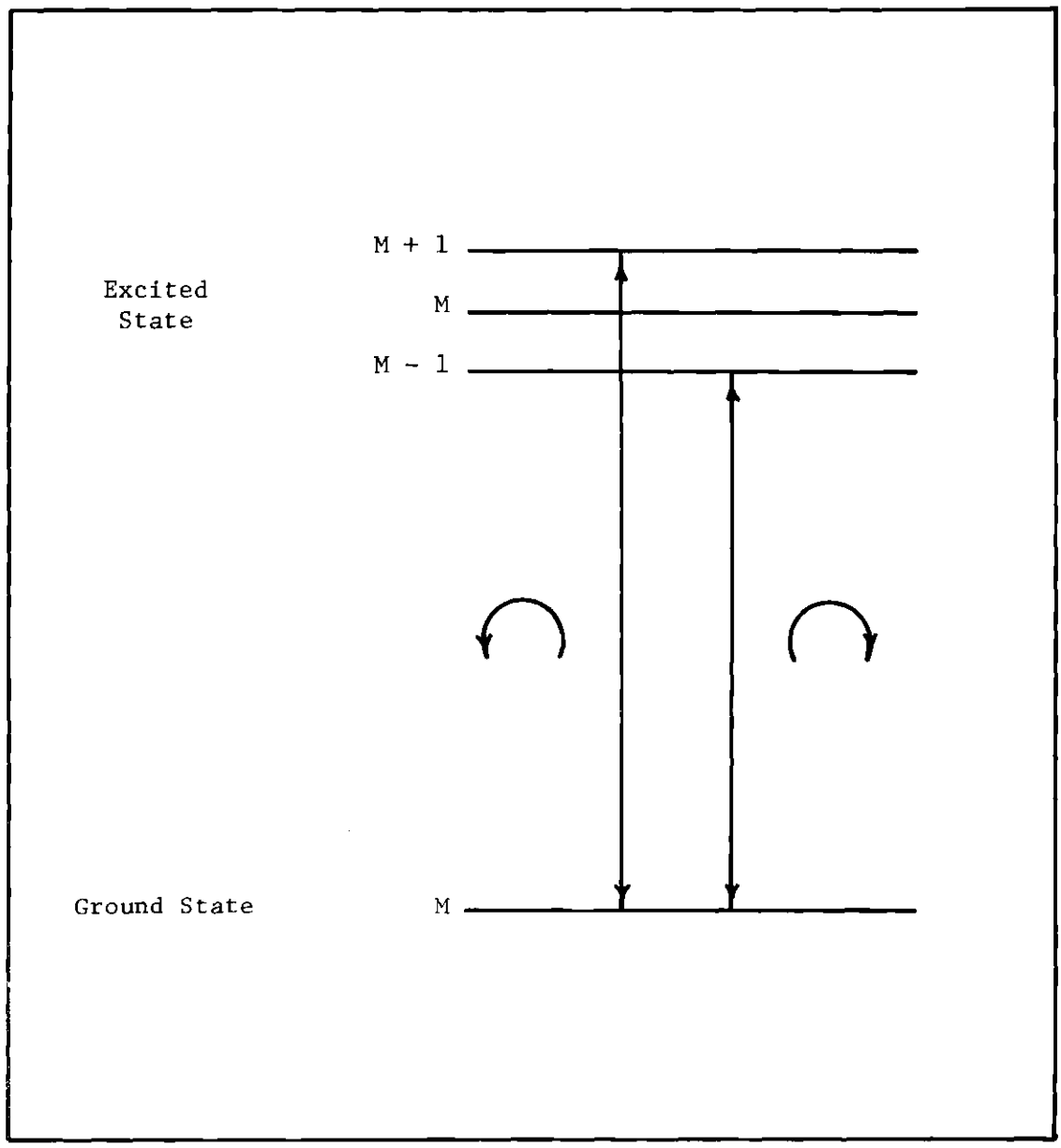

Fig. 1. Polarization of Transitions Between Magnetic States.

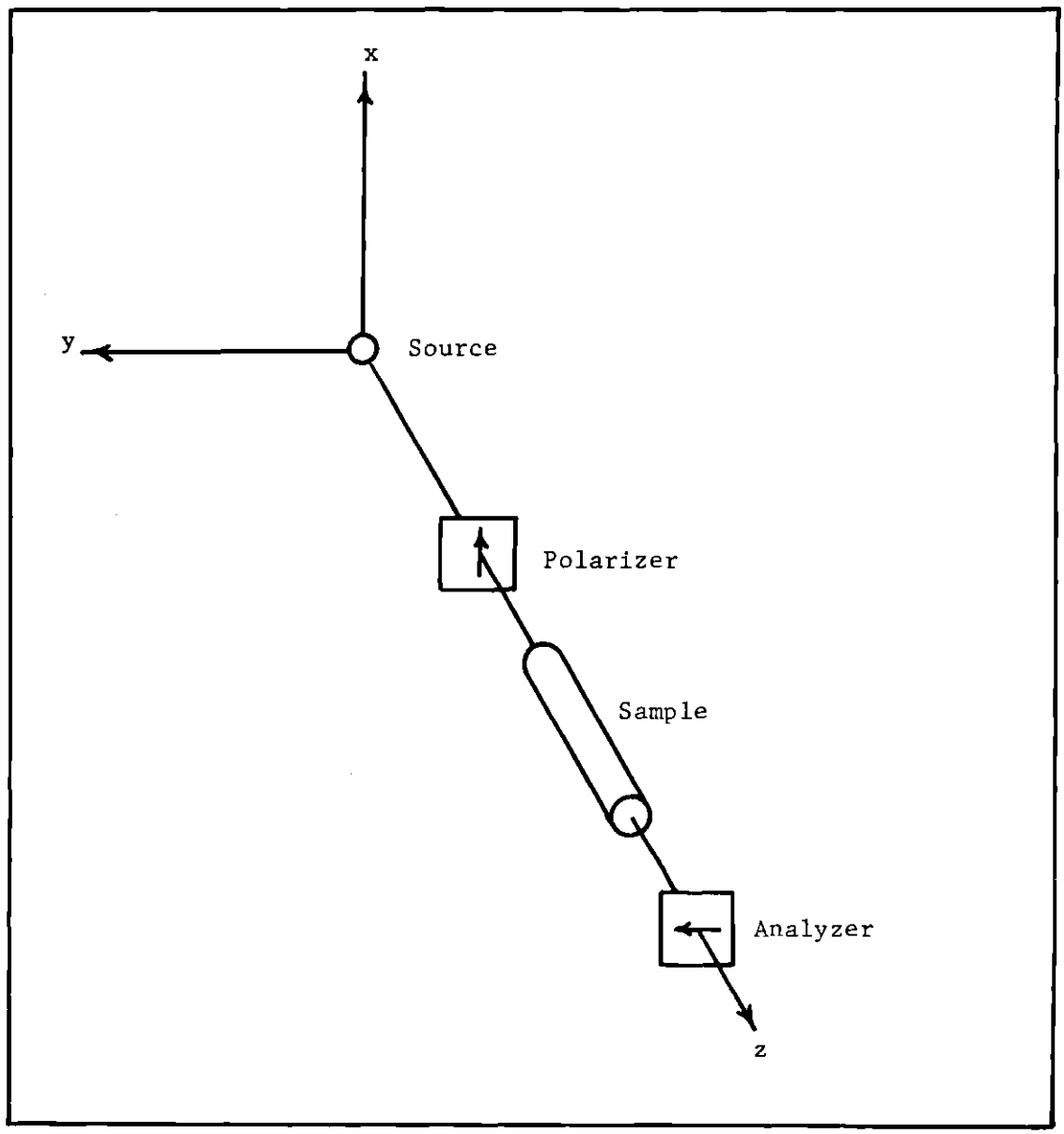

Fig. 2. Optical System for the Measurement of Magnetic Rotation.

In general, the light leaving the sample will be elliptically rather than plane polarized, and can be described in terms of right and left circularly polarized components. These circular components are given by the equations

$$E_L = E_L^o \, e^{2\pi i(\nu t - z/\lambda_L)} \, e^{-(\alpha_L/2)\, z} \tag{1}$$

$$E_R = E_R^o \, e^{-2\pi i(\nu t - z/\lambda_R)} \, e^{-(\alpha_R/2)\, z} \tag{2}$$

where E_L and E_R are the magnitudes of the electric vectors, ν is the frequency of the observed radiation, z is the path length through the sample that the light has traveled, λ refers to the wavelength of the radiation in the sample, and α is the absorption coefficient in the sample. The wavelength is related to that in a vacuum by the relation $\lambda = \lambda_o/n$, where λ_o is the vacuum wavelength and n is the index of refraction in the sample.

Before light plane polarized along the x-axis enters the sample, $z = 0$ and $E_R^o = E_L^o$. The vector sum of equations (1) and (2) reduces to plane polarized radiation with its electric vector parallel to the x-axis, which must be the case if the representation of the radiation in terms of circular components is valid. Generally, after passing a finite distance through the sample, the radiation will no longer be plane polarized, and components of the electric vector will appear parallel to both the x and y axes. These components are expressed in the following equations:

$$E_x = \text{Real Part of } \frac{E_L + E_R}{2} \tag{3}$$

$$E_y = \text{Imaginary Part of } \frac{E_L + E_R}{2} \tag{4}$$

For the system shown in Figure 3, the electric vector of the light passed through the analyzer, E_A, can be expressed as

$$E_A = E_x \sin \phi - E_y \cos \phi \tag{5}$$

If the path length through the sample is ℓ, and $E_R^o = E_L^o = E$, the light passing through the sample in terms of its circular components is shown below:

$$E_L = E\, e^{-(\alpha_L/2)\ell}\, e^{2\pi i(\nu t - \ell n_L/\lambda_o)} \tag{6}$$

$$E_R = E\, e^{-(\alpha_R/2)\ell}\, e^{-2\pi i(\nu t - \ell n_R/\lambda_o)} \tag{7}$$

The electric vector of the light passing through the analyzer is

$$E_A = \frac{E}{2}\left\{e^{-\left(\frac{\alpha_L}{2}\right)\ell} \sin\left[\phi - 2\pi\left(\nu t - \frac{\ell n_L}{\lambda_o}\right)\right] + e^{-\left(\frac{\alpha_R}{2}\right)\ell} \sin\left[\phi + 2\pi\left(\nu t - \frac{\ell n_R}{\lambda_o}\right)\right]\right\} \tag{8}$$

The intensity of the light passing through the analyzer is the time average of E_A^2,

$$\begin{aligned}\langle E_A^2 \rangle = \Bigg\langle \frac{E^2}{4} \Bigg\{ & \frac{e^{-\alpha_L \ell}}{2}\left[1 - \cos 2\left(\phi - 2\pi\left(\nu t - \frac{\ell n_L}{\lambda_o}\right)\right)\right] \\ & + \frac{e^{-\alpha_R \ell}}{2}\left[1 - \cos 2\left(\phi + 2\pi\left(\nu t - \frac{\ell n_R}{\lambda_o}\right)\right)\right] \\ & + e^{-\left(\frac{\alpha_L + \alpha_R}{2}\right)\ell}\left[\cos 2\pi\left(-\nu t + \frac{\ell(n_L + n_R)}{\lambda_o}\right)\right] \\ & - e^{-\left(\frac{\alpha_L + \alpha_R}{2}\right)\ell}\left[\cos 2\left(\phi + \frac{\pi \ell}{\lambda_o}(n_L - n_R)\right)\right] \Bigg\} \Bigg\rangle\end{aligned} \tag{9}$$

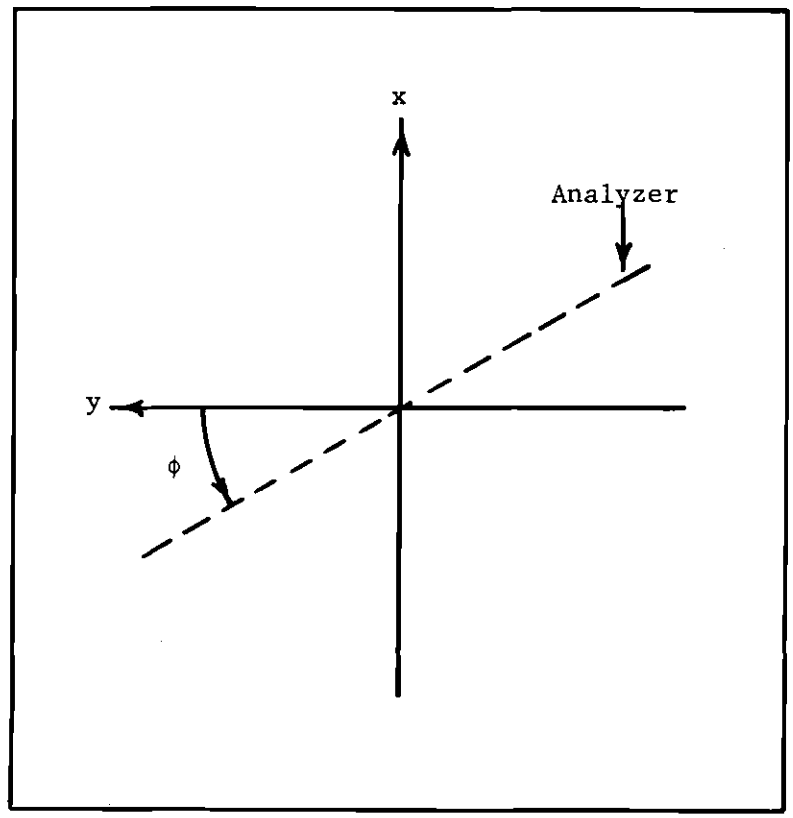

Fig. 3. Coordinate System for Magnetic Rotation.

or

$$\langle E_A^2 \rangle = \frac{E^2}{2}\left\{\left(\frac{e^{-\left(\frac{\alpha_L}{2}\right)\ell} - e^{-\left(\frac{\alpha_R}{2}\right)\ell}}{2}\right)^2 + e^{-\left(\frac{\alpha_L+\alpha_R}{2}\right)\ell} \sin^2\left(\phi + \frac{\pi\ell}{\lambda_o}(n_L - n_R)\right)\right\} \qquad (10)$$

Equation (10) is the equation of an ellipse with its major axis at an angle $\frac{\pi\ell}{\lambda_o}(n_R - n_L)$ relative to the positive y-axis. The minimum intensity will appear at the Faraday angle, $\phi = \frac{\pi\ell}{\lambda_o}(n_R - n_L)$. The ellipticity of the curve described in equation (10) is given by

$$\frac{E_A(minimum)}{E_A(maximum)} = \left(\frac{e^{-\left(\frac{\alpha_L}{2}\right)\ell} - e^{-\left(\frac{\alpha_R}{2}\right)\ell}}{e^{-\left(\frac{\alpha_L}{2}\right)\ell} + e^{-\left(\frac{\alpha_R}{2}\right)\ell}}\right) \approx \left(\frac{\alpha_R - \alpha_L}{4}\right)\ell \qquad (11)$$

Looking at the right side of equation (10) it can be seen that the intensity is partly a function of the circular dichroism, given by the first term in the sum, and partly a function of the Faraday rotation indicated in the second term. Only if $\alpha_R = \alpha_L$ would the MRS signal be due to simple Faraday rotation. This equality is never realized in any system exhibiting an MRS, for the existence of a difference in the indices of refraction for circularly polarized light implies a difference in the absorption coefficients. The absorption coefficient $\alpha(\nu)$ and index of refraction $n(\nu)$ as functions of frequency are related through the Kramers-Kronig relations (11,12).

$$n(\nu)^2 - 1 = \frac{c}{2\pi^2}\int_0^\infty \frac{\nu'\alpha(\nu')\,d\nu'}{\nu[(\nu')^2 - \nu^2]} \qquad (12)$$

$$\alpha(\nu) = \frac{-8\nu^2}{c} \int_0^\infty \frac{[n(\nu)^2 - 1]\, d\nu'}{(\nu')^2 - \nu^2} \qquad (13)$$

Here c is the velocity of light. The relationship between the index of refraction and absorption coefficient will be seen again in the formulas presented in the next section of this thesis.

The mechanism whereby differences in the absorption coefficients and indices of refraction for circular light occur remains to be considered. Differences may occur due to the Zeeman splitting of transitions involving right and left circular light, or because of perturbations in the relative intensities of transitions involving right and left circular light. If a molecular absorption spectrum exhibiting rotational structure exists and is observed in the absence of any magnetic field, each rotational line should appear as a single feature with an absorption half width determined by the experimental conditions and properties of the species. If either of the electronic states involved in a specific transition has a magnetic momnet, a magnetic field will split the M levels, and a line which appeared single and sharp will become a set of closely spaced Zeeman components. When the system is viewed along the axis of the magnetic field, only those absorption transitions involving $\Delta M = +1$ (left circularly polarized) and $\Delta M = -1$ (right circularly polarized) will be observed. The spacing between the Zeeman components will depend on the magnitude of the splitting of the M levels in the two states. Although the $\Delta M = \pm 1$ transitions are distributed more or less uniformly throughout the Zeeman pattern, their relative intensities are not. From this point forward, we will only consider the case where the upper state involved in a transition possesses a magnetic moment. Under this condition an R-type transition in a molecule

exhibiting the normal Zeeman effect* will have $\Delta M = +1$ transitions most intense on the high frequency side of the Zeeman pattern, and $\Delta M = -1$ transitions most intense at the low frequency side.

The intensities of the various Zeeman components may be calculated from the electric dipole moment matrix elements using appropriate wave functions. A qualitative idea of the relative intensities of Zeeman components can be obtained from the vector model shown in Figure 4. Using this model, the most intense transition involves the least change in the direction of the total angular momentum vector. This reflects the quantum mechanical requirement for intense transitions which demands wave functions which overlap well (3,13). The relative intensities of $\Delta M = \pm 1$ transitions are shown for a P and an R line in Figure 5.

Associated with each Zeeman component of a transition is a frequency dependent function representing the index of refraction, and another representing the absorption coefficient. If $(n_R - n_L)$ and $(\alpha_R - \alpha_L)$ are computed within the frequency range including a whole Zeeman pattern, both functions will have nonzero values throughout most of the Zeeman pattern. In Figure 6a and Figure 7a these quantities are calculated for a simple transition in which only one $\Delta M = +1$ and one $\Delta M = -1$ component occur. The addition of more components will complicate the calculation, but leave the shape of the curves quite similar to those found in the simple case of two components. The curves drawn in Figure 6a and 7a would be applicable to an R-type transition. For a P transition, the location of the $\Delta M = \pm 1$ components would be reversed and the sign of the resultant curves would thereby be reversed also (7,8).

---

*The normal Zeeman effect splits the M levels in such a way as to make those with the largest positive M lie highest in energy.

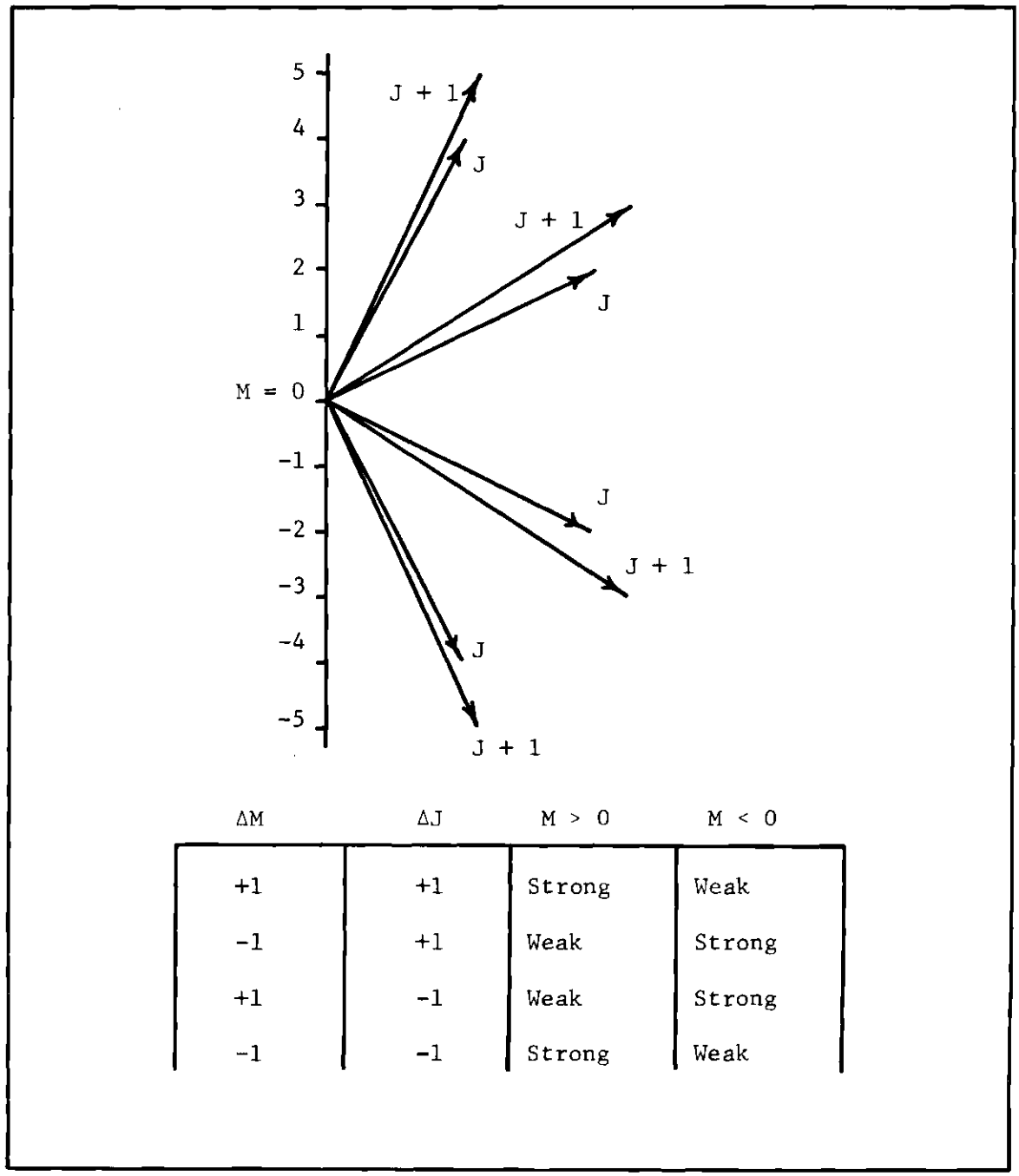

ΔM	ΔJ	M > 0	M < 0
+1	+1	Strong	Weak
-1	+1	Weak	Strong
+1	-1	Weak	Strong
-1	-1	Strong	Weak

Fig. 4. Vector Model Indicating Transition Intensities--(Only some of the states with J = 4 and J = 5 are shown. These are adequate to illustrate the point in question, and the same results may be obtained using any pair of states with $\Delta J = \pm 1$.)

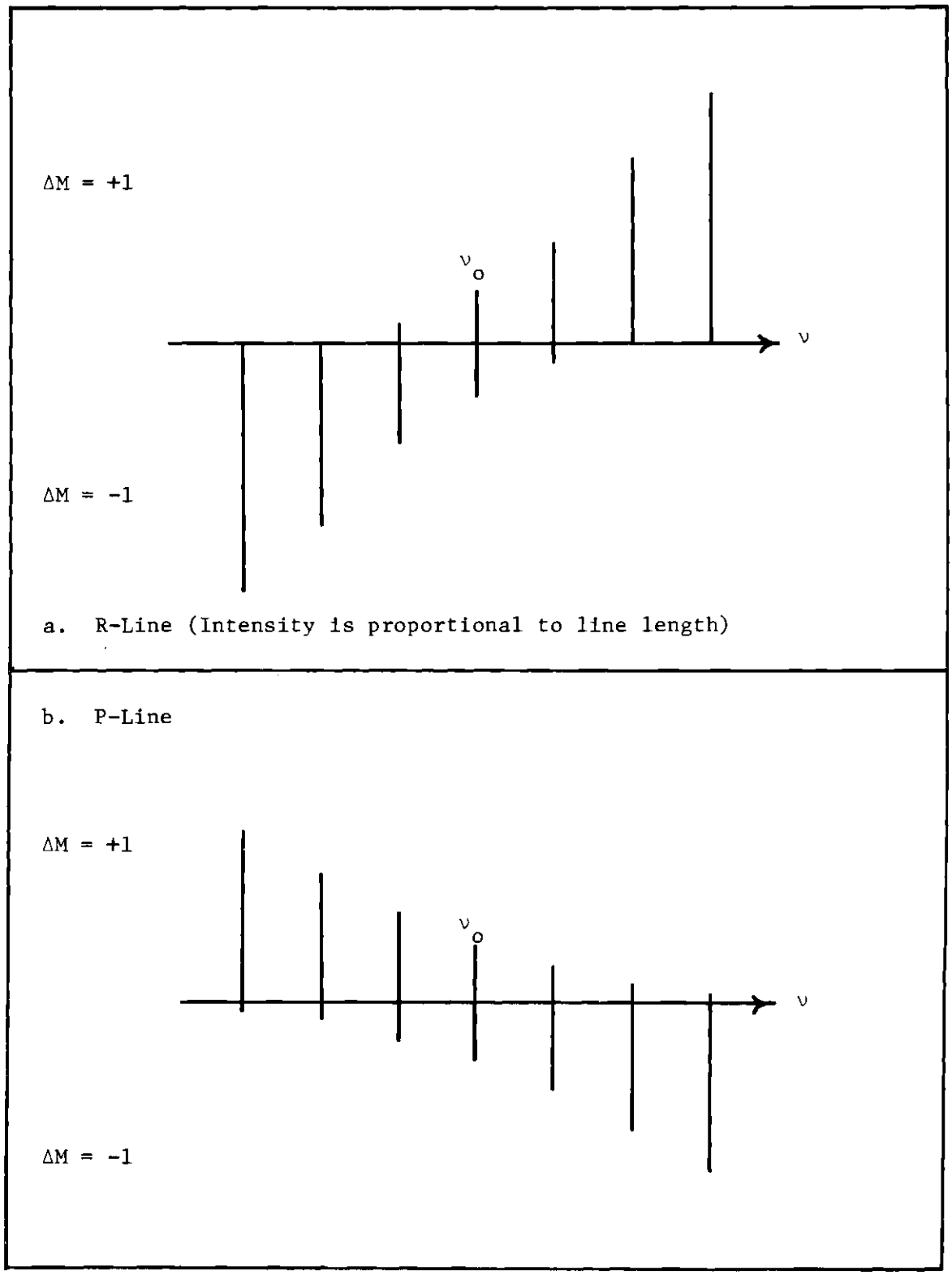

Fig. 5. Intensity of Zeeman Components.

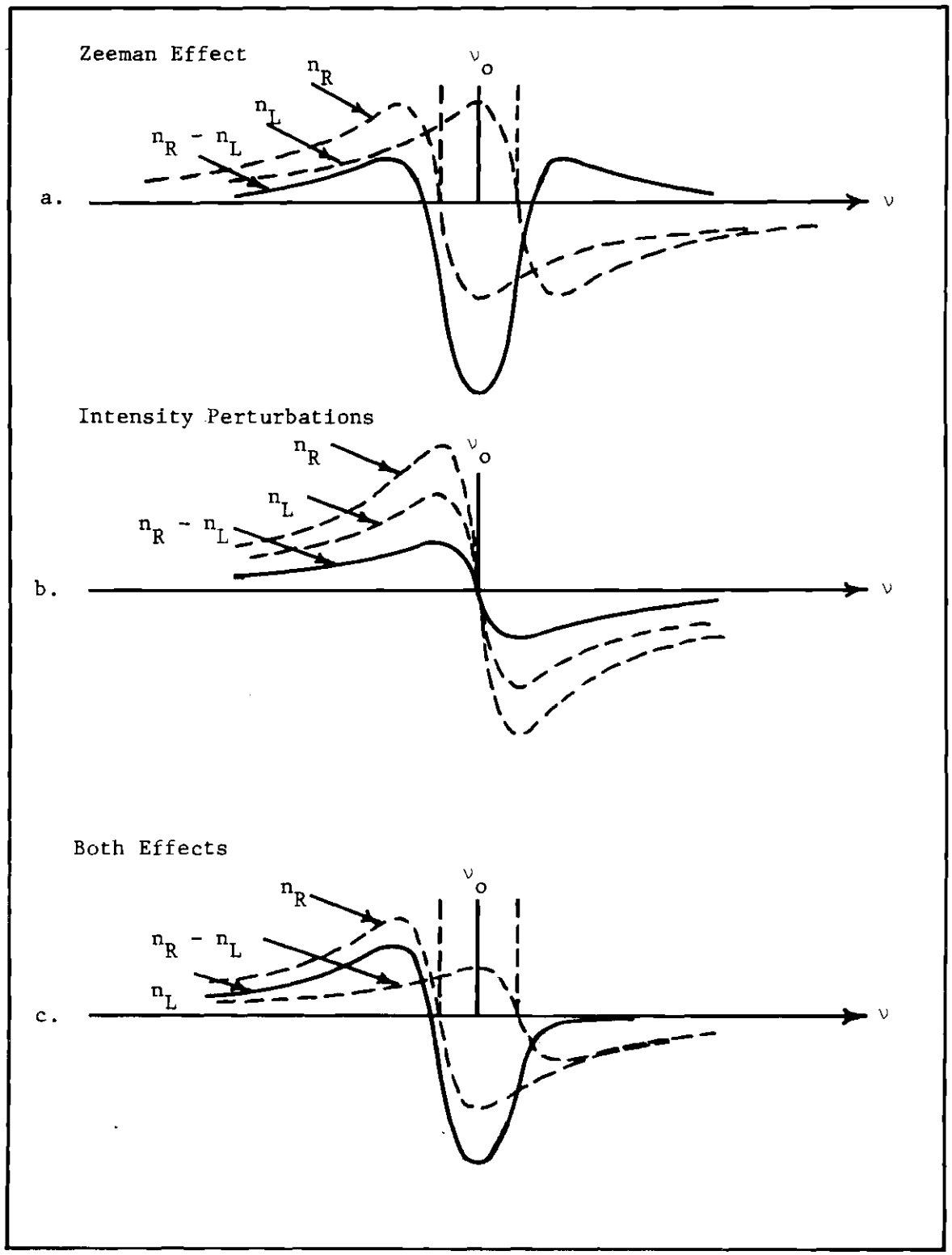

Fig. 6. Angle of Rotation.

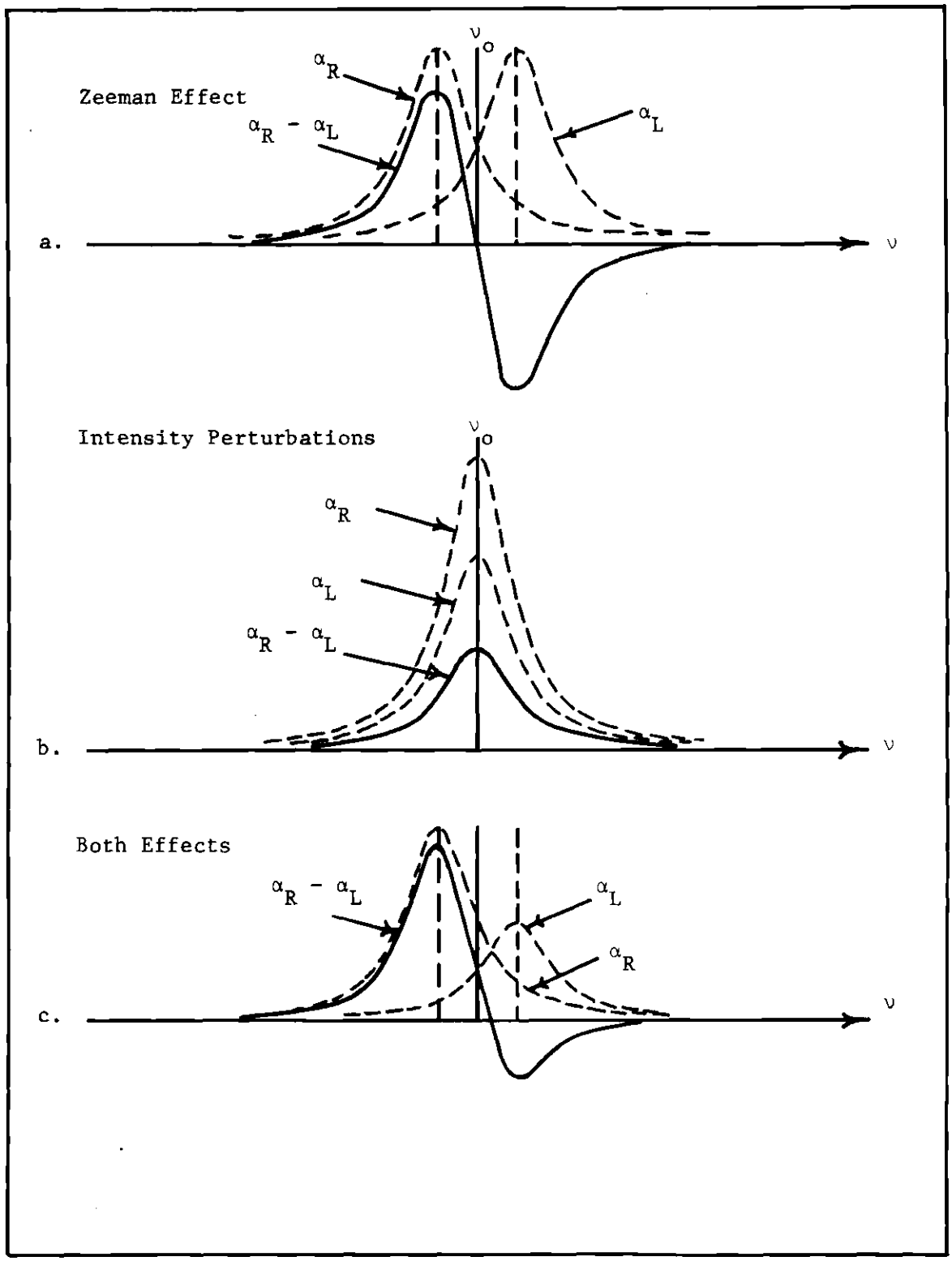

Fig. 7. Circular Dichroism

It can be seen from Figure 5 that each $\Delta M = +1$ transition has a $\Delta M = -1$ transition of equal intensity placed symmetrically on the opposite side of the zero field transition frequency. When the field is removed, all of the lines become superposed, and if no intensity perturbations occur, both $(n_R - n_L)$ and $(\alpha_R - \alpha_L)$ will be zero throughout the region of absorption. Intensity perturbations may occur in one of two ways: 1. In a magnetically active ground state all of the various M levels split by the field will not be equally populated, and this will affect the transition intensities in a Zeeman pattern. 2. The presence of a magnetic field can cause mixing to occur between adjacent J states in a molecule, which will affect transition probabilities in a Zeeman pattern.

The second method of producing intensity perturbations is the most important. In terms of quantum mechanics, the mixing is done by the magnetic dipole moment operator. The matrix of this operator in a zero field basis set has some off diagonal terms which lead to mixing of the zero field states. The mixing will occur between states having the same value of M, but differing in J by ±1. The amount of mixing will depend on the magnetic dipole moment matrix elements and on the energy difference between the states. Let the zero field wave function be designated by $| n', J, M >$, where n' includes all of the quantum numbers necessary to describe the state except J and M. The wave function in the magnetic field given by first order perturbation theory is

$$|n',J,M\rangle^{H} = |n',J,M\rangle + \left(\frac{\langle n',J+1,M|-\vec{\mu}\cdot\vec{H}|n',J,M\rangle}{E_{n',J,M} - E_{n',J+1,M}}\right)|n',J+1,M\rangle$$

$$+ \left(\frac{\langle n',J-1,M|\vec{\mu}\cdot\vec{H}|n',J,M\rangle}{E_{n',J,M} - E_{n',J-1,M}}\right)|n',J-1,M\rangle \qquad (14)$$

where E is the energy of the state denoted by the subscripts, and $-\vec{\mu} \cdot \vec{H}$ is the magnetic dipole moment operator (14).

When the electric dipole moment transition probability for the Zeeman components of a transition are calculated using the perturbed wave functions, the symmetry which existed between $\Delta M = \pm 1$ transitions is destroyed. The destruction of this symmetry will leave either $\Delta M = +1$ or $\Delta M = -1$ transitions more intense, and MORD and MCD will be nonzero even when no Zeeman splitting occurs. This effect is demonstrated in Figure 6b and Figure 7b.

In Figures 6c and 7c are shown a combination of the effects caused by Zeeman splitting and intensity perturbations on MORD and MCD. These last figures would be expected to provide the most realistic picture of any real system, for both effects must be considered.

Any theoretical approach to MCD and MORD must be able to determine the relative importance of the Zeeman and perturbation effects. Any calculations of such magnetic optical phenomena will require specific assumptions about the molecular system in question. It will be necessary to know the nature of the electronic states involved as well as the absorption line width, if not the line shape. In order to test the theory experimentally, the slit width and any other important experimental parameters must be taken into account. These requirements appear to be quite demanding, but past experience in this laboratory has indicated that only by considering all of them will an adequate understanding of magnetic optical effects in simple molecules be obtained.

Formulas

Serber presented one of the earliest theoretical developments on magnetic rotation in molecules, and his approach is still used in more

modern theories on magnetic optical activity (2). He calculated the Verdet constant, starting from an equation given by Kramers (15). This equation gave the rotation, ϕ, of the plane of polarization of a light beam passing through a sample in the expression

$$\frac{\phi}{\ell} = \frac{8\pi^2 \nu^2 N i}{ch} \sum_{S,S'} \frac{1}{(\nu^2 - \nu_{ss'}^2)} \left(\frac{e^{\frac{-W_s}{KT}}}{Q} \right) \langle s|x|s' \rangle \langle s'|y|s \rangle \tag{15}$$

$\frac{\phi}{\ell}$ is the rotation of the plane per centimeter of sample traversed, $\nu_{ss'}$ is the transition frequency between quantum states defined by s and s', N is the number density of the molecules, w_s is the ground state energy and Q the partition function. The operators x and y are components of the electric dipole moment operator relative to a space fixed coordinate system.

It is not obvious that Kramer's equation is related to right and left circularly polarized light, but such a relationship is easily demonstrated. First let equation (15) be rewritten as

$$\phi = \frac{-8\pi^2 \nu^2 N}{ch} \sum_{S,S'} \frac{1}{(\nu^2 - \nu_{ss'}^2)} \left(\frac{e^{\frac{-W_s}{KT}}}{Q} \right) Im \left[\langle s|x|s' \rangle \langle s'|y|s \rangle \right] \tag{16}$$

The matrix elements can be rearranged as in

$$\langle s|x|s' \rangle \langle s'|y|s \rangle = \langle s|x + iy|s' \rangle \langle s'|y|s \rangle - i \langle s|y|s' \rangle \langle s'|y|s \rangle \tag{17}$$

where the first term on the right is zero if the transition from s to s' involves $\Delta M = +1$, or they may be rearranged to give

$$\langle s|x|s'\rangle\langle s'|y|s\rangle = \langle s|x - iy|s'\rangle\langle s'|y|s\rangle + i\langle s|y|s'\rangle\langle s'|y|s\rangle \quad (18)$$

where the first term on the right is zero for a $\Delta M = -1$ transition. Equation (16) may then be rewritten as the difference between two terms.

$$\phi = \frac{-8\pi^2\nu^2 N}{ch}\left\{\sum_{S,S'}^{\Delta M=-1}\frac{1}{(\nu^2-\nu_{ss'}^2)}\left(\frac{e^{\frac{-W_s}{KT}}}{Q}\right)[\langle s|y|s'\rangle\langle s'|y|s\rangle] - \sum_{S,S'}^{\Delta M=+1}\frac{1}{(\nu^2-\nu_{ss'}^2)}\left(\frac{e^{\frac{-W_s}{KT}}}{Q}\right)[\langle s|y|s'\rangle\langle s'|y|s\rangle]\right\} \quad (19)$$

Equation (19) can be given as

$$\phi = \frac{-8\pi^2\nu^2 N}{ch}\left\{\sum_{S,S'}^{\Delta M=-1}\frac{1}{(\nu^2-\nu_{ss'}^2)}\left(\frac{e^{\frac{-W_s}{KT}}}{Q}\right)|\langle s|x|s'\rangle|^2 - \sum_{S,S'}^{\Delta M=+1}\frac{1}{(\nu^2-\nu_{ss'}^2)}\left(\frac{e^{\frac{-W_s}{KT}}}{Q}\right)|\langle s|x|s'\rangle|^2\right\} \quad (20)$$

Since the sums in equations (19) and (20) involve terms associated with circular light, it is now apparent that equation (20) represents the difference between quantities associated with right and left circular polarization. Because of the nature of the frequency dependence in equation (20), this formula is not applicable when ν is very near $\nu_{ss'}$.

To go from equation (15) to a formula for the Verdet constant, Serber expanded the matrix elements, transition frequency, ground state

energy, and partition function in power series of the magnetic field intensity. These series were of the form $w_s = w_s^o + Hw_s' + \ldots$. The expanded terms were substituted into equation (15), and the terms first order in H collected to give the following type of formula for the Verdet constant:

$$V = B \sum_{S,S'} \left\{ \frac{\nu^2 a(S,S')}{(\nu_{SS'}^2 - \nu^2)^2} + \frac{\nu^2 b(S,S')}{(\nu_{SS'}^2 - \nu^2)} + \frac{\nu^2 c(S,S')}{T(\nu_{SS'}^2 - \nu^2)} \right\} e^{\frac{-W_S}{kT}} \qquad (21)$$

where B is a constant dependent on the system to be studied. The "a" terms arise from Zeeman splitting in the ground and excited states, and include matrix elements of the following form:

$$[\langle S|\vec{\mu}\cdot\vec{H}|S\rangle - \langle S'|\vec{\mu}\cdot\vec{H}|S'\rangle][\mathcal{Z}\langle S|X|S'\rangle\langle S'|Y|S\rangle]$$

The "b" terms are due to the perturbation of intensities of the $\Delta M = \pm 1$ transitions. The perturbations are caused by the mixing of states in the ground and excited state due to the presence of the magnetic field. The matrix elements that appear in the "b" terms have the form

$$[\langle S|X|S'\rangle\langle S'|\vec{\mu}\cdot\vec{H}|S''\rangle\langle S''|Y|S\rangle - \langle S|Y|S'\rangle\langle S'|\vec{\mu}\cdot\vec{H}|S''\rangle\langle S''|X|S\rangle]$$

or

$$[\langle S|\vec{\mu}\cdot\vec{H}|S''\rangle\langle S''|X|S'\rangle\langle S'|Y|S\rangle - \langle S|\vec{\mu}\cdot\vec{H}|S''\rangle\langle S''|Y|S'\rangle\langle S'|X|S\rangle]$$

The "c" terms are also due to intensity perturbations, but these are caused by population effects in a magnetically active ground state. These "c" terms are generally called the paramagnetic terms, due to the nature of

their temperature dependence, and they involve matrix elements of the form

$$[\langle s|\vec{\mu}\cdot\vec{H}|s\rangle\langle s|x|s'\rangle\langle s'|y|s\rangle - \langle s|\vec{\mu}\cdot\vec{H}|s\rangle\langle s|y|s'\rangle\langle s'|x|s\rangle]$$

Serber's formula was applied to some experimental data available on I_2 and the dialkali vapors. The data were explained on the basis of "a" terms only, even though the formula was applied without justification near regions of absorption. Carroll used Serber's formula to consider I_2 as well as Na_2 and K_2, but this time the "b" terms were included in the calculations. Even though the formula was again applied near absorption, Carroll was able to explain the data in a manner which did not agree in all of its details with Serber's previous explanation based on "a" terms only.

Since Serber's formula was only suitable far from absorption, it remained to develop a theory which would be applicable within areas of absorption. Recently, Stephens has presented formulas to calculate MCD and MORD (10,16,17). He applied a damped frequency function and in so doing made the formulas suitable for use within regions of absorption. To develop his formulas, Stephens assumed that the absorption line width was very much greater than any Zeeman splitting that could occur. These formulas are especially suited to the study of solutions and solids, where absorption line widths are very large. If $\theta_{ss'}$ is taken to be the circular dichroism induced in a sample near a transition from s to s' by a magnetic field and $\phi_{ss'}$ the Faraday rotation, then $\theta_{ss'} \propto (\alpha_R - \alpha_L)$ and $\phi_{ss'} \propto (n_R - n_L)$. Stephens' formulas give

$$\Theta_{SS'} = \frac{-7Z\,N\,H}{\hbar c}\left\{\frac{4\nu_{SS'}\nu^3(\nu_{SS'}^2-\nu^2)\,\Gamma_{SS'}\,A_{SS'}}{\hbar\left[(\nu_{SS'}^2-\nu^2)^2+\nu^2\Gamma_{SS'}^2\right]^2}\right.$$

$$\left. + \frac{\nu^3\,\Gamma_{SS'}}{(\nu_{SS'}^2-\nu^2)^2+\nu^2\Gamma_{SS'}^2}\left[B_{SS'}+\frac{C_{SS'}}{kT}\right]\right\} \qquad (22)$$

and

$$\Phi_{SS'} = \frac{-7Z\,N\,H}{\hbar c}\left\{\frac{2\nu_{SS'}\nu^2\left[(\nu_{SS'}^2-\nu^2)^2-\nu^2\Gamma_{SS'}^2\right]\,A_{SS'}}{\hbar\left[(\nu_{SS'}^2-\nu^2)^2+\nu^2\Gamma_{SS'}^2\right]^2}\right.$$

$$\left. + \frac{\nu^2(\nu_{SS'}^2-\nu^2)}{(\nu_{SS}^2-\nu^2)^2+\nu^2\Gamma_{SS'}^2}\left[B_{SS'}+\frac{C_{SS'}}{kT}\right]\right\} \qquad (23)$$

where ν is in cm^{-1} and Γ is the absorption line half width. The A, B and C terms in Stephens' formulas include the same types of matrix elements as those appearing in Serber's "a", "b", and "c" terms, and are ascribed to the same causes.

Neither the formulas of Serber nor those of Stephens are applicable to the case where the absorption line width is of the same order of magnitude as the Zeeman splitting. Theories have been presented by Sage and Groenewege, but they are not applicable under the conditions existing when an MRS is observed (18,19).

Starting from formulas for the index of refraction and absorption coefficient for a classical oscillator, and using the Van Vleck-Weisskopf

damped line shape, it is possible to derive formulas for Faraday rotation and circular dichroism applicable under the conditions imposed by magnetic rotation. Based on the assumption that the index of refraction squared is approximately equal to the dielectric constant,

$$n^2 = 1 + \frac{Ne^2}{\pi m(\nu_0^2 - \nu^2)} \left\{ 1 - \frac{\nu \Gamma^2}{2\nu_0} \left[\frac{(\nu_0 + \nu)}{\Gamma^2 + (\nu_0 - \nu)^2} + \frac{(\nu_0 - \nu)}{\Gamma^2 + (\nu_0 + \nu)^2} \right] \right\} \tag{24}$$

where e is the electronic charge, m the mass of the oscillator, and ν_o the frequency of the classical oscillator transition. When $\nu \to \nu_o$,

$$n^2 \approx 1 + \frac{Ne^2}{2\pi \nu_0 m} \left[\frac{(\nu_0 - \nu)}{\Gamma^2 + (\nu_0 - \nu)^2} \right] \tag{25}$$

Since n ≈ 1 in a gas at low pressure,

$$n = 1 + \frac{Ne^2}{4\pi \nu_0 m} \left[\frac{(\nu_0 - \nu)}{\Gamma^2 + (\nu_0 - \nu)^2} \right] \tag{26}$$

To go from the classical expression to its quantum mechanical counterpart ν_o will become $\nu_{ss'}$, and e^2/m will be replaced by $(8\pi^2 \nu_{ss'}/3h)|\xi_{ss'}|^2$, where $\xi_{ss'}$ is the electric dipole moment matrix element between s and s'. The expression for n will become

$$n = 1 + \frac{2\pi N}{3h} \left[\frac{(\nu_{ss'} - \nu)}{\Gamma_{ss'} + (\nu_{ss'} - \nu)^2} \right] |\mathcal{E}_{ss'}|^2 \tag{27}$$

or if ν is expressed in cm^{-1},

$$n = 1 + \frac{2\pi N}{3hc} \left[\frac{(\nu_{ss'} - \nu)}{\Gamma_{ss'}^2 + (\nu_{ss'} - \nu)^2} \right] |\mathcal{E}_{ss'}|^2 \tag{28}$$

where N is now the ground state population density.

The matrix element $|\xi_{ss'}|^2$ can be expressed in terms of its x, y and z components relative to a space fixed coordinate system.

$$|\mathcal{E}_{ss'}|^2 = |\langle s|x|s'\rangle|^2 + |\langle s|y|s'\rangle|^2 + |\langle s|z|s'\rangle|^2 \tag{29}$$

When considering the index of refraction for circularly polarized light, only the x and y components contribute, and

$$|\langle s|x|s'\rangle|^2 = |\langle s|y|s'\rangle|^2$$

The index of refraction for circularly polarized light can be expressed as

$$n_{CIRC.} = 1 + \frac{4\pi N}{3hc}\left[\frac{(\nu_{ss'}-\nu)}{\Gamma_{ss'}^2+(\nu_{ss'}-\nu)^2}\right]|\langle s|x|s'\rangle|^2 \tag{30}$$

If more than one transition occurs in the same region of the spectrum, the index of refraction for circularly polarized light will be

$$n_{CIRC.} = 1 + \frac{4\pi}{3h}\sum_{s,s'}\frac{(\nu_{ss'}-\nu)N}{\Gamma_{ss'}^2+(\nu_{ss'}-\nu)^2}|\langle s|x|s'\rangle|^2 \tag{31}$$

The Faraday rotation per unit path length through the sample can be expressed as

$$\frac{\phi}{\ell} = \frac{4\pi^2}{3hc} \left\{ \sum_{S,S'}^{\Delta M=-1} \frac{\nu_{SS'}(\nu_{SS'}-\nu)\, N}{\Gamma_{SS'}^2 + (\nu_{SS'}-\nu)^2} \, |\langle S|x|S'\rangle|^2 \right.$$

$$\left. - \sum_{S,S'}^{\Delta M=+1} \frac{\nu_{SS'}(\nu_{SS'}-\nu)\, N}{\Gamma_{SS'}^2 + (\nu_{SS'}-\nu)^2} \, |\langle S|x|S'\rangle|^2 \right\}. \tag{32}$$

Returning to the classical oscillator, the absorption coefficient is given by

$$\alpha = \frac{2N\nu^2 e^2}{mc\,\nu_0^2} \left[\frac{\Gamma}{(\nu-\nu_0)^2 + \Gamma^2} + \frac{\Gamma}{(\nu+\nu_0)^2 + \Gamma^2} \right] \tag{33}$$

If $\nu \to \nu_0$

$$\alpha \approx \frac{2Ne^2}{cm} \left[\frac{\Gamma}{(\nu-\nu_0)^2 + \Gamma^2} \right] \tag{34}$$

and the quantum mechanical substitution yields

$$\alpha = \frac{16N\pi^2}{3hc} \left[\frac{\nu_{SS'}\Gamma_{SS'}}{(\nu-\nu_{SS'})^2 + \Gamma_{SS'}^2} \right] |\mathcal{E}_{SS'}|^2 \tag{35}$$

For circularly polarized light,

$$\alpha_{CIRC.} = \frac{32N\pi^2}{3hc} \left[\frac{\nu_{SS'}\Gamma_{SS'}}{(\nu-\nu_{SS'})^2 + \Gamma_{SS'}^2} \right] |\langle S|x|S'\rangle|^2 \tag{36}$$

and if several transitions occur in the same vicinity,

$$\alpha_{circ.} = \frac{32 N \pi^2}{3hc} \sum_{S,S'} \frac{\nu_{SS'} \Gamma_{SS'} N}{(\nu - \nu_{SS'})^2 + \Gamma_{SS'}^2} \left| \langle S | x | S' \rangle \right|^2 \qquad (37)$$

where ν is expressed in cm^{-1}. The circular dichroism per unit path length $\theta/\ell = \alpha_R/4 - \alpha_L/4$, and

$$\frac{\theta}{\ell} = \frac{8\pi^2}{3hc} \left\{ \sum_{S,S'}^{\Delta M=-1} \frac{\nu_{SS'} \Gamma_{SS'} N}{(\nu - \nu_{SS'})^2 + \Gamma_{SS'}^2} \left| \langle S | x | S' \rangle \right|^2 \right.$$
$$\left. - \sum_{S,S'}^{\Delta M=+1} \frac{\nu_{SS'} \Gamma_{SS'} N}{(\nu - \nu_{SS'})^2 + \Gamma_{SS'}^2} \left| \langle S | x | S' \rangle \right|^2 \right\} \qquad (38)$$

Equations (32) and (38) provide a starting point for the development of a theory of magneto-optics similar to that provided for Serber in equation (15). Since it is desired to produce a theory suitable for applications where Γ is the same size as the Zeeman splitting, an expansion similar to Serber's will not work. The frequency dependent functions would lend themselves to such an expansion if Γ were much larger than the Zeeman effect, or vice versa. Because the frequency dependent functions cannot be simply expanded in powers of the magnetic field intensity, the magnetic field effects must be introduced into equations (32) and (38) in some other way.

The ICℓ transition ($^3\pi_1 \leftarrow {}^1\Sigma+$) studied in this laboratory involves only a magnetically active excited state. Because the ground state will exhibit no Zeeman splitting, it should be possible to neglect the population factor when calculating magneto-optical effects. The only terms remaining

in equations (32) and (38) which can be affected by a magnetic field are the frequency $\nu_{ss'}$ and the matrix elements. If the summations are taken over all of the Zeeman components of a transition, the effect of the magnetic field on the frequency will be taken into account.

Magnetic effects on the matrix elements must be considered in terms of the magnetic field perturbations on the wave functions used to calculate the matrix elements. The magnetic dipole moment will mix nearby states having J different by ±1 with the zero field states. A zero field matrix element $\langle s|x|s'\rangle$ will now become

$$\left\langle s \left| x \right| s' - \sum_{s''} \frac{\langle s'|\vec{\mu}\cdot\vec{H}|s''\rangle}{E_{s'} - E_{s''}} \; s'' \right\rangle$$

from equation (14). This matrix element can be expanded to give

$$\langle s|x|s'\rangle - \sum_{s''} \left(\frac{\langle s'|\vec{\mu}\cdot\vec{H}|s''\rangle}{E_{s'} - E_{s''}} \right) \langle s|x|s''\rangle$$

where the sum will consist of at most two terms, corresponding to J's different from that in s' by ±1.

When the magnetically perturbed matrix elements are substituted into equations (32) and (38), and terms second order in their field dependence are neglected,

$$\frac{\phi}{\ell} = \frac{4\pi^2}{3hc} \left\{ \sum_{s,s'}^{\Delta M=-1} \frac{\nu_{ss'}(\nu_{ss'}-\nu)}{\Gamma_{ss'}^2 + (\nu_{ss'}-\nu)^2} \left[\langle s|x|s'\rangle^2 - 2\sum_{s''} \left(\frac{\langle s'|\mu\cdot H|s''\rangle}{E_{s'} - E_{s''}} \right) \langle s|x|s'\rangle\langle s|x|s''\rangle \right] \right.$$

$$\left. - \sum_{s,s'}^{\Delta M=+1} \frac{\nu_{ss'}(\nu_{ss'}-\nu)}{\Gamma_{ss'}^2 + (\nu_{ss'}-\nu)^2} \left[\langle s|x|s'\rangle^2 - 2\sum_{s''} \left(\frac{\langle s'|\vec{\mu}\cdot\vec{H}|s''\rangle}{E_{s'} - E_{s''}} \right) \langle s|x|s'\rangle\langle s|x|s''\rangle \right] \right\} \qquad (39)$$

and

$$\frac{\theta}{\ell} = \frac{8\pi^2}{3hc}\left\{\sum_{s,s'}^{\Delta M=-1}\frac{\nu_{ss'}\Gamma_{ss'}}{(\nu-\nu_{ss'})^2+\Gamma_{ss'}^2}\left[\langle s|x|s'\rangle^2 - 2\sum_{s''}\left(\frac{\langle s'|\vec{\mu}\cdot\vec{H}|s''\rangle}{E_{s'}-E_{s''}}\right)\langle s|x|s'\rangle\langle s|x|s''\rangle\right]\right.$$

$$\left. -\sum_{s,s'}^{\Delta M=+1}\frac{\nu_{ss'}\Gamma_{ss'}}{(\nu-\nu_{ss'})^2+\Gamma_{ss'}^2}\left[\langle s|x|s'\rangle^2 - 2\sum_{s''}\left(\frac{\langle s'|\vec{\mu}\cdot\vec{H}|s''\rangle}{E_{s'}-E_{s''}}\right)\langle s|x|s'\rangle\langle s|x|s''\rangle\right]\right\} \quad (40)$$

In order to use equations (39) and (40), it is necessary to assume a molecular model, so that the magnetic moment, wave functions and line widths can be approximated. If the formulas are to be tested against experimental data, experimental parameters such as the slit function must be taken into account. When calculating the matrix elements in equations (39) and (40), it is usually assumed that the rotational wave function will separate from the remainder of the wave function describing a state. This reduces the matrix elements to a constant term, depending on all but the rotational wave functions, multiplied by a matrix element depending only on the rotational states involved. In many cases the symmetric rotor wave functions can be used to evaluate these rotational matrix elements.

The two types of terms appearing in equations (39) and (40) under the summations over s and s' correspond to Serber's "a" and "b" terms. The paramagnetic terms would appear if ground state populations were considered. Given a suitable molecular model, it should be possible to calculate magnetic optical effects using equations (39) and (40), if the paramagnetic terms are negligible.

CHAPTER III

EXPERIMENT--PULSED DISCHARGES

Apparatus for Pulsed Energy Experiments

The $^3\pi_1 \leftarrow {}^1\Sigma^+$ transition in ICℓ was studied by three different experimental techniques. Two of the experiments involved the use of capacitor discharges, and the components of the apparatus used for the pulsed experiments will be discussed in this section.

Three ICℓ samples were used in the experiments. Sample A was enriched in the $Cℓ^{35}$ isotope to 96.8 per cent. The chlorine was obtained from the Isotopes Division of the Oak Ridge National Laboratory, in the form of NaCℓ. The NaCℓ was oxidized with $KMnO_4$ in 3F H_2SO_4, and the $Cℓ_2$ produced was reacted with a weighed amount of I_2, to produce ICℓ. The sample was contained in a Pyrex tube 25 mm in diameter and 50 cm long, with obtical windows sealed to the ends. Samples B and C were prepared with Fisher practical grade ICℓ, which was distilled twice before being used. The purity of these samples was checked by searching for evidence of I_2 in the MRS. Sample B was placed into a Pyrex tube 35 mm in diameter and 50 cm long, and Sample C utilized a tube 22 mm in diameter and 25 cm long. The pressure in both of these samples was adjusted to maximize the intensity of the magnetic rotation signals they produced.

Two spectrographs were used in the experiments. Low resolution was obtained on a Bausch and Lomb Model 11 Eagle type mount, equipped with a 635.3 lines per mm grating blazed at 6000 Å. The dispersion obtained with this instrument was 10.6 Å per mm, in the focal plane. High resolution

was obtained on a Jarrell-Ash Mark IV 3.4 meter Ebert type spectrograph. A 7,500 lines per inch grating blazed at 59^{o} was used, and the instrument was modified to improve its focussing properties by adjusting the plane of the entrance slit to coincide with the focal plane. The spectrum of ICℓ ($^{3}\pi_{1} \leftarrow {}^{1}\Sigma^{+}$) occurs around 6000 Å, and was observed in the ninth and tenth orders. Dispersion in the ninth order was .55 Å per mm and .50 Å per mm in the tenth. The detection was photographic or photoelectric. Photographic data were recorded on Eastman Kodak 103 a-F and 103 a-D plates, 103 a-F film, and a high speed recording film, Kodak type 2475.

Pulsed experiments were recorded photometrically with an E.M.I. 9558-B photomultiplier tube. A cathode follower was placed inside the photomultiplier housing to reduce the output impedence. The output from the cathode follower was amplified and displayed on the screen of a Tektronix Model 564 storage oscilloscope. The oscilloscope display was examined using the storage facility, and recorded permanently on Polaroid Type 107 film when it was necessary. The cathode follower and amplifier circuit are shown in Figure 8. The power supply used with the photomultiplier for the pulsed experiments produced 0 to -1100 V, and was filtered but unregulated. To limit extraneous fields reaching the photomultiplier, a mu-metal shield was placed around the tube, and the body of the housing was made of nickel. Facilities were provided to cool the photomultiplier housing to dry ice temperature.

Three solenoids were used to produce pulsed magnetic fields. The coils were wound on plastic tubes, and those used to produce fields in excess of 10,000 gauss were externally supported by plastic (mycarta) sleeves. Solenoid I was used to produce fields up to 10,000 gauss in a

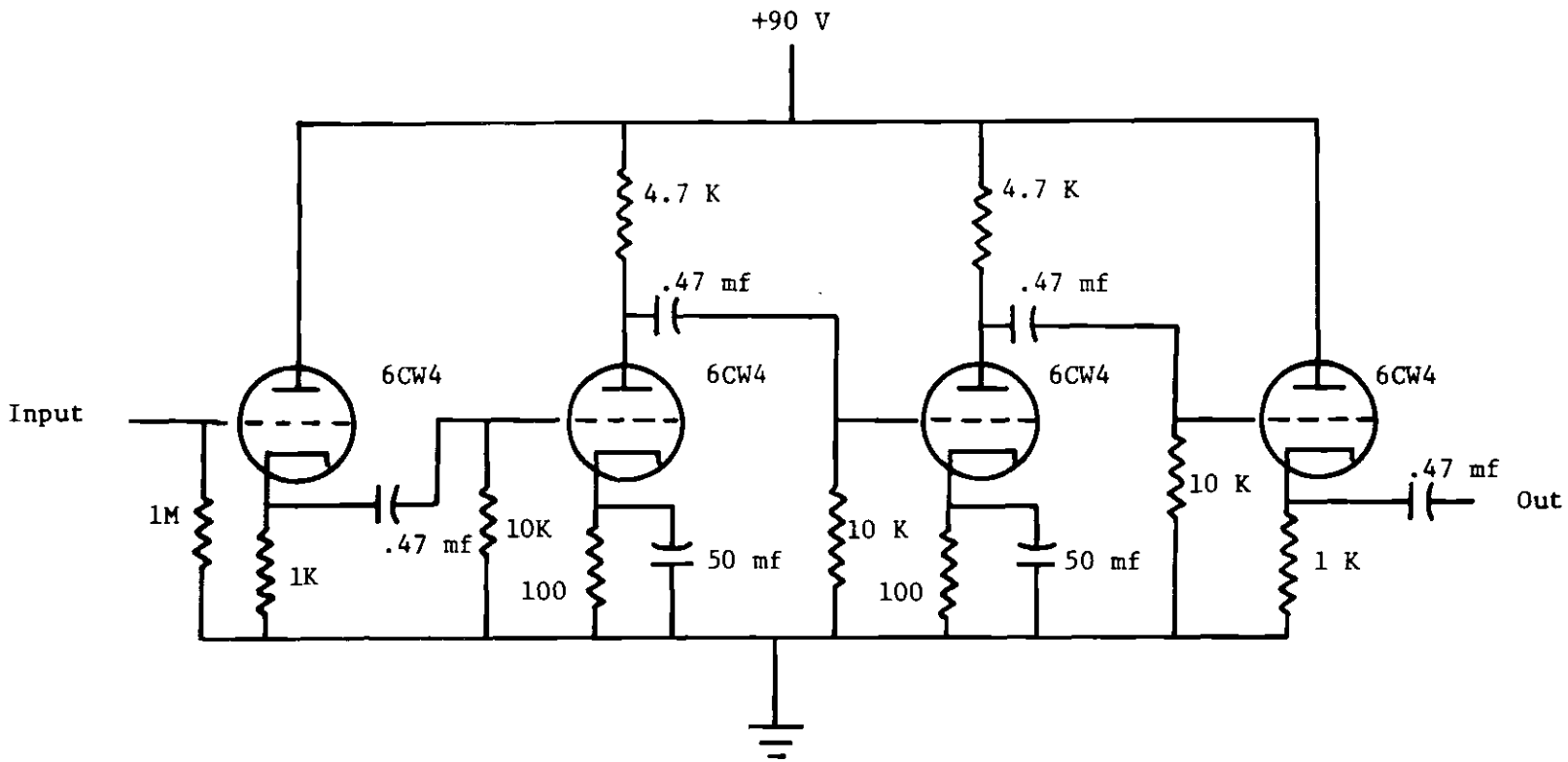

Fig. 8. Cathode Follower and Preamplifier Circuit.

relatively large volume. The coil was wound on a Lucite tube 45 mm O.D., 38 mm I.D., and 70 cm long, and consisted of three layers of cotton and Formvar insulated A.W.G. No. 16 copper wire. Teflon insulation .010 inches thick was placed between the layers, and a layer of Scotch No. 33 electrical tape was wound around the outer layer to hold the wire in place. The length of the coil was 65 cm. The magnetic field was produced by the discharge of a 61.5 mf capacitor, and the maximum field produced was 2.1 times the discharge voltage of the capacitor. The period of oscillation of this circuit was 3.5 msec.

Solenoids II and III produced higher fields, and were retained by external plastic sleeves. These coils were used with a 241.5 mf bank of capacitors. A partial cross section of solenoid II is shown in Figure 9. This coil was wound on a mycarta core 38 mm O.D., 26 mm I.D., and 25.5 cm long, and consisted of a single layer of Formvar insulated A.W.G. No. 14 copper wire. It was retained by three mycarta sleeves 88 mm O.D., 43 mm I.D., and 7.2 cm long. The maximum field produced by this coil was 10 times the discharge voltage of the capacitor bank, and had an oscillation period of 960 microseconds. Solenoid III was wound on a mycarta core 32 mm O.D., 25 mm I.D., and 49 cm long, and consisted of a single layer of Formvar insulated A.W.G No. 14 copper wire. It was retained by five mycarta sleeves 95 mm O.D., 37 mm I.D., and 7.2 cm long, which were fitted with brass fittings to allow air to be blown around the coil for cooling during repeated pulse experiments. The maximum field produced by this coil was 8.5 times the discharge voltage, with a period of 1070 microseconds. The important characteristics of the three solenoids are summarized in Table 1.

The capacitors used with the solenoids consisted of two banks stored in a single unit, which contained the switching and safety circuits

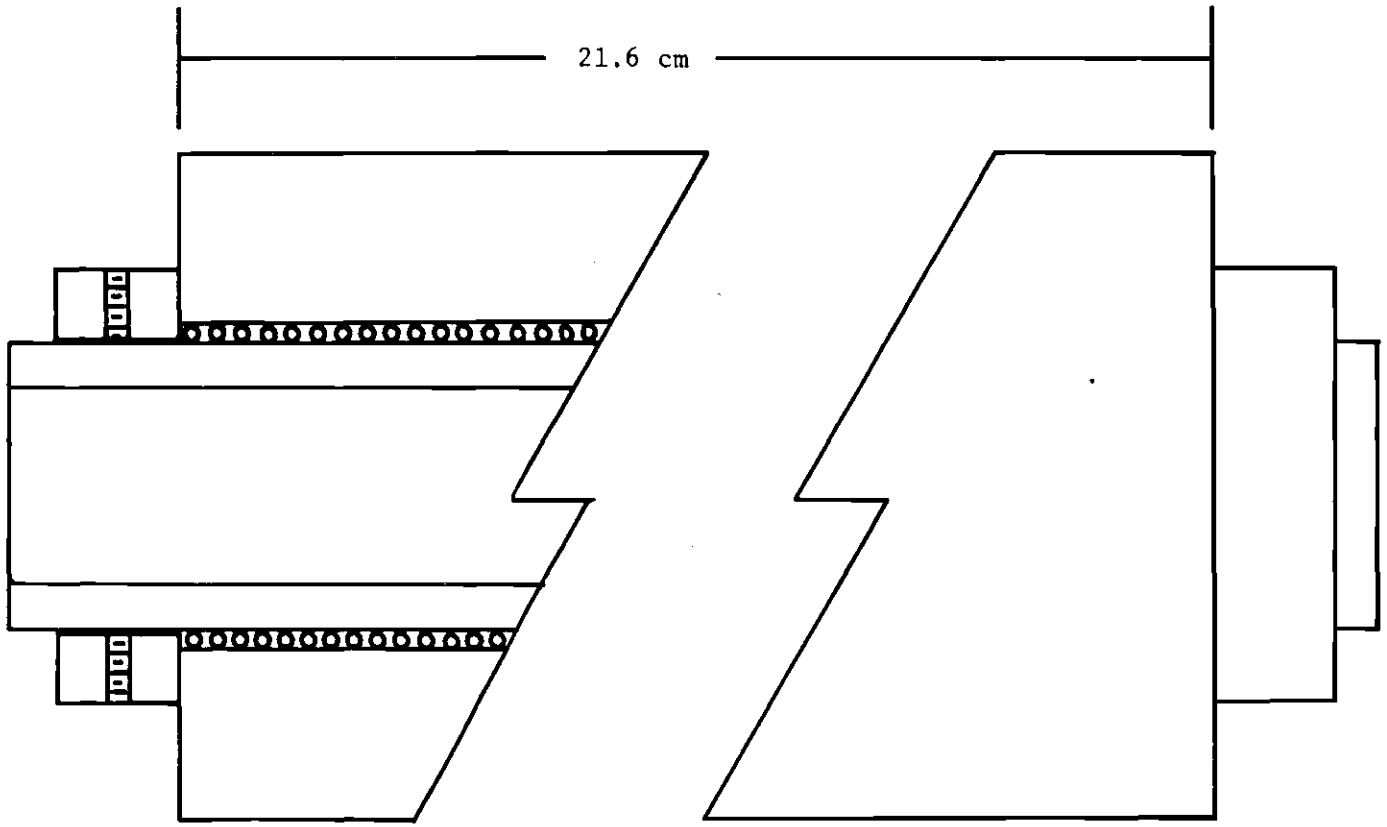

All dimensions full scale except overall length.

All parts Mycarta, wire AWG No. 14 Formvar covered copper.

Fig. 9. Pulsed Field Solenoid.

Table 1. Solenoid Specifications

Solenoid	Wire Size (AWG)	Average Radius of Coil (cm)	Length of Coil (cm)	Discharge Capacitor (mf)	Max. Field (Gauss per Volt on Cap)	Number of Layers in Coil	Period of Oscillation (microsecs)
I	16	2.5	64.5	61.0	2.07	3	3,500
II	14	2.0	21.5	241.5	10.04	1	960
III	14	1.7	36.0	241.5	8.52	1	1,070

as well as the capacitors. The circuit for this unit is shown in Figure 10. The design of this circuit, as well as the remainder of the pulsed circuitry was derived from the literature (20-45). The capacitors used in these banks were Cornell-Dubilier NRG Type 211 capacitors, with a nominal capacitance of 60 mf at 10 kv, and were designed especially for pulsed discharges. For safety purposes, each capacitor bank was equipped with a solenoid operated copper shorting bar, which had to be deliberately activated before a bank could be charged. The charging resistors were provided to isolate the power supply from the capacitors. Spark gaps were used as switches, and were triggered by pulses from 12 v automobile ignition coils. Argon was bled through the spark gaps to prevent oxidation and increase the stability of their operation. A spark gap is shown in Figure 11. The electrodes were chrome steel ball bearings welded to 1/4 inch steel rods. The trigger electrode was made of steel, the end plates and electrode supports were mycarta, and the envelope was Pyrex pipe.

Two power supplies were used to charge the capacitors. A 0 to +8.5 kv voltage doubler, shown in Figure 12, was used to charge the two capacitor banks mentioned above. The other supply, used to charge the flash lamp, produced 0 to +20 kv and was obtained from government surplus.

The flash lamp and associated circuitry were stored in an aluminum box. The circuit is described in Figure 13. The capacitor was a Cornell-Dubilier NRG Type 323 capacitor, with 1.6 mf at 25 kv. A solenoid operated copper shorting bar was placed acorss this capacitor. The discharge of this circuit was controlled by a 4C35 hydrogen thyratron, triggered by a positive voltage pulse applied to its grid. Two types of flash lamps were used, both of which provided Lyman discharges through a capillary section.

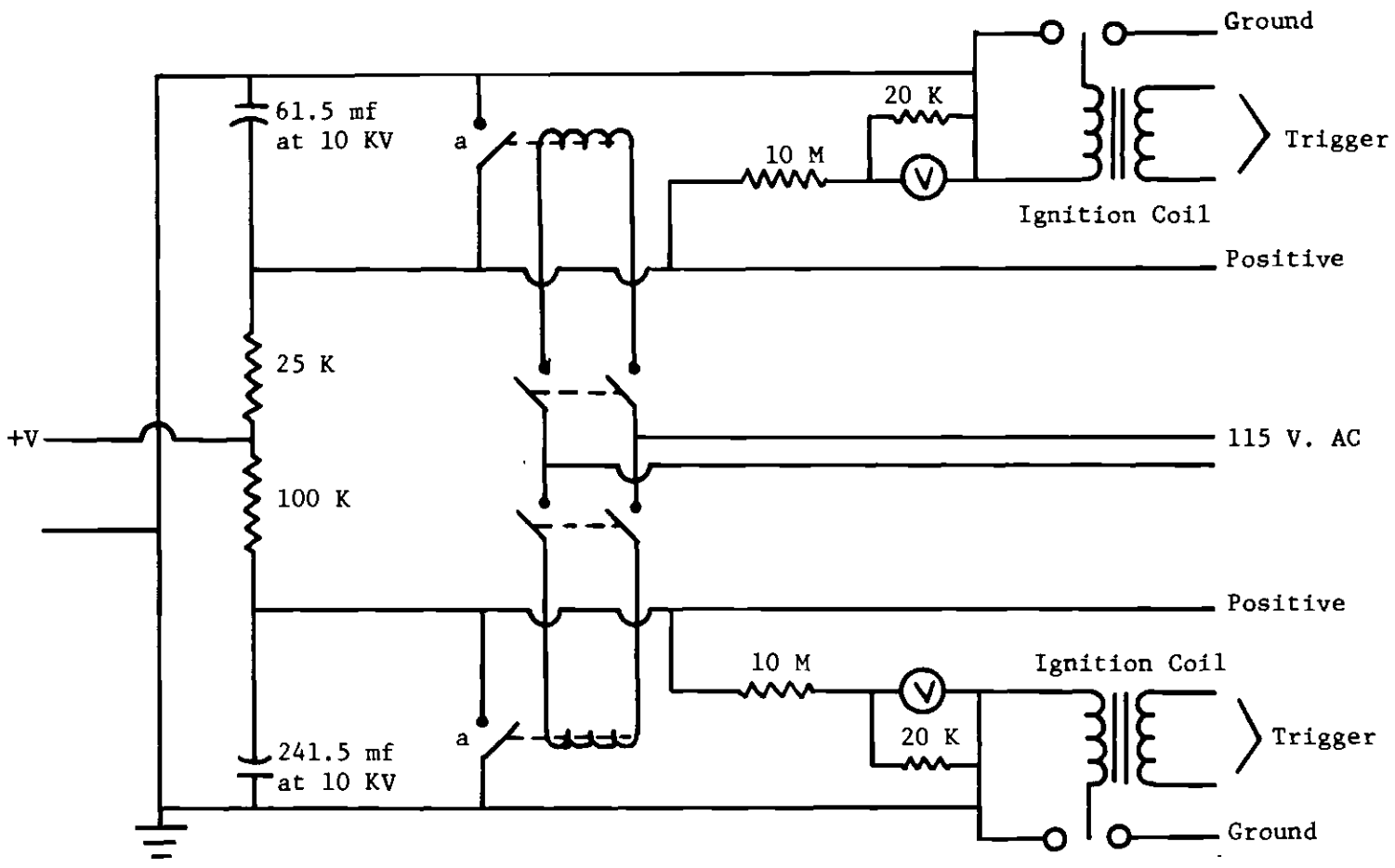

[a]Copper shorting bar, Solenoid activated.

Fig. 10. Capacitor Storage Bank

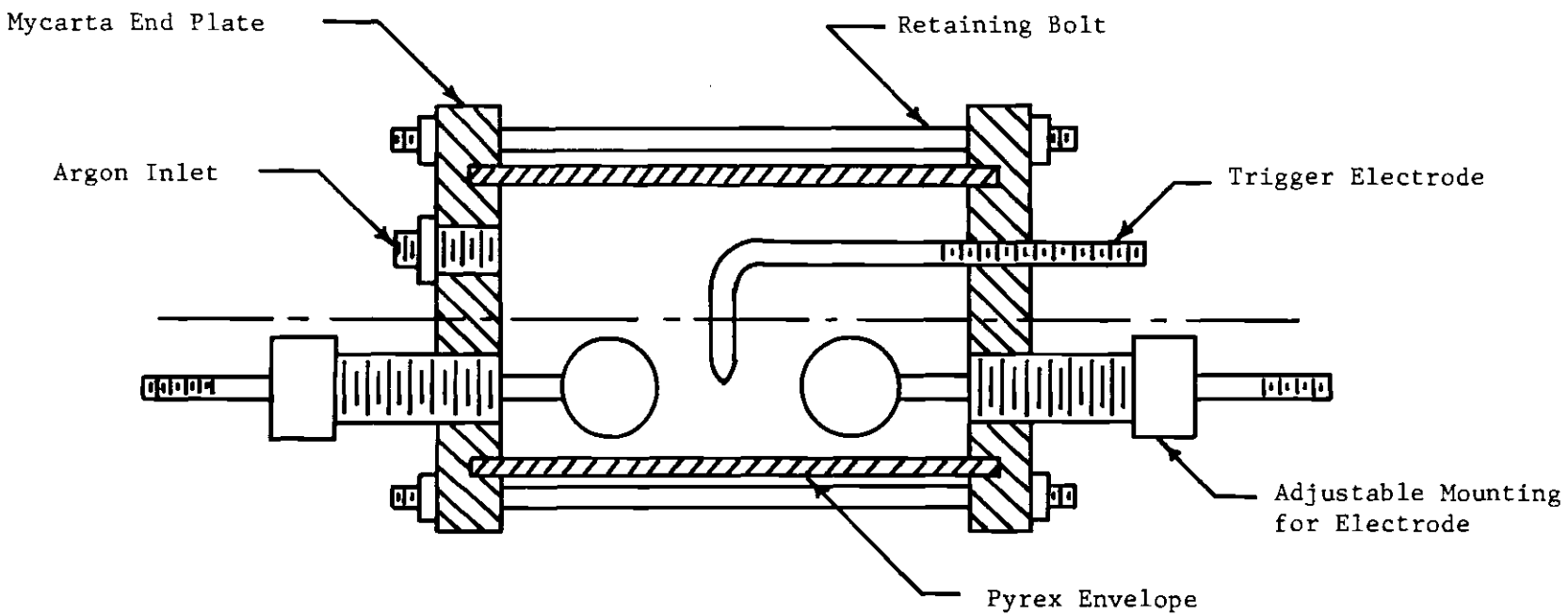

Fig. 11. Spark Gap.

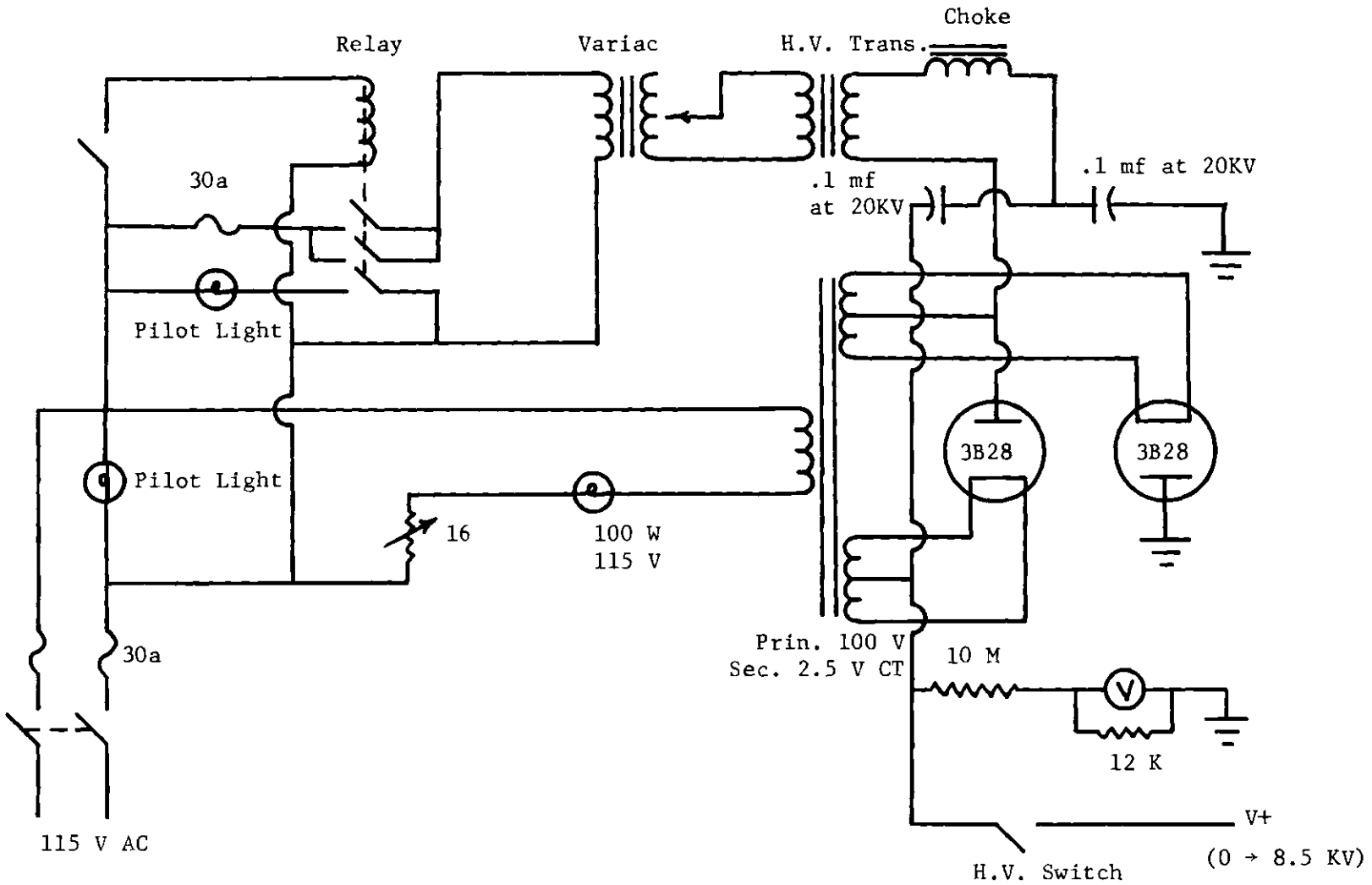

Fig. 12. Voltage Doubler Circuit (8.5 KV).

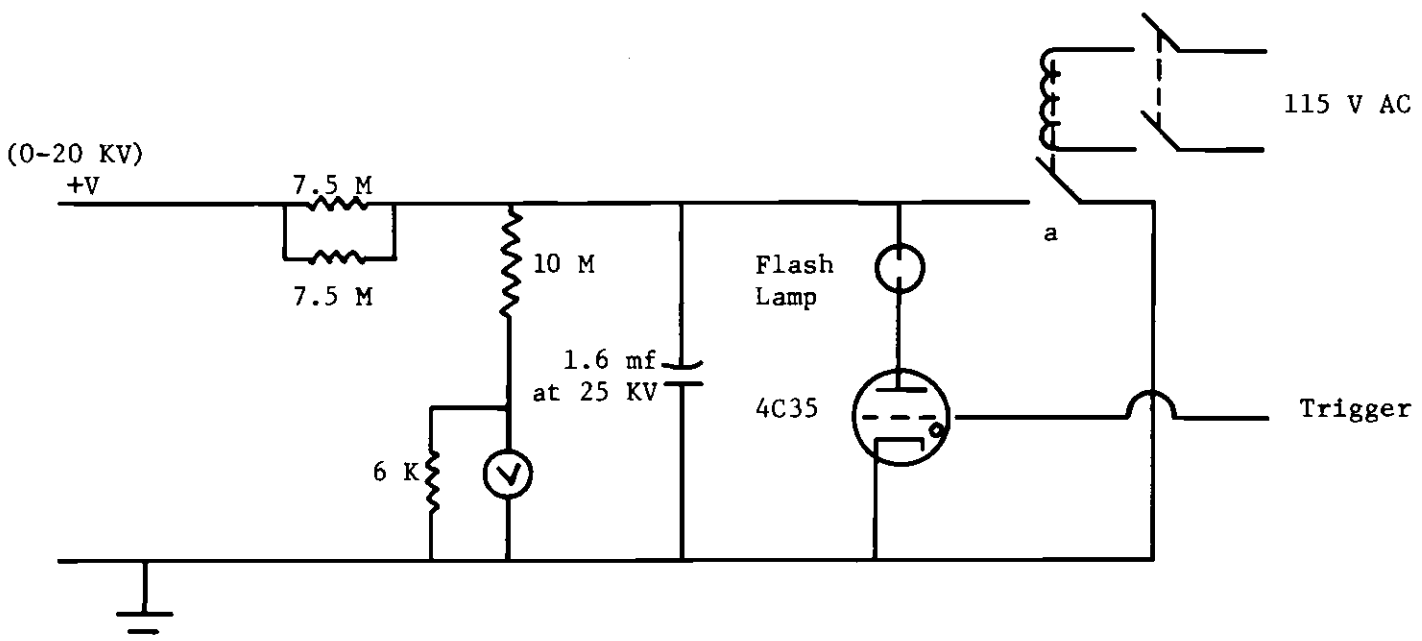

[a]Copper shorting bar, Solenoid activated.

Fig. 13. Flash Lamp Circuit.

One was viewed from the side of the capillary section, and is shown in Figure 14. The envelope of the tube was made of quartz, with a 2 mm I.D. capillary in the center. The electrode fittings were made by modifying brass Swagelok fittings, and the electrodes were 1/4 inch in diameter and consisted of tungsten with two per cent thorium. The electrodes were silver soldered into place in the brass fittings. One of the electrode fittings was connected to a glass tube leading to a vacuum system. This facilitated the evacuation and filling of the tube with Argon, which was used at pressures between one and five mm Hg. After repeated use, it was necessary to evacuate and refill the flash tube, since the pressure increased, ostensibly due to gas being driven from the capillary walls. The second flash lamp allowed the capillary section to be viewed from the end, and is shown in Figure 15. The envelope was made of Pyrex with a capillary section of 2 mm I.D. quartz supported in Teflon mounts. The Teflon mounts were sealed to the Pyrex tube by o-rings to prevent the discharge from going around the capillary section. The electrode fittings were the same fittings used with the other lamps, and a third modified Swagelok fitting held a window in place, which allowed an unobstructed view of the capillary. This tube was filled in the same way as the side view flash lamp. In both lamps, the capillary sections were enlarged to the point of breaking after about 3000 flashes and had to be replaced. The end view tube was more easily renewed, since only the capillary section required replacement.

The primary trigger circuit is shown in Figure 16. It was used to trigger spark gaps by discharging 10 mf at +230 v into the primary winding of an automobile ignition coil. The secondary winding was

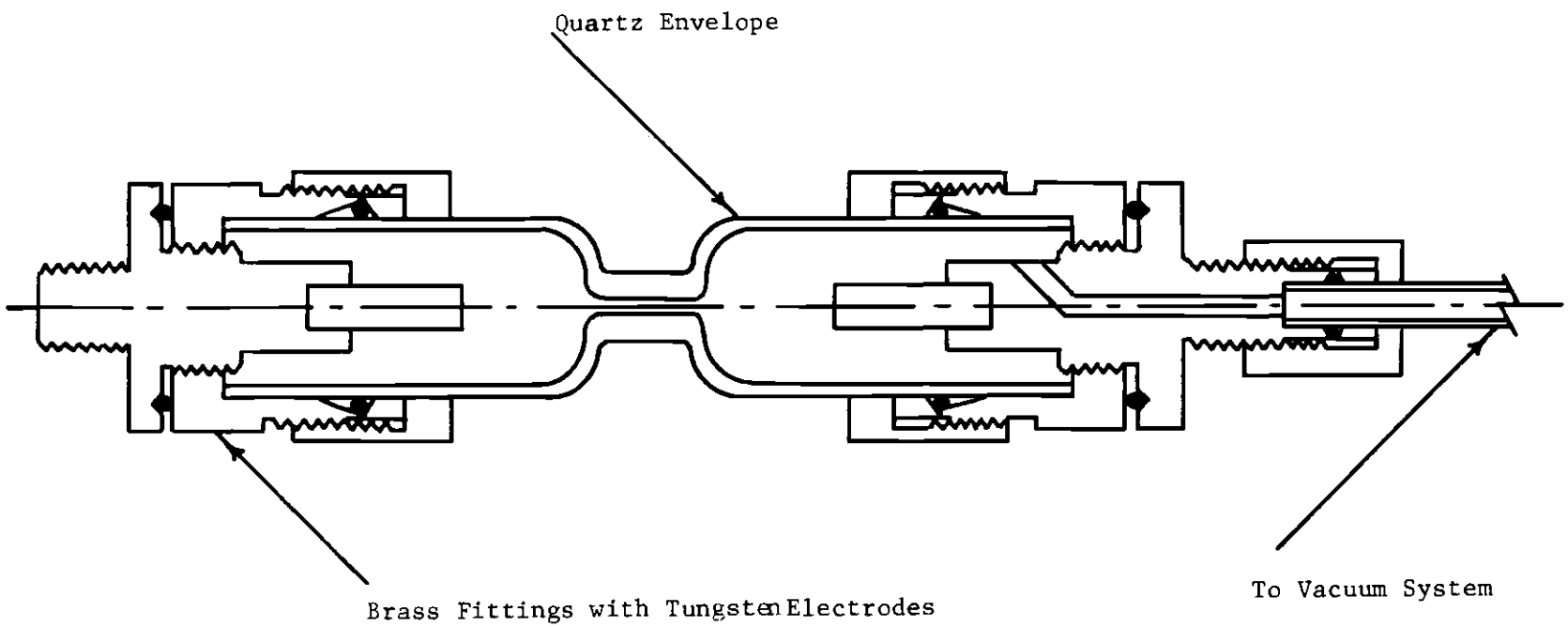

Full scale.

Fig. 14. Side View Flash Tube.

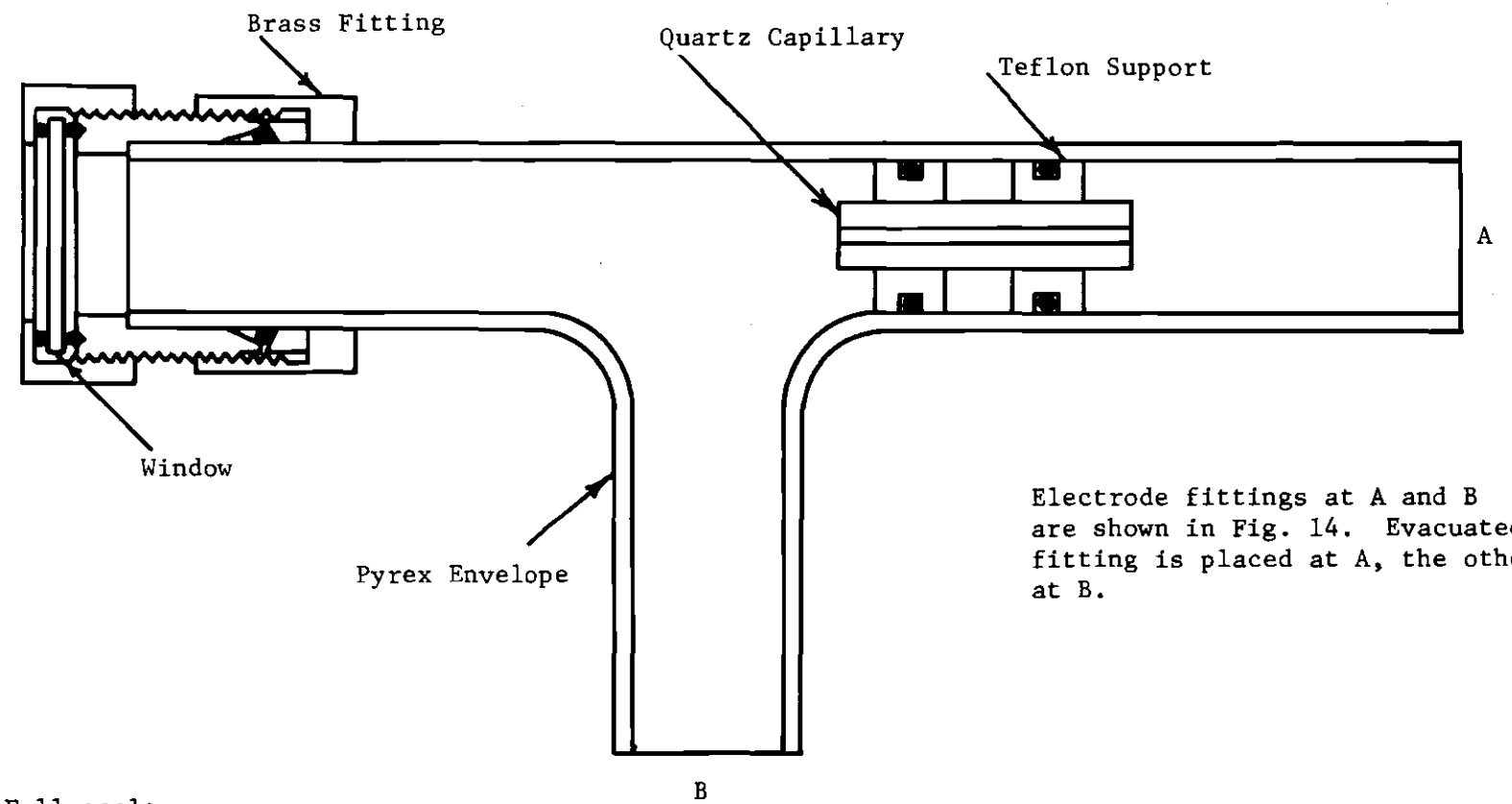

Fig. 15. End View Flash Tube.

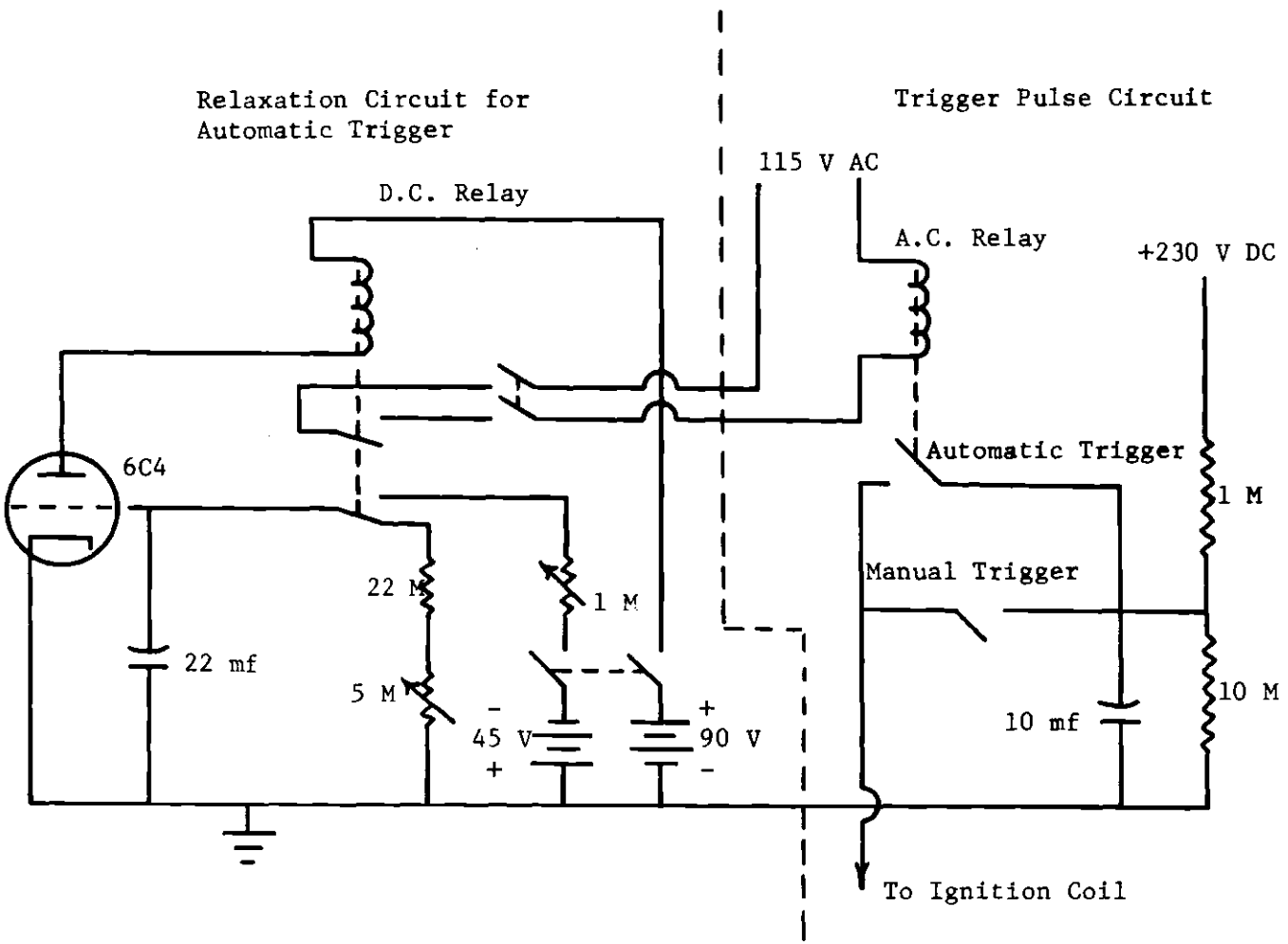

Fig. 16. Manual and Automatic Trigger Circuit.

connected to the trigger electrode in the spark gap. A circuit was provided to fire the trigger periodically at times variable from 12 to 38 seconds.

Most of the experiments involved two energy pulses, and required a means to control the time lapse between them. The time delay circuit is shown in Figure 17. The input to the time delay was derived from a 929 vacuum phototube situated to observe the spark gap involved in the initial discharge. The output of the time delay involved the discharge of a capacitor through a 4C35 hydrogen thyratron. The capacitor could be discharged directly into an ignition coil, or through a 10 ohm resistor, when it was desired to trigger a flash lamp. The voltage across the resistor was used to trigger the flash lamp circuit. After the time delay was triggered, it was necessary to deionize the thyratrons in the time delay circuit before the circuit could be used again. The reset circuit shown in Figure 18 was used to deionize the thyratrons and also had incorporated into it a pulse counter. A positive voltage pulse was required to trigger the reset circuit, and was usually supplied by the time delay output.

The quarter wave plate used in the Ne source experiment was designed to be used with the Hg line at 5460 Å, but it worked reasonably well at 5852 Å and 6266 Å. The quarter wave plates used with the flash lamp included one designed for the Na lines at 5890 Å and some plates prepared in this laboratory by peeling mica to the proper thickness.

Some preliminary experiments were done with a D.C. light source, provided by a high pressure Xe arc. The lamp was a P.E.K. Labs., Inc. Type X-75. The lamp was powered by a P.E.K. Labs., Inc. Model 401 power supply.

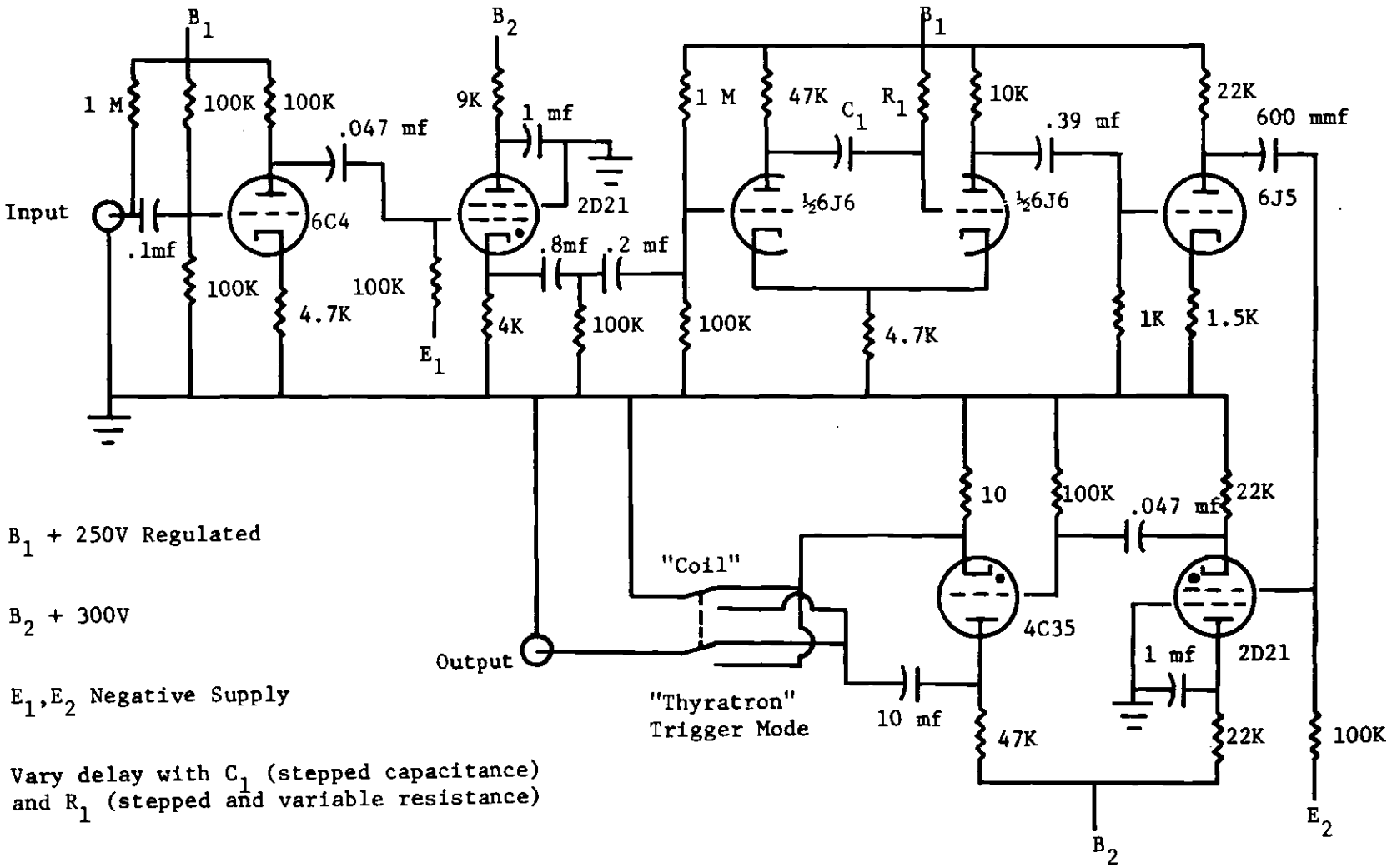

Fig. 17. Time Delay Circuit.

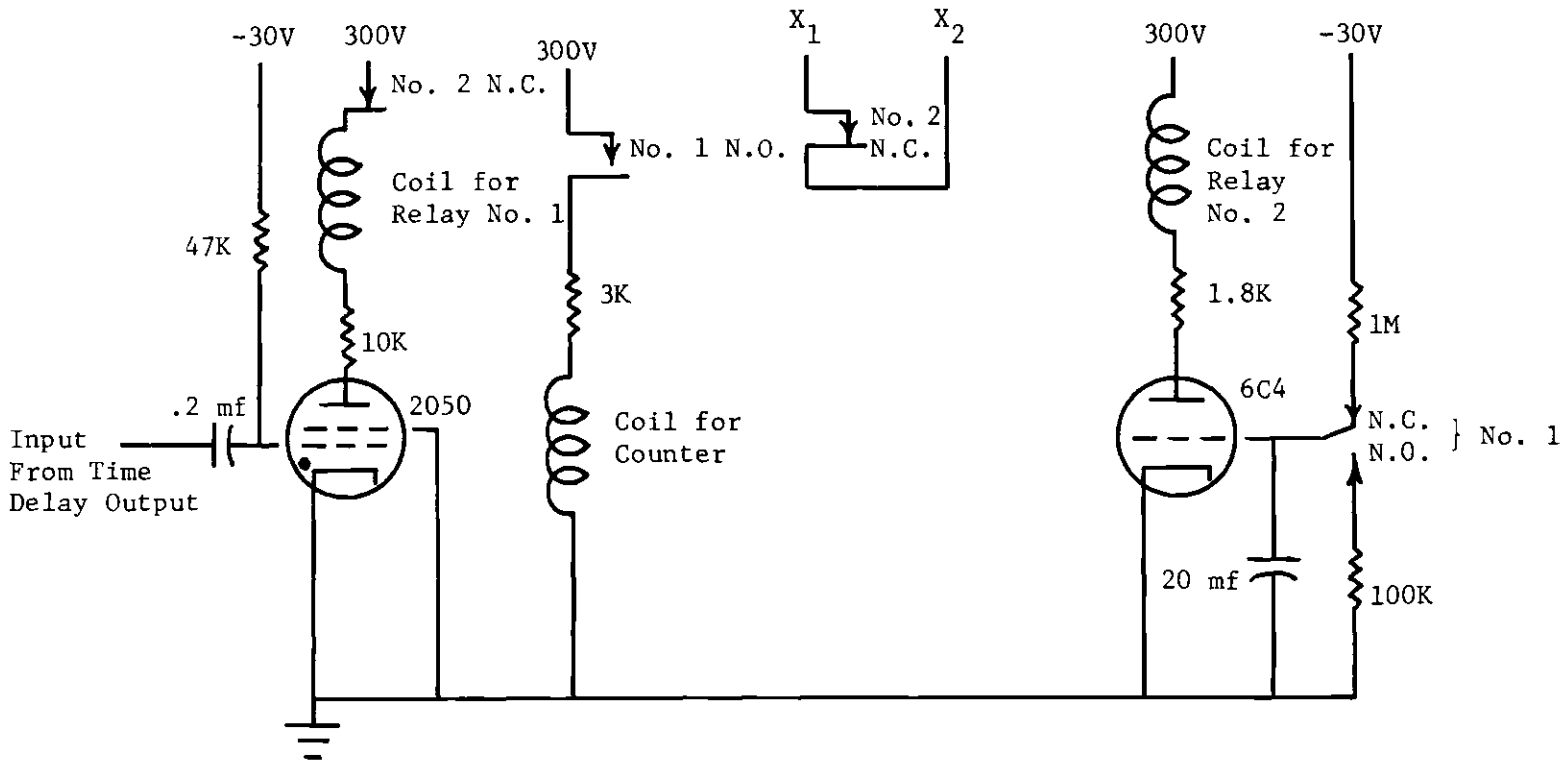

X_1,X_2 go to plate supply for thyratrons in time delay, removes B_2 (+v) from thyratrons to deionize them and reset the circuit.

Fig. 18. Counter and Time Delay Reset Circuit.

The Ne discharge was produced with an 11 mHz oscillator, capable of delivering up to 300 watts of power. The Ne discharge tubes were made of Pyrex tubing 3 to 7 mm I.D., and were viewed through one end. The tubes varied in length, but were usually around 5 cm long. The geometry of the tubes was not critical for the production of a satisfactory discharge, and was limited only by the size of the magnet which contained it. To construct a satisfactory discharge tube, it was necessary to flame the tube repeatedly while under vacuum to completely outgas it. A small piece of copper wire was placed into some of the tubes to act as a collector, and this seemed to improve the quality of the discharge. The tubes were filled with Matheson Research Grade Ne, 99.995 per cent by volume, and the pressure was adjusted to maximize the discharge intensity as observed with the eye. The electrical connections to the tubes were made by soldering the oscillator leads to 1/2 inch wide brass bands wrapped around the tubes, which were made of brass shim stock about .003 inch thick. The lifetime of the Ne discharge tubes varied considerably, and was as long as 30 hours in some cases and as short as 10 minutes in others.

Ne Source

In the first studies done on ICℓ, an attempt was made to produce experimentally the theoretically ideal nearly monochromatic light source of variable frequency. The nearly monochromatic light source was provided by an atomic emission line, and the frequency variations were produced by the Zeeman effect. When an atomic emission line exhibiting a normal Zeeman triplet in the presence of a magnetic field is viewed along the field axis, only two Zeeman components are visible. These correspond to $\Delta M = \pm 1$ transitions, and hence they are circularly polarized. By passing

the light through a quarter wave plate followed by a plane polarizer, it is possible to selectively pass just one of the Zeeman components, and either that component displaced to high frequencies or that displaced to low frequencies may be chosen. The frequency shift is controlled by the intensity of the magnetic field inducing the Zeeman splitting. The frequency of a laser transition in a gas laser was varied by this method in the infrared region of the spectrum. This variable frequency laser was used to study the fine structure in some vibrational transitions which occurred near the lasing line (46).

To study the ICℓ system the Ne emission spectrum was chosen. The lines are intense and easily separated by a low resolution spectrograph or monochromator. The Ne emission spectrum occurs in the same region as the ICℓ $^3\pi_1 \leftarrow {}^1\Sigma^+$ transition, and two intense Ne lines exhibiting normal Zeeman triplets occur in the immediate vicinity of some magnetic rotation features of the ICℓ molecule (47). These two Ne lines appear at 5852 Å and 6266 Å. In Table 2 are listed the Ne lines and adjacent ICℓ features. The ICℓ features and assignments are from the absorption data of Hulthen, et al., and only those features which also occurin the MRS of ICℓ are tabulated (48-50). The details of the two transitions are shown in Figure 19, with the notation given by Moore (51). Both of these Ne lines exhibit the normal Zeeman effect, so that the $\Delta M = +1$ (right circularly polarized) emission transition occurs at the lowest frequency (52). These Ne transitions, as they appear when viewed along the axis of the magnetic field, are shown in Figure 20.

The line width in the Ne emission spectrum is determined by the temperature, pressure, and magnetic and electric field effects (53). Lang

Table 2. Neon Emission Lines and Nearby ICℓ Features

Line Position [a]	Assignment
15,953.481 cm^{-1}	Neon
15,952.881	ICℓ, V" = 0 → V' = 14, R type, J' = 57
15,951.867	ICℓ, V" = 0 → V' = 14, P type, J' = 52
15,951.524	ICℓ, V" = 0 → V' = 15, P type, J' = 73
17,082.027	Neon
17,082.141	ICℓ, V" = 0 → V' = 29, R type, J' = 45
17,082.613	ICℓ, V" = 0 → V' = 28, P type, J' = 38
17,082.838	ICℓ, V" = 0 → V' = 28, R type, J' = 41

[a] From References (46) and (47).

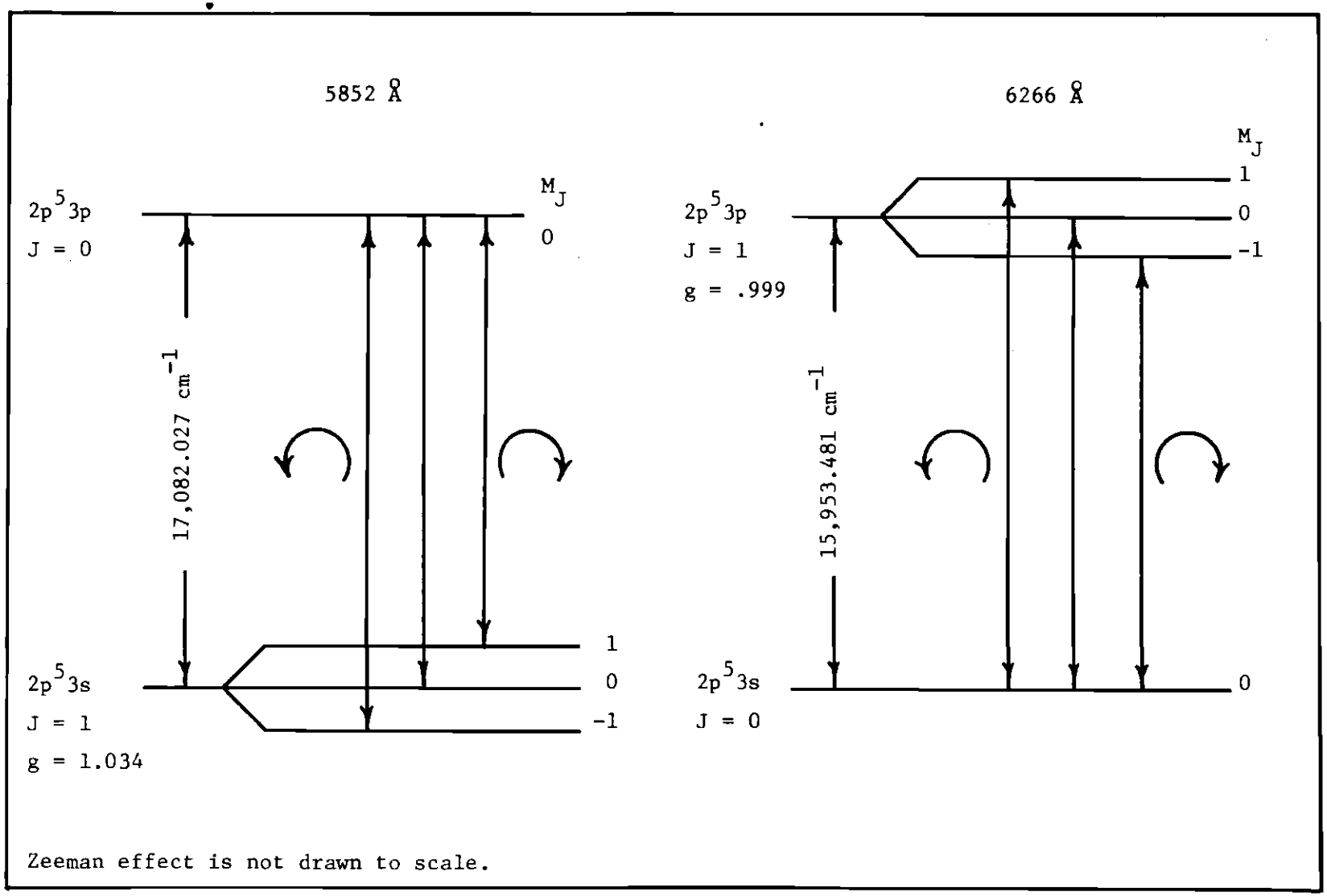

Fig. 19. Neon Lines Used in Zeeman Source Experiment.

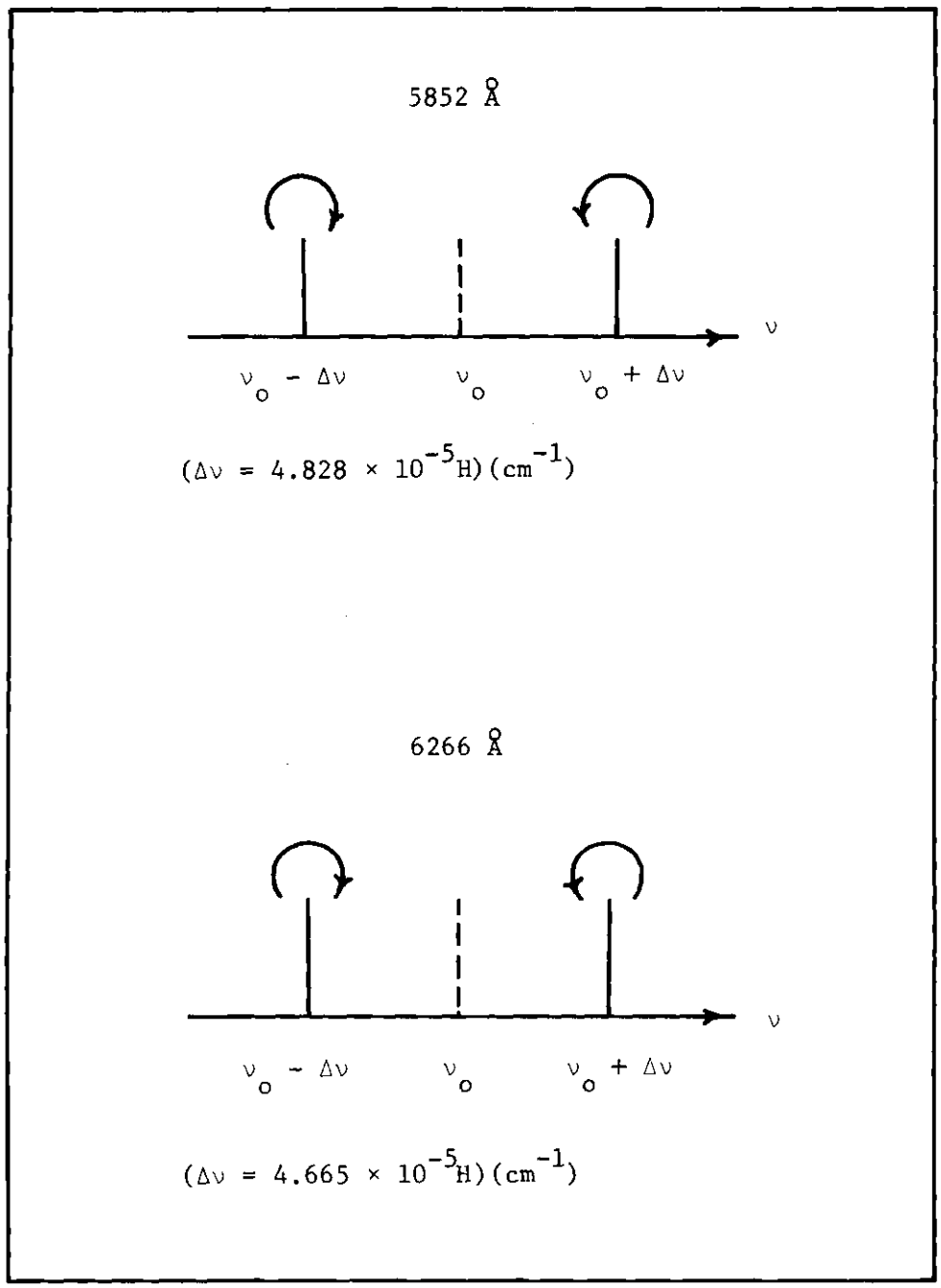

Fig. 20. Ne Lines Viewed Along a Longitudinal Field (H).

investigated the line width of a Ne emission spectrum excited by a 22 mHz oscillator (54). The Stark effect and Doppler broadening were negligible; the principal factor affecting the line width was the pressure of the Ne itself. Even at pressures as low as 0.1 mm Hg, the half width of the 5852 Å line was .115 cm^{-1}. The half width of several Ne lines was recorded and although the line at 6266 Å was not among them, it seems safe to assume that its half width must be on the order of .100 cm^{-1}. Thus the Ne emission provided two source lines, with half widths of about .100 cm^{-1} and frequencies variable up to 2.0 cm^{-1} with the magnetic fields available.

The magnetic fields used to produce the Zeeman effect in Ne and to induce magnetic effects in ICℓ were provided by pulsed fields. Solenoid I contained the ICℓ sample A, and the Ne discharge was placed within solenoid II. The field produced by solenoid I oscillated very slowly compared to solenoid II, so that by delaying the discharge of II by 840 microseconds relative to that of I, the field produced by I remained almost constant while the field from II varied from zero to its maximum value. The field produced by solenoid I is plotted as a function of time in Figure 21, and the time interval during which solenoid II was pulsed is marked. The magnetic fields were monitored by observing the voltage induced in a small coil of wire placed near the solenoids.

The current as a function of time in a simple R-L-C circuit is given by

$$i(t) = A\,V\,e^{-\left(\frac{R}{2L}\right)t}\sin\left\{\left[\frac{1}{LC}-\left(\frac{R}{2L}\right)^2\right]^{1/2}t\right\} \qquad (41)$$

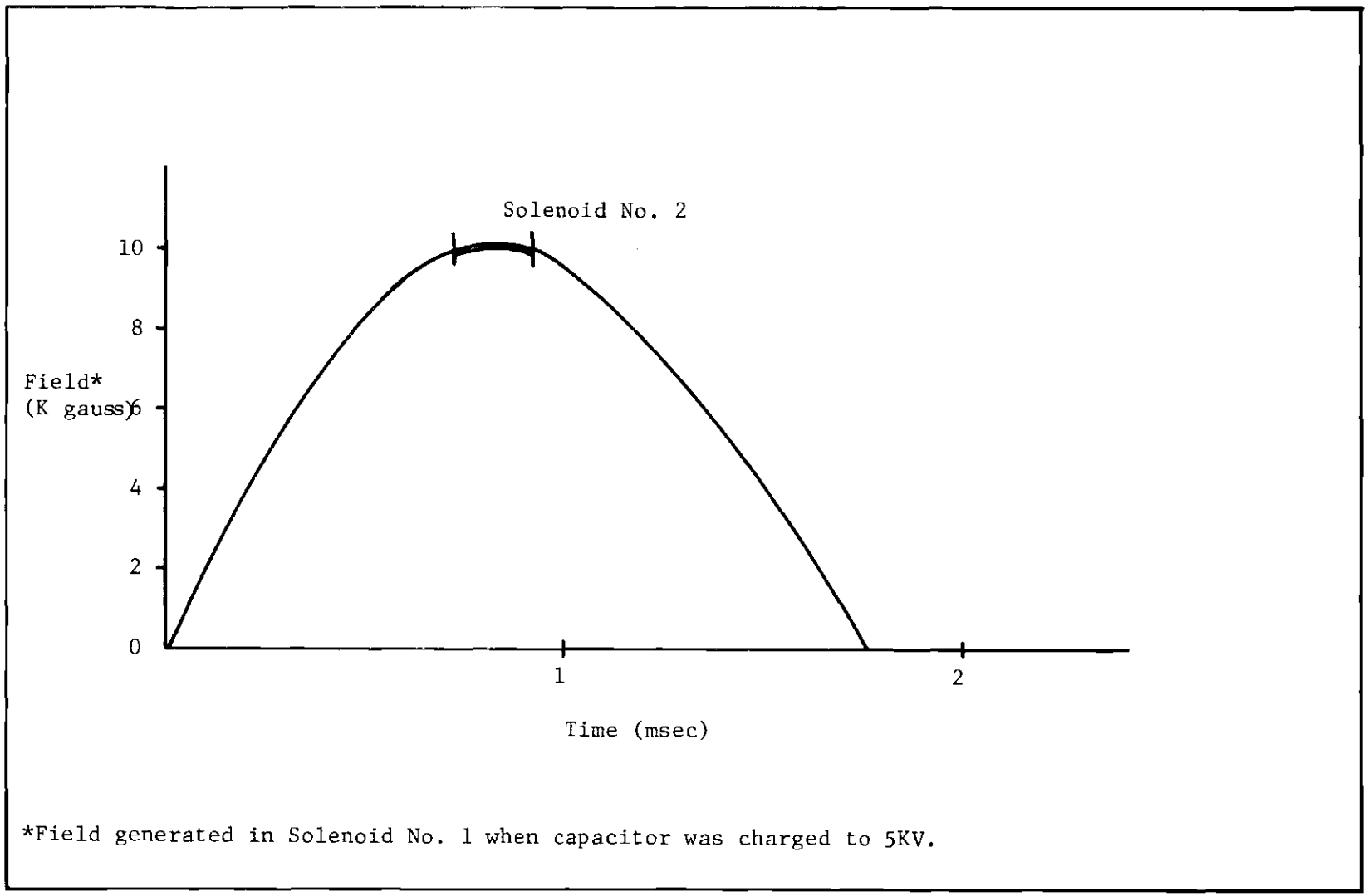

Fig. 21. Field Generated in a Pulsed Solenoid.

A is a constant dependent on the circuit parameters and V is the initial voltage on the capacitor. If the capacitance of the circuit is assumed to be in the capacitor bank, only two parameters remain to be computed, and these can be determined from the rate of exponential decay and period of oscillation of the circuit. Once the current as a function of time is determined, the magnetic field intensity in gauss in the center of a long solenoid is given by

$$H = 4\pi \times 10^{-3} \times n \times i(t) \tag{42}$$

Here n is the number of turns per meter in the solenoid and i(t) is the current in amperes. Since the Zeeman shift, $\Delta\nu$, is assumed to be a first order function in H, it too can be given as a time dependent function for any particular Zeeman component. The current, magnetic field intensity, and Zeeman shift can all be represented by the same time dependent curve, if appropriate changes are made in the scale of the ordinate. This is shown for solenoid II in Figure 22. In this Figure, it is assumed that the Zeeman shift is given by

$$\Delta\nu = g\beta H \tag{43}$$

which is the case for the normal Zeeman triplets in question. β is the Bohr magneton and g is the Landé g factor.

A block diagram of the apparatus used in this experiment is shown in Figure 23. The Bausch and Lomb Model 11 spectrograph was adequate to isolate the Ne lines at 5852 Å and 6266 Å, even when the entrance and exit slits were about 2 mm wide. The detection was done photoelectrically, using the photomultiplier, preamplifier, and oscilloscope described previously. Solenoids I and II were used for the ICℓ sample and Ne discharge,

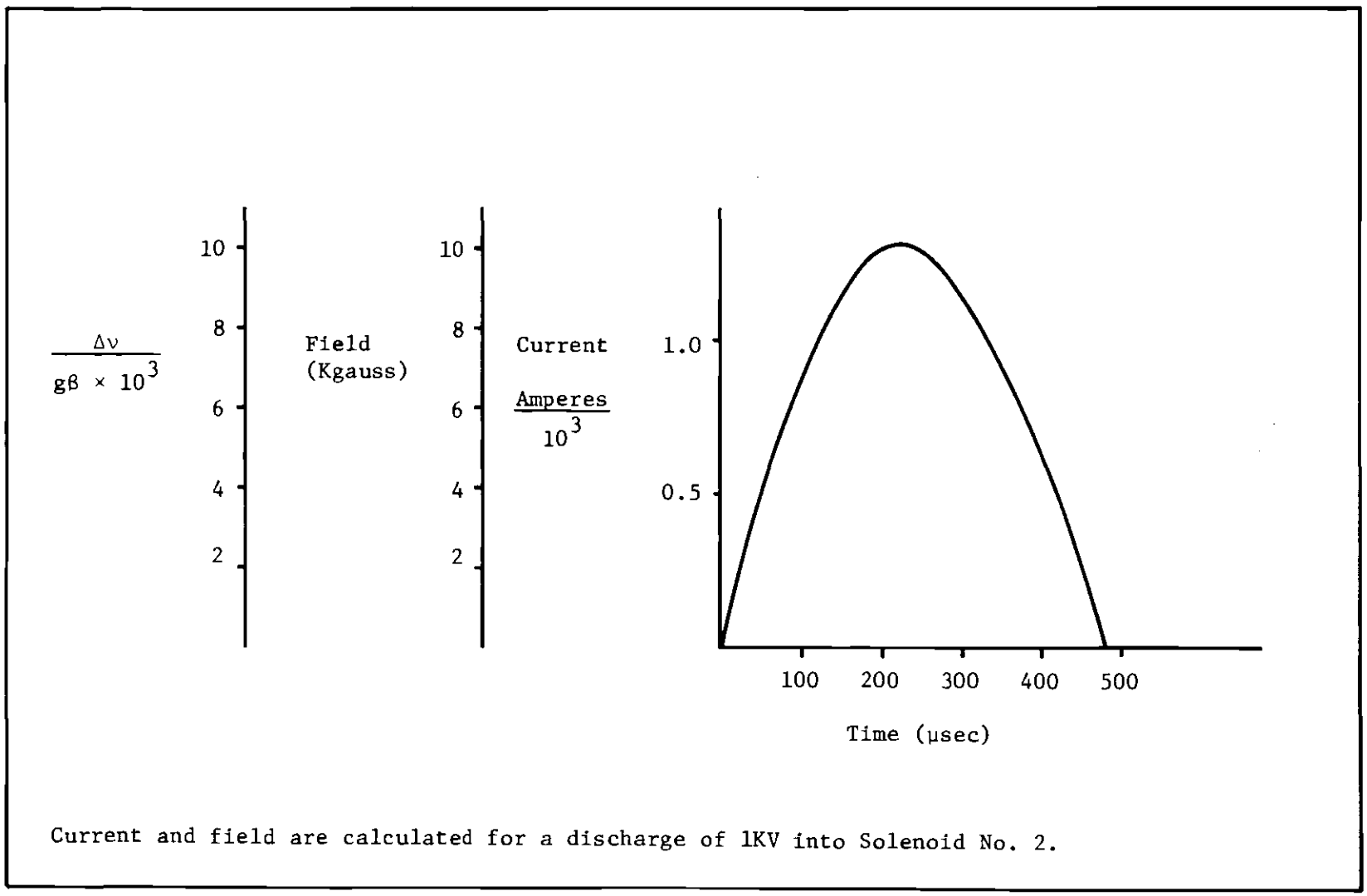

Fig. 22. Current, Field and Zeeman Effect in Pulsed Magnet.

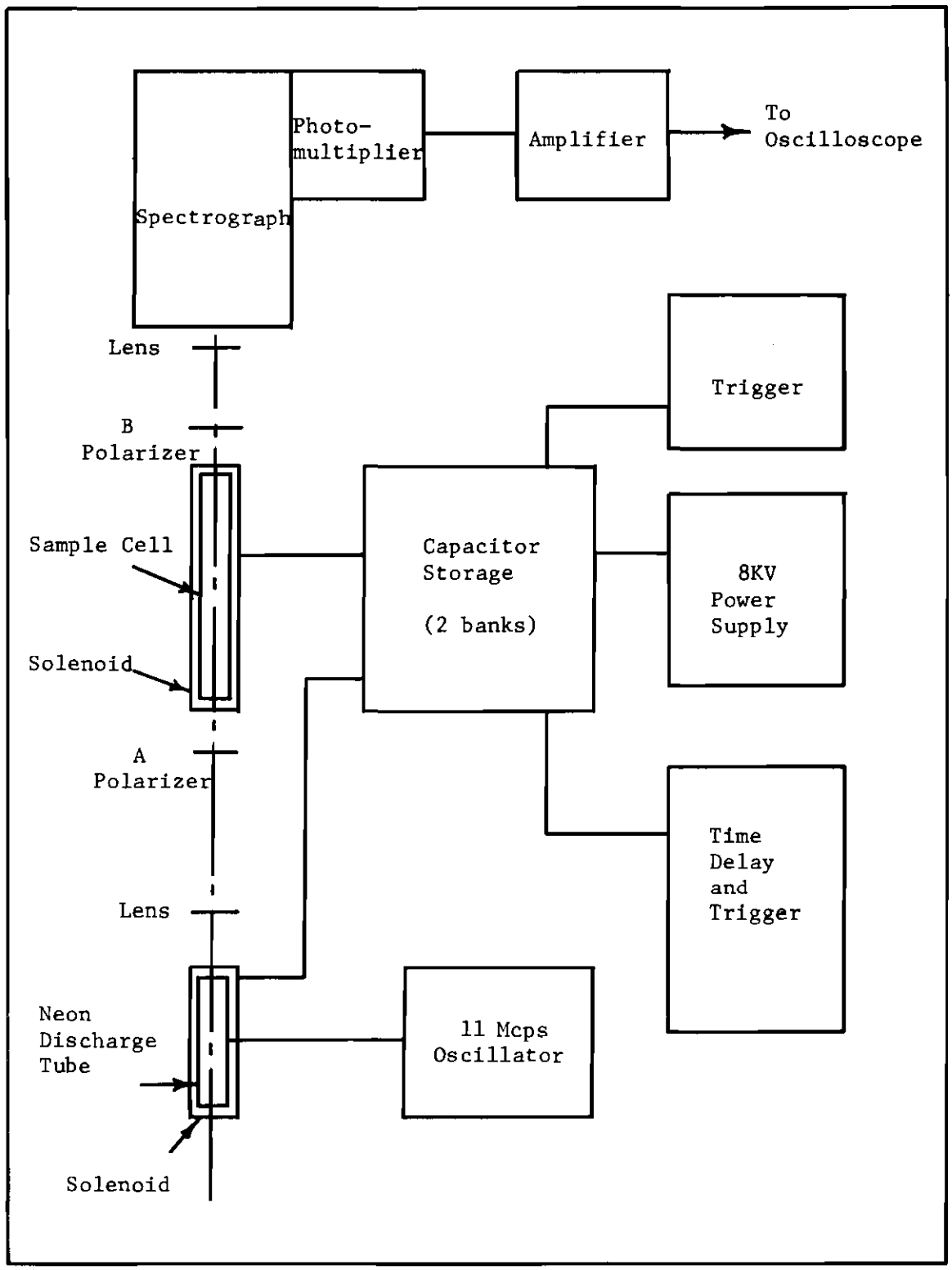

Fig. 23. Neon Source Experiment.

respectively, and both the discharge and sample were located to avoid the field gradients which occur at the ends of a solenoid. The fields were uniform to within five per cent throughout the discharge and sample volumes. The trigger, power supply, time delay, capacitor storage bank, and 11 mHz oscillator were described in the previous section. A lens was used near the source to collimate the light and another to focus the light onto the slit of the spectrograph.

To do a magnetic rotation experiment, a quarter wave plate followed by a plane polarizer was placed at position A, and an analyzer at position B. The angular dependence of the magnetic rotation could be determined by changing the orientation of the analyzer relative to the polarizer. The absorption of circularly polarized radiation was obtained when the analyzer was removed, and its place taken by a quarter wave plate followed by a plane polarizer.

To perform an experiment involving two pulsed fields, the trigger was used to initiate the discharge in solenoid I. The time delay, monitoring the light from the spark gap in series with solenoid I, discharged the second capacitor bank through solenoid II, approximately 840 microseconds after the first pulse was initiated. The oscilloscope was triggered by the first pulse, but it was operated in a delayed sweep mode, and only the first half period of the field produced by solenoid II was observed.

Due to the sensitivity of the detection system to extraneous radiation, it was necessary to separate the detection circuit from the pulsed fields as much as possible, and to shield the 11 mHz oscillator. Connections were made with coaxial leads, and wherever possible circuit elements were shielded by grounded steel boxes. The necessary shielding and the location of various detector elements was determined on a trial-and-error basis,

and that arrangement which appeared to minimize the observation of extraneous signals was used.

Flash Source

A flash lamp and pulsed magnetic field were used in conjunction with the high resolution Jarrell-Ash spectrograph in an attempt to determine directly the Zeeman splitting of single lines in ICℓ. A block diagram of the apparatus is shown in Figure 24. The spectrograph was used with a 25 micron entrance slit which gave resolution on the order of .013 Å or .04 cm^{-1} in the region studied, and most of the data were recorded on Kodak Type 2475 high speed recording film.

ICℓ sample B was used in conjunction with solenoid I, and sample C with solenoid III. The latter sample solenoid pair was prepared in an attempt to use fields up to 25,000 gauss to study magnetic effects in ICℓ. However, it became apparent upon using it that sample C exhibited very broad absorption lines, and hence was unsuitable for use in these experiments. The solenoids were powered by the appropriate capacitor banks in the capacitor storage unit described previously. The 8.5 kv power supply was used to charge the solenoid capacitors, and the 20 kv supply charged the flash lamp circuit. Since most of the experiments involved many pulses, the trigger used to initiate the solenoid discharge was operated in its automatic mode. The time delay was used to trigger the flash lamp when the solenoid reached its first maximum in field intensity. The flash lamp discharged in about 20 microseconds, so that the magnetic field was essentially constant while the lamp was discharging.

The spectrograph was located about 15 feet from the sample. Since the flash lamp did not provide a point source of radiation it was im-

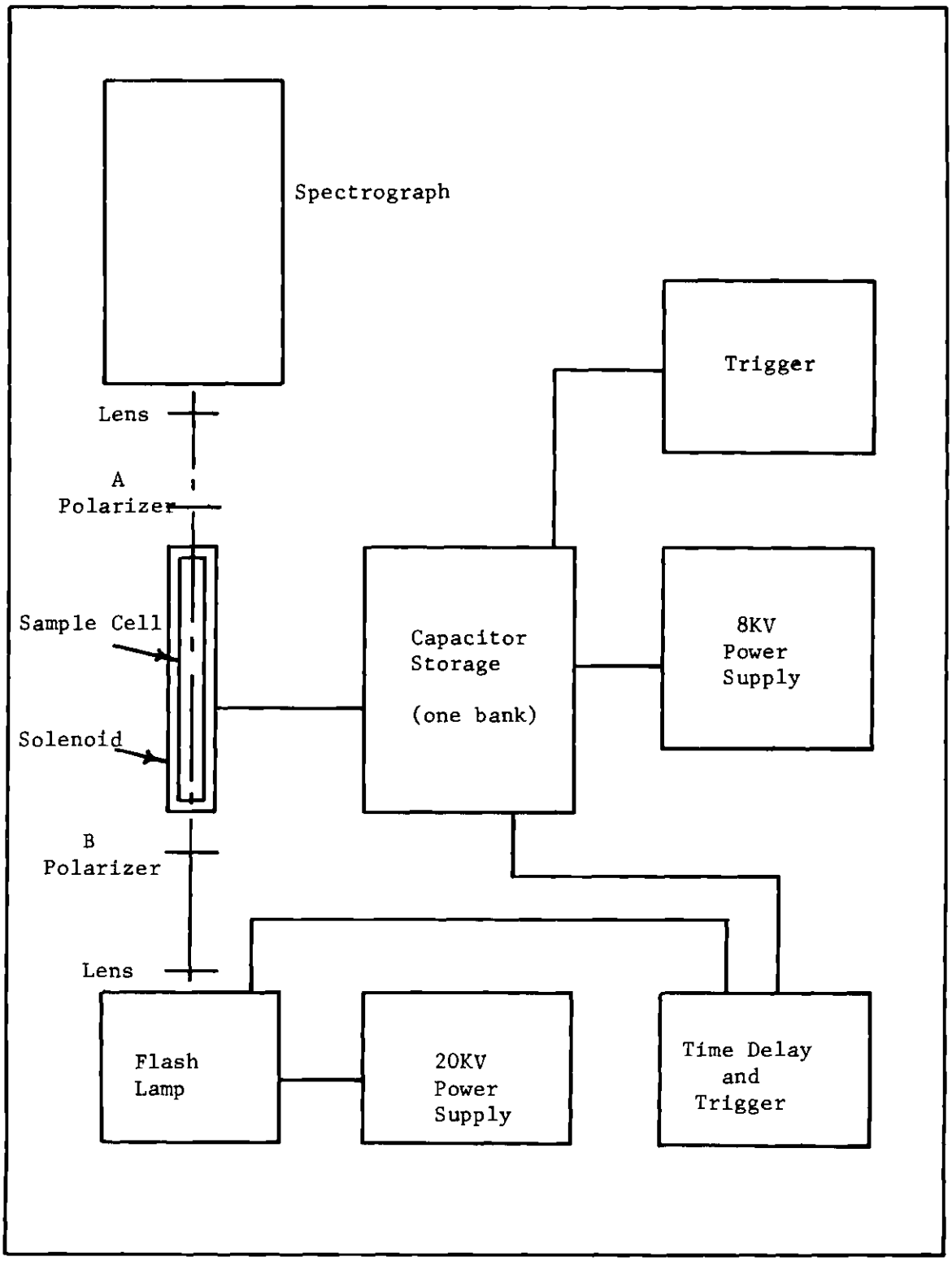

Fig. 24. Flash Source Experiment.

possible to collimate the light beam, and a series of lenses were used between the sample and the spectrograph to keep the beam from diverging. The lens closest to the spectrograph was adjusted to produce an image of the source on the slit. In some experiments a cylinder lens was used to concentrate the image in the focal plane of the spectrograph.

Magnetic rotation could be studied by placing crossed plane polarizers at A and B. To photograph the absorption of circularly polarized light a plane polarizer followed by a quarter wave plate was located at A. The $^3\pi_1 \leftarrow {}^1\Sigma^+$ transition in ICℓ appeared in two orders near the angle for which the grating was blazed. The red region (ninth order) was isolated with a high frequency cut-off filter, Corning No. 2412. The yellow (tenth order) was isolated by using a Corning No. 3482 in series with a Corning No. 4308 or a Kodak Wratten filter No. 56 or 66.

Results--Ne Source

Interactions between the magnetic field inducing the Zeeman effect and the Ne discharge limited the usefulness of this device as a radiation source. The oscillating nature of the magnetic field caused the intensity of the Ne emission to fluctuate. These fluctuations were not reproducible, which made it impossible to make a calibration of the light intensity taking them into account.

The magnetic rotation signal obtained using the Ne source was of such low intensity that the low signal to noise ratio became quite significant. The signal intensity was so low that it appeared to change during repetitions of the same experiment, due to fluctuations in the background noise from the photomultiplier and other detection circuitry. Because of this low signal level, uncrossing the polarizers even slightly

almost completely obliterated the magnetic rotation signal, and this made it impossible to determine any angular dependence.

In Table 3 the ICℓ features observed using the Ne source are listed, and compared to those obtained photographically in MRS by Eberhardt and in abosrption by Hulthén, et al. (48-50). The ICℓ features near the 5852 Å Ne line fell within one cm^{-1} of the Ne line. The nearness of these features to the Ne line, compared to two cm^{-1} at the 6266 Å Ne line, allowed a more expanded time scale to be used with the 5852 Å system, which yielded slightly better resolution.

The magnetic rotation and absorption data observed for ICℓ near both Ne lines are shown in Figure 25. The fluctuations in the Ne light intensity caused by the magnetic field are especially noticeable in the absorption near 6266 Å. The background variations have made it almost impossible to locate the ICℓ features. Absorption of circularly polarized light by ICℓ in a magnetic field of 8000 gauss in shown in Figure 26.

Results--Flash Source

A side-view type of flash lamp was first used with the Bausch and Lomb Model 11 spectrograph to test the feasibility of these experiments. Using a 60 micron entrance slit, absorption was photographically recorded with 10 flashes or less and MRS in 200 flashes. However, this spectrograph did not provide the resolution necessary for the observation of the Zeeman effect in ICℓ.

The Jarrell-Ash Ebert spectrograph was used to obtain the necessary resolution. With the entrance slit at 25 microns, it required at least 1000 flashes dissipating 80 joules apiece to produce a photographic record of absorption, when only the sample and lenses were in the optical path.

Table 3. Comparison of Photographic and Pulsed Data on ICl

Type of Data	Photographic[c] Experiment	Ne Source Experiment	Assignment[a]
MRS	17,082.190	17,082.18 ± .05	29 R 45
MRS	17,082.626	17,082.58 ± .10	28 P 38
MRS	17,082.843	17,082.88 ± .10	28 R 41
ABS	17,082.141	17,082.19 ± .05	29 R 45
ABS	17,082.613	17,082.67 ± .10	28 P 38
ABS	17,082.838	17,082.93 ± .10	28 R 41
MRS	15,952.064[b]	15,952.08 ± .15[b]	?
MRS	15,951.798[b]	15,951.76 ± .15[b]	14 P 52
MRS	15,951.473[b]	15,951.58 ± .15[b]	15 P 73
ABS	15,952.881	15,952.81 ± .10	14 R 57
ABS	15,951.867	15,951.83 ± .15	14 P 52
ABS	15,951.524	15,951.62 ± .15	15 P 73

[a]All transitions are from V" = 0. The first term is V', the second indicates the type of transition, and the third is J'.

[b]Not resolved.

[c]Magnetic Rotation Data from Reference (48), Absorption from (46) and (47).

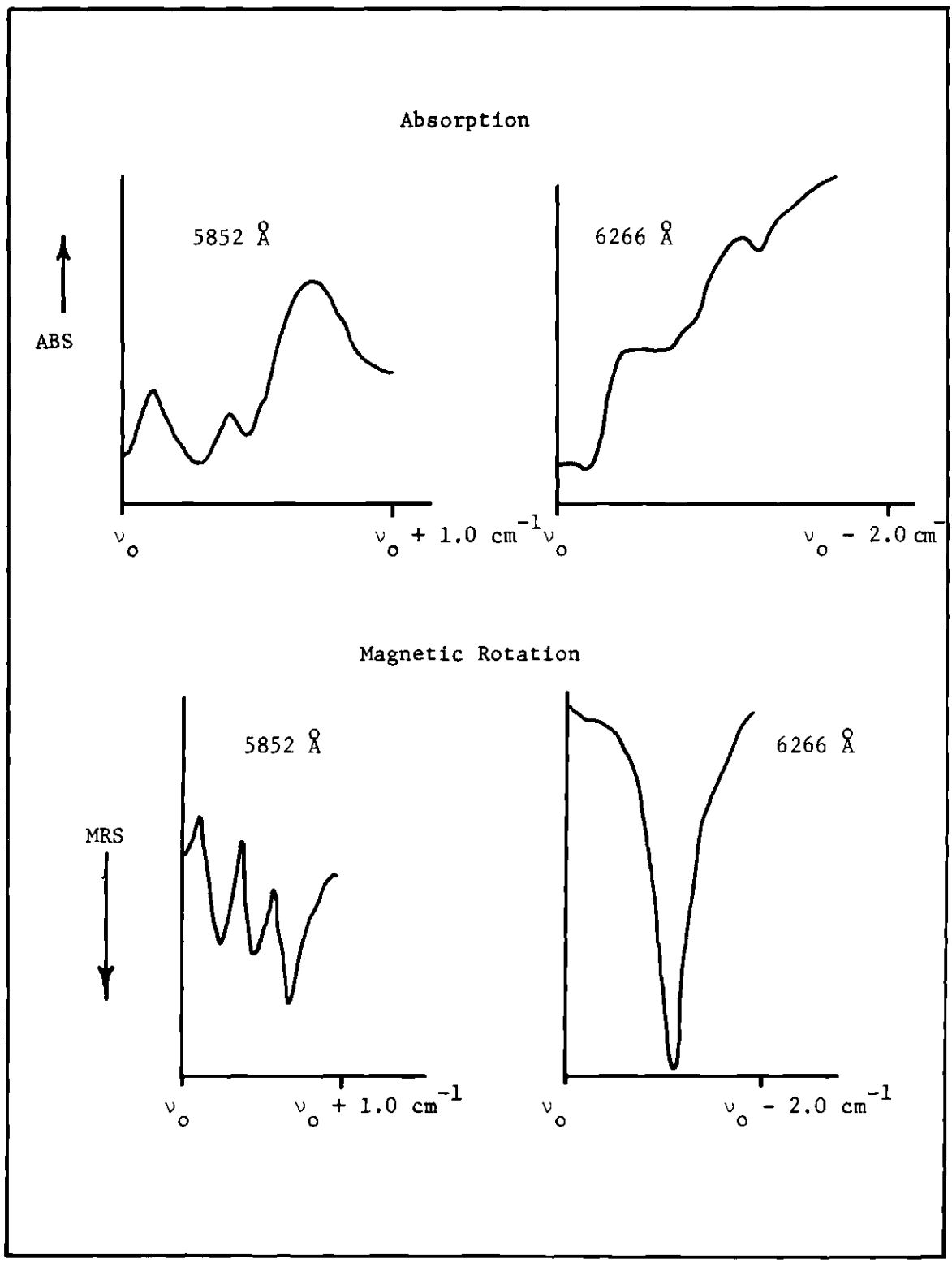

Fig. 25. Absorption and Magnetic Rotation from Ne Source Experiment.

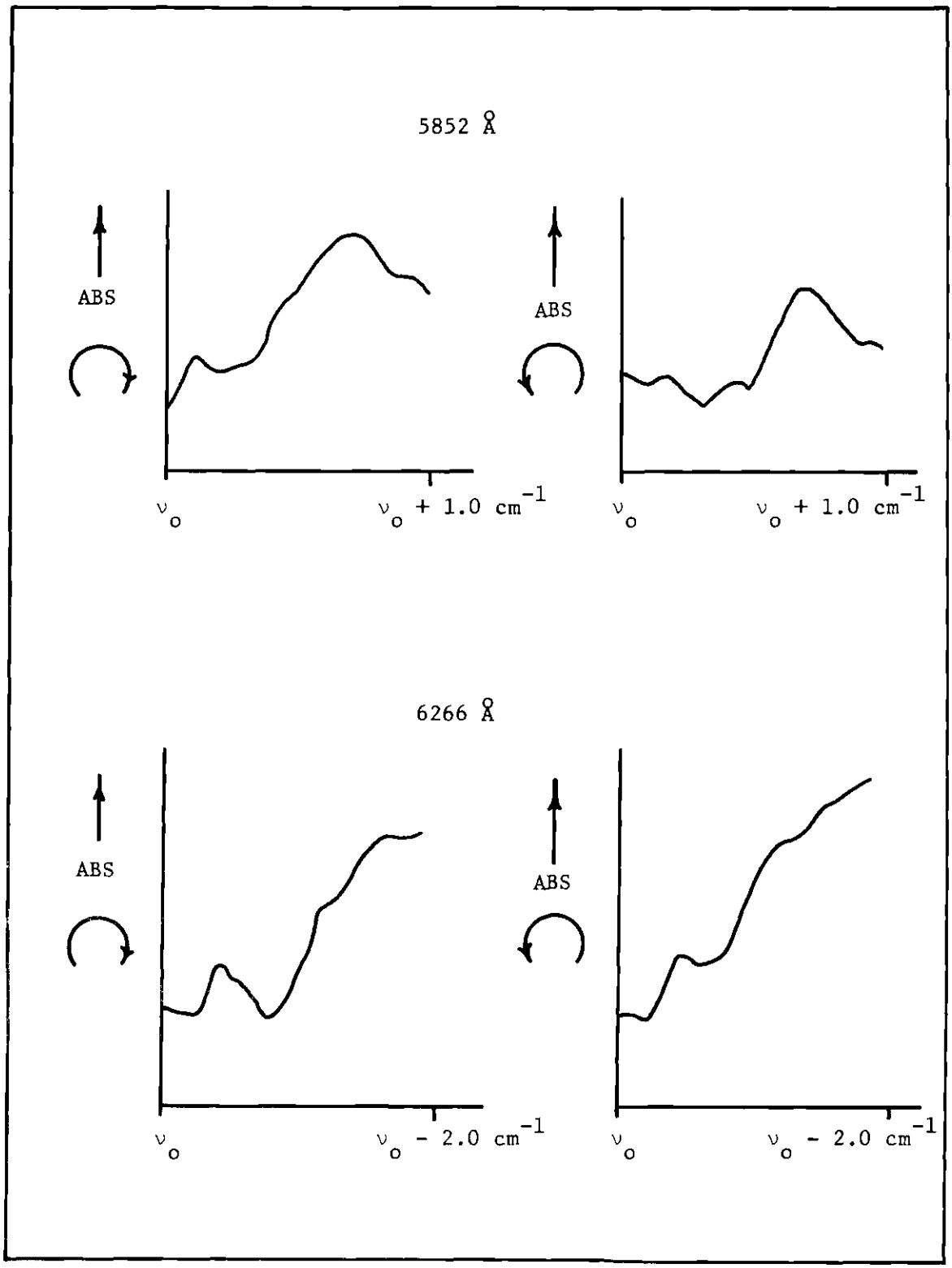

Fig. 26. Absorption of Circularly Polarized Light by ICℓ in a Pulsed Field of 8000 Gauss, Neon Swept Source.

The magnetic rotation phenomenon is at least two to three orders of magnitude less intense than absorption, so that the use of this type of flash lamp to study MRS was not feasible.

The end view type of flash tube was developed, but even with this type of lamp, 400-500 flashes were required to produce a simple absorption picture on a photographic plate or film. Using the end view tube, the ICℓ absorption in a field of 8000 gauss was measured for the V" = 1 → V' = 12,13 and V" = 0 → V' = 10 bands in the $^3\pi_1 \leftarrow {}^1\Sigma^+$ transition. Although no quantitative measurements were possible, a slight broadening of the features nearest the head of each band was observed. A plane polarizer and quarter wave plate were added to the optical system and an attempt was made to measure the absorption of polarized light for the V" = 1 → V' = 13 band, when the sample was in a field of 8000 gauss. At least 3000 flashes were required to make an adequate photographic record of the absorption. No difference between the absorption of right and left circular light was immediately apparent, and only when traces were made on a Leeds and Northrup recording densitometer did any difference appear. The absorption of left circular light at the band head extended slightly farther toward high frequencies than did the absorption of right circular light. No quantitative measurement was made on this data, and due to the low intensity of the absorption phenomena, no attempt was made to view the MRS with a flash lamp and the high resolution spectrograph.

Conclusions--Ne and Flash Sources

The experimental difficulties associated with the use of the Ne source eliminated the possibility of obtaining any really useful data on the ICℓ system. The magnetic rotation experiments did no more than confirm

the existence of the phenomena in the region of the spectrum observed. Absorption data was obtained, but better data is easily obtained photographically with a high resolution spectrograph. Absorption of circular light by the ICℓ sample in a magnetic field did indicate that a difference existed in the absorption of right and left circularly polarized light. From the data collected near 5852 Å, it appeared that the P transition absorbed more right than left circular light, but no conclusions about the R lines were immediately obvious. The information on the P line did agree with the data obtained later using phase sensitive detection.

The flash lamp, as a source of radiation, provided even less information than the Ne source. It was completely impossible to measure the high resolution MRS of ICℓ with this source. Simple absorption was possible, but the same data were collected much more readily using a D.C. arc lamp. Absorption in a magnetic field indicated that the Zeeman effect existed in ICℓ, but no quantitative measurements were possible. Absorption of circular light by ICℓ in a magnetic field indicated that the $V'' = 1 \rightarrow V' = 13$ band head, consisting of overlapping R lines, absorbed more left than right circularly polarized light at the high frequency end of the spectrum.

CHAPTER IV

EXPERIMENT--PHASE SENSITIVE DETECTION

Apparatus for Phase Sensitive Detection

The source of radiation in this experiment was the P.E.K. Labs, Inc. high pressure Xe arc lamp described previously. Filters were used to separate the two orders in which the ICℓ spectrum occurs.

The magnet used for this experiment was manufactured by Spectromagnetic Industries. It consisted of 12 coils 6 1/2 inches I.D., 19 inches O.D., and 1 3/4 inches thick separated by cooling coils. The assembly was 24 inches long and provided a nearly homogeneous field in a volume 6 inches in diameter and 20 inches long. It was powered by a Spectromagnetic Industries Model TU 250-30 power supply, and D.C. fields up to 2800 gauss were obtained.

The fixed polarizers were Glan prisms. The polarizer mounted on the chopper assembly was Baush and Lomb polarizing light film, Cat. No. 31-52-62-20. The quarter wave plates were prepared in this laboratory by peeling mica to the proper thickness.

The chopper is shown in Figure 25. The chopper consisted of a bearing-mounted brass tube, driven through O-ring belts by a Leeds and Northrup 1800 r.p.m. synchronous motor. The chopper rotated at approximately 14 cps. A beam chopper, polarizer, or quarter wave plate was attached to one end of the brass tube. The opposite end of the brass tube held a slotted cylinder of thin metal, which acted as a beam chopper to produce a reference signal at twice the fundamental frequency of the

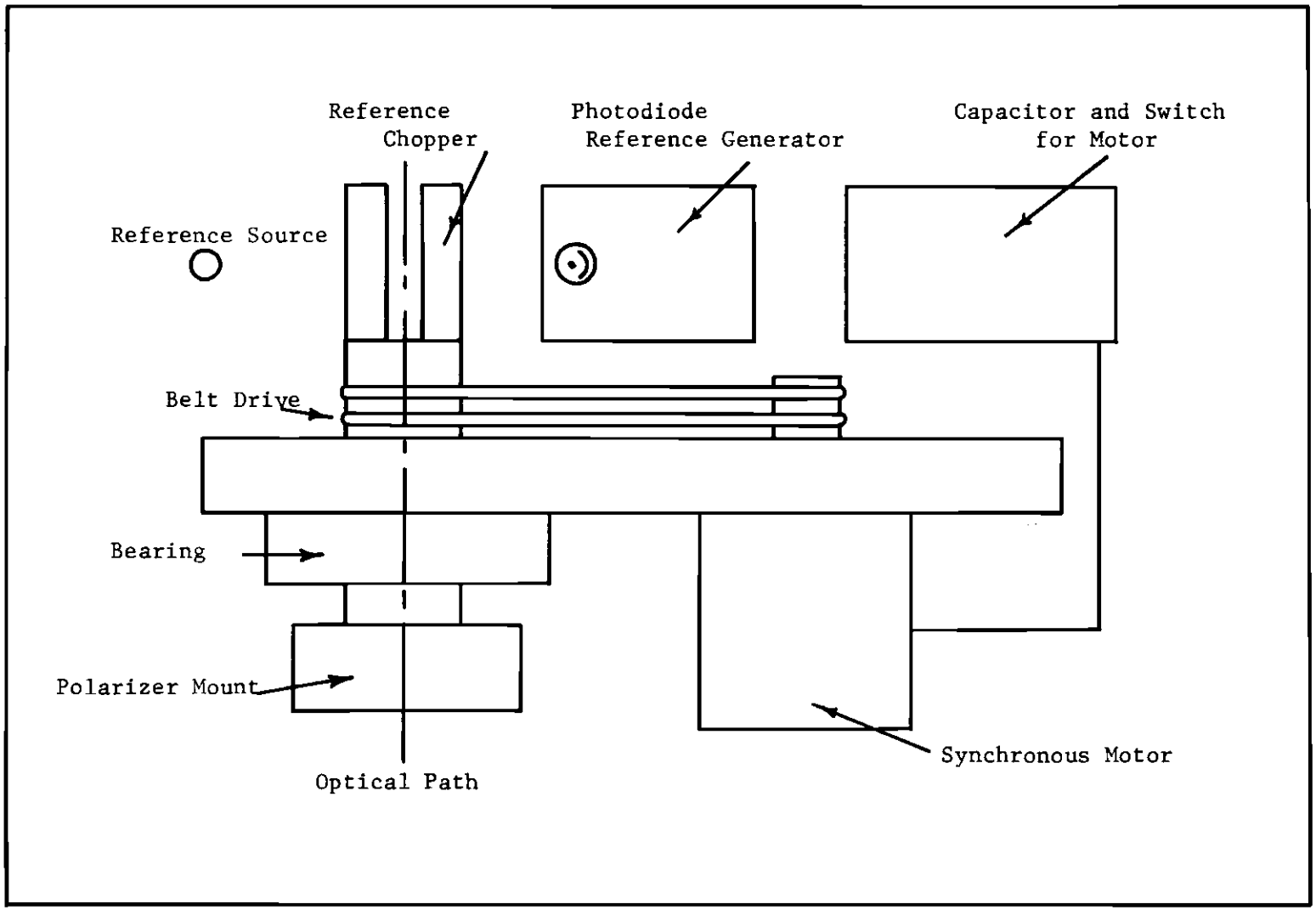

Fig. 27. Chopper Assembly, Top View.

chopper rotation. The reference signal was produced by breaking a beam of light falling onto a photodiode, and using the voltage across the diode as a signal. This voltage was fed directly into the lock-in amplifier, where it was filtered to produce a pure sine wave.

The spectrograph used was the Jarrell-Ash instrument described previously. A mechanical drive was provided to turn the grating at .01° per minute, or at .01° per 25 minutes using a pair of 5:1 planetary reducers. The detection was photoelectric, using the E.M.I. 9558-B photomultiplier tube. The cathode follower was removed from the housing for this experiment, and a voltage divider was constructed of wire wound resistors. The photomultiplier circuit is shown in Figure 26.

The anode of the photomultiplier was connected to an electrometer amplifier and filter; the circuitry is described in Figure 27. The filter was a low pass type of filter, with a cut-off point at 40 cps. In some experiments, additional amplification was obtained with a Keithley Model 610B electrometer, before the signal was fed to the lock-in amplifier. A Princeton Applied Research Model JB-5 lock-in amplifier was used. The output from the JB-5 was recorded on a Bausch and Lomb V.O.M. 5 chart recorder.

Phase Sensitive Detection Used to Measure Magnetic Effects in ICℓ

Phase sensitive detection was used to measure the Faraday rotation and circular dichroism in several vibrational bands of the ICℓ $^3\pi_1 \leftarrow {}^1\Sigma^+$ transition. The optical system used to measure the Faraday rotation is shown in Figure 28a. The orientation of the polarizers relative to the coordinate system is illustrated in Figure 28b.

The intensity of the radiation passed by the rotating polarizer was derived earlier and can be expressed as

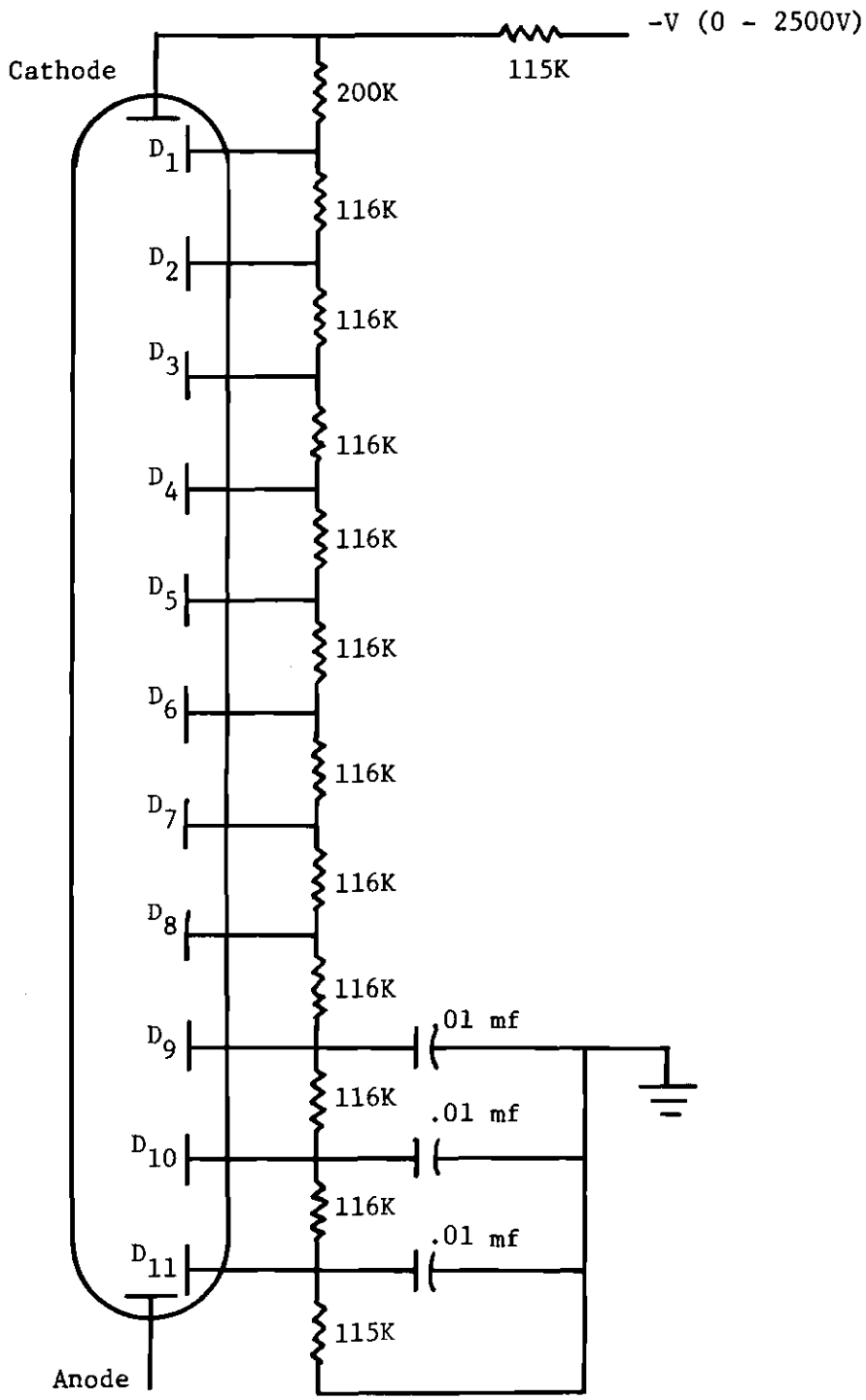

Fig. 28. E.M.I. 9558B Photomultiplier Circuit.

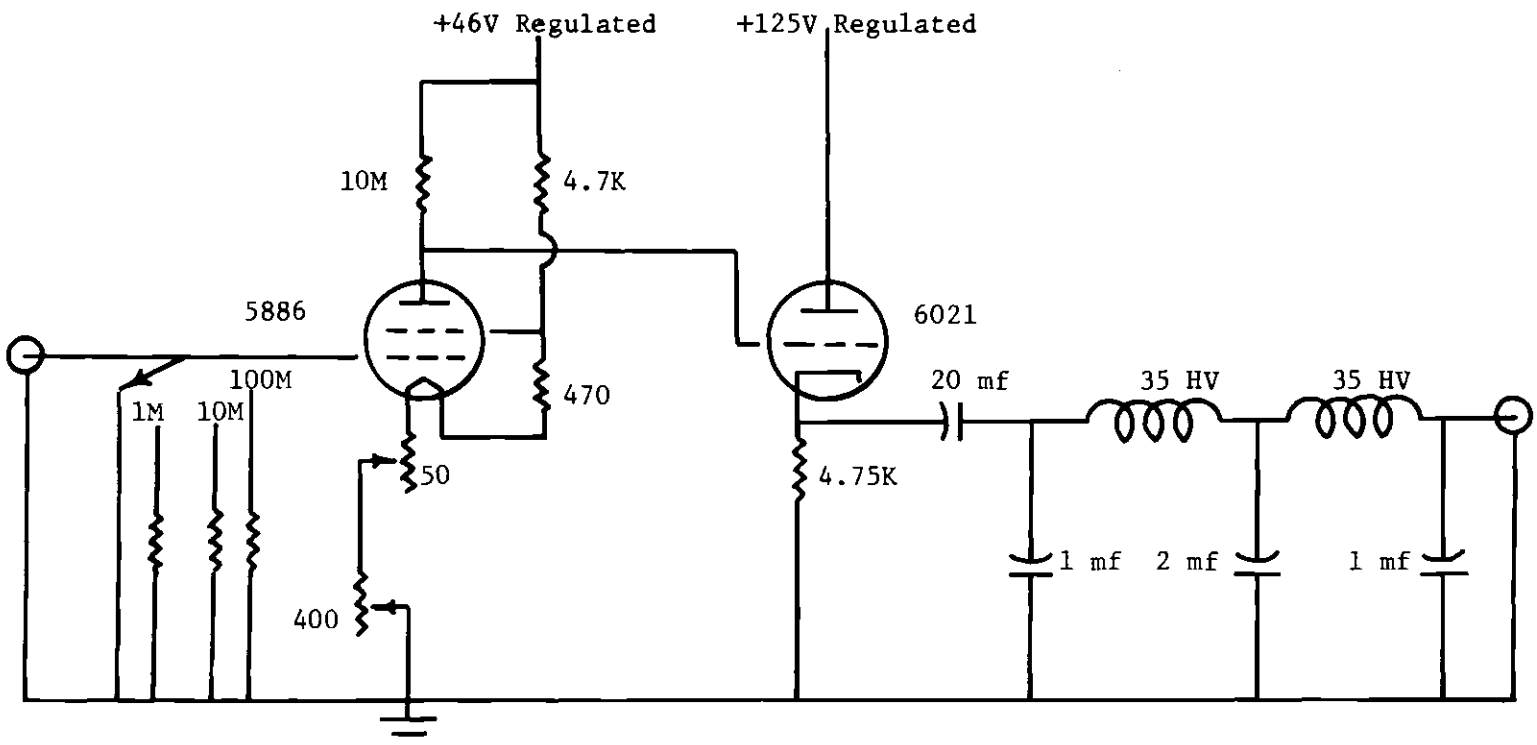

Fig. 29. Electrometer Amplifier and Filter Circuit.

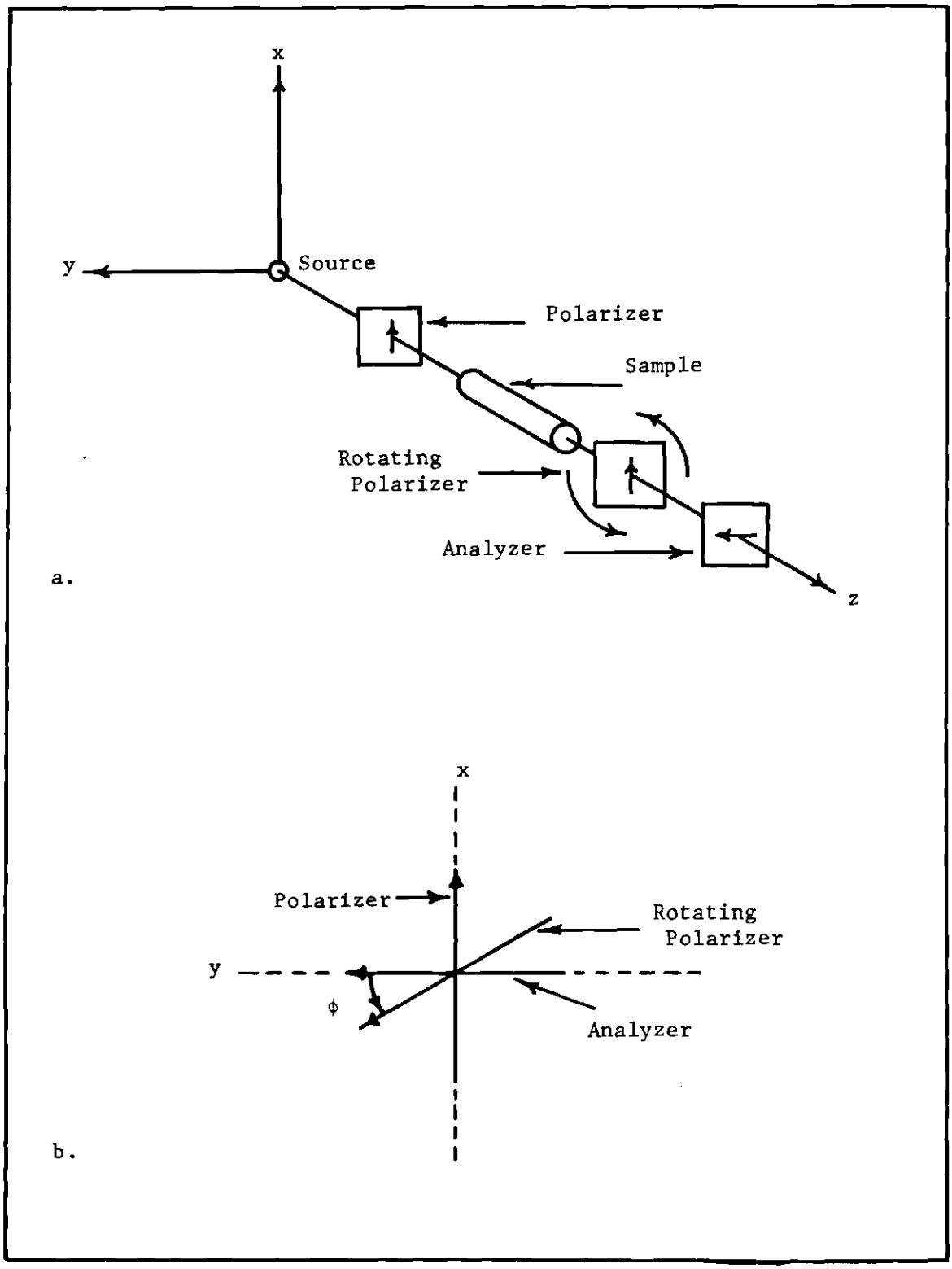

Fig. 30. Optical System and Coordinates for Angle of Rotation Studies with Phase Sensitive Detection.

$$I = \frac{E^2}{2}\left\{\left(\frac{e^{-\alpha_L \ell} + e^{-\alpha_R \ell}}{2}\right) - e^{-\frac{(\alpha_L+\alpha_R)\ell}{2}} \cos 2\left[\phi + \frac{\pi \ell}{\lambda_o}(n_L - n_R)\right]\right\} \tag{44}$$

If the electric vector passed by the analyzer is denoted E_A, and that passed by the rotating polarizer denoted E_p, then

$$E_A = E_p \cos \phi \tag{45}$$

and the radiation intensity passed by the analyzer will be

$$E_A^2 = E_p^2 \cos^2 \phi \tag{46}$$

Substituting from equation (44) yields

$$\langle E_A^2 \rangle = \frac{E^2}{2}\left\{\left(\frac{e^{-\alpha_L \ell} + e^{-\alpha_R \ell}}{2}\right)\cos^2\phi - e^{-\left(\frac{\alpha_L+\alpha_R}{2}\right)\ell} \cos^2\phi \cos 2\left[\phi + \frac{\pi \ell}{\lambda_o}(n_L - n_R)\right]\right\} \tag{47}$$

Substituting

$$\beta = \frac{\pi \ell}{\lambda_o}(n_R - n_L) \tag{48}$$

in equation (47)

$$\langle E_A^2 \rangle = \frac{E^2}{2}\left\{\left(\frac{e^{-\alpha_L \ell} + e^{-\alpha_R \ell}}{2}\right)\cos^2\phi - e^{-\left(\frac{\alpha_L+\alpha_R}{2}\right)\ell} \cos^2\phi \cos 2\left[\phi - \beta\right]\right\} \tag{49}$$

Expanding cos $2(\phi - \beta)$ yields

$$\langle E_A^2 \rangle = \frac{E^2}{2}\left\{\left[\left(\frac{e^{-\alpha_L \ell} + e^{-\alpha_R \ell}}{2}\right) - e^{-\left(\frac{\alpha_L+\alpha_R}{2}\right)\ell}\right]\cos^2\phi \right.$$
$$\left. + e^{-\left(\frac{\alpha_L+\alpha_R}{2}\right)\ell}\left[\sin^2(2\phi-\beta) + \sin^2\beta - 2\sin\beta\sin(2\phi-\beta)\right]\right\} \qquad (50)$$

and collecting the terms depending on (2ϕ) gives

$$\langle E_A^2 \rangle_{2\phi} = \frac{E^2}{2}\left\{\left(\frac{e^{-\left(\frac{\alpha_L}{2}\right)\ell} - e^{-\left(\frac{\alpha_R}{2}\right)\ell}}{2}\right)^2 \cos 2\phi - e^{-\left(\frac{\alpha_L+\alpha_R}{2}\right)\ell}\sin\beta\sin(2\phi-\beta)\right\} \qquad (51)$$

The first term on the right side of equation (51) depends on the circular dichroism, and if this is very small

$$\therefore \langle E_A^2 \rangle_{2\phi} = -\frac{E^2}{2} e^{-\left(\frac{\alpha_R+\alpha_L}{2}\right)\ell}\sin\beta\sin(2\phi-\beta) \qquad (52)$$

Equation (52) gives that part of the intensity which depends on (2ϕ), in terms of β, the Faraday angle. The signal for $\beta > 0$ will be 180° out of phase with a signal produced when $\beta < 0$. If a phase sensitive detector is tuned to (2ϕ), which is twice the rotational frequency of the polarizer, an arbitrary base line can be established for $\beta = 0$. Deviations of β from zero will cause the output signal to deflect from the base line, and the sign of the deflection will depend on the sign of β.

Recording the light intensity passed by the optical system described in Figure 28 as measured by a phase sensitive detector tuned to twice the rotational frequency of the polarizer will give a measure of the Faraday

angle, $\frac{\pi \ell}{\lambda_o} (n_R - n_L)$. The system may be calibrated by rotating the analyzer relative to the polarizer.

For the measurement of circular dichroism by phase sensitive detection, the optical system shown in Figure 29 was used. The rotating quarter wave plate has four apertures, and their location relative to the retardation axis is shown in Figure 31. When the rotating plate is properly oriented, the light passing through it and into the sample is alternately right and left circularly polarized. The fixed quarter wave plate and analyzer can be oriented relative to each other so that they will pass right and left circular light in any ratio. They are usually oriented to pass equal amounts of right and left circularly polarized light, unless a calibration is necessary.

The light intensity passed by the system in Figure 29 will be proportional to the difference between the intensities of right and left circular light passed by the sample, and will have a frequency twice the rotational frequency of the quarter wave plate. The signal observed by a properly tuned phase sensitive detector will be proportional to $(I_R - I_L) \sin (2\phi + \gamma)$, where I refers to intensity, ϕ the rotation of the quarter wave plate, and γ is an arbitrary phase factor dependent on the instrumentation. The phase of this signal is seen to change by 180^o when the relative magnitudes of I_R and I_L change. If the lock-in amplifier forms on its output an arbitrary base line for $I_R = I_L$, deflections will occur when $I_R \neq I_L$, and the sign of the deflection will depend on the relative magnitudes of I_R and I_L.

The electric vectors of the right and left circular light will be of equal magnitude, E, before the light enters the sample. After traversing a path length ℓ through the sample, the magnitudes of the electric

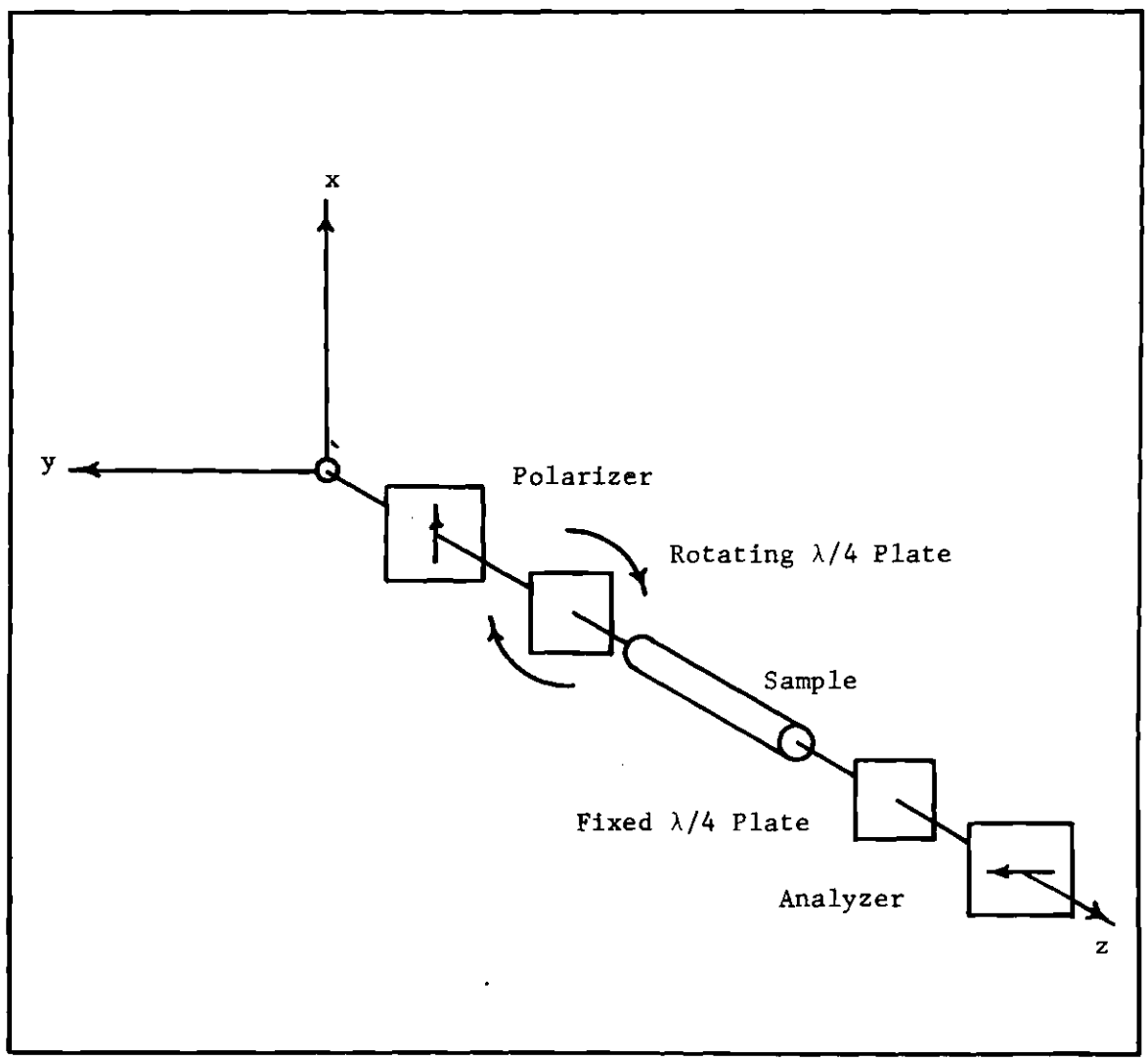

Fig. 31. Optical System and Coordinates for Circular Dichroism Studies with Phase Sensitive Detection.

vectors can be expressed as $E\, e^{\frac{-\alpha_L \ell}{2}}$ and $E\, e^{\frac{-\alpha_R \ell}{2}}$, for left and right circular light, respectively. Therefore the difference in intensities for right and left circular light will be

$$I_R - I_L = E^2 \{e^{-\alpha_R \ell} - e^{-\alpha_L \ell}\} \quad , \tag{53}$$

or approximately,

$$I_R - I_L \simeq E^2 \ell(\alpha_L - \alpha_R) \quad . \tag{54}$$

Thus the intensity of the light passed by the optical system in Figure 29 and measured by a phase sensitive detection system tuned to the proper frequency will be proportional to the circular dichroism, or $(\alpha_R - \alpha_L)$.

A block diagram of the phase sensitive detection apparatus is shown in Figure 30. To measure the angle of rotation a polarizer mounted on the chopper is located at A. To measure circular dichroism a fixed quarter wave plate is placed at A, and the chopper carrying the quarter wave plate shown in Figure 31 is placed at B.

To tune the apparatus when measuring the angle of rotation, a signal can be generated by rotating the analyzer. A test signal can be obtained when measuring circular dichroism by changing the relative orientation of the analyzer and fixed quarter wave plate.

The ICℓ spectrum was scanned by rotating the grating in the spectrograph, and features measured with the phase sensitive detector were identified by comparison with the MRS of ICℓ, which was obtained photometrically and at the same scanning rate.

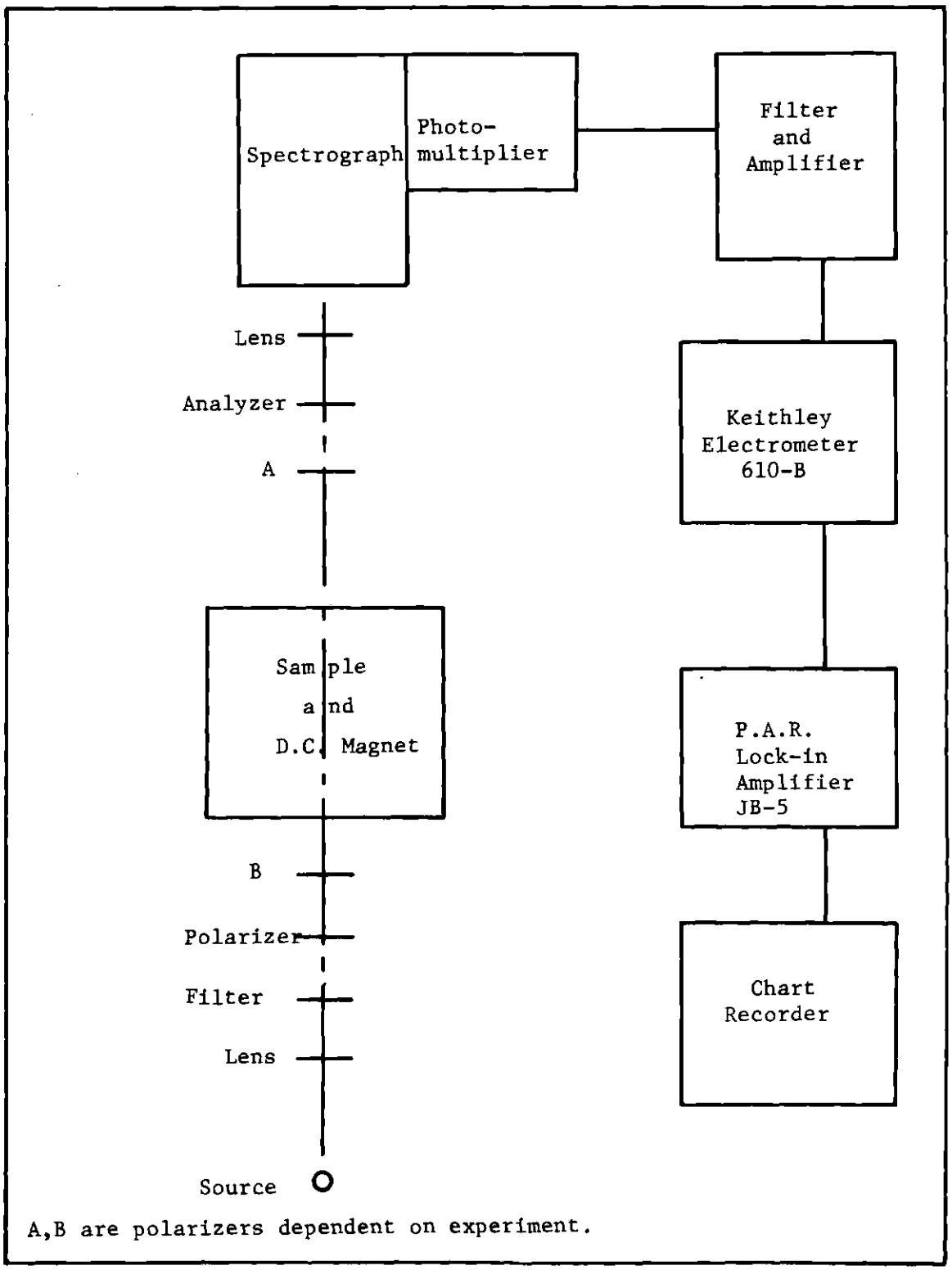

Fig. 32. Apparatus for Phase Sensitive Detection.

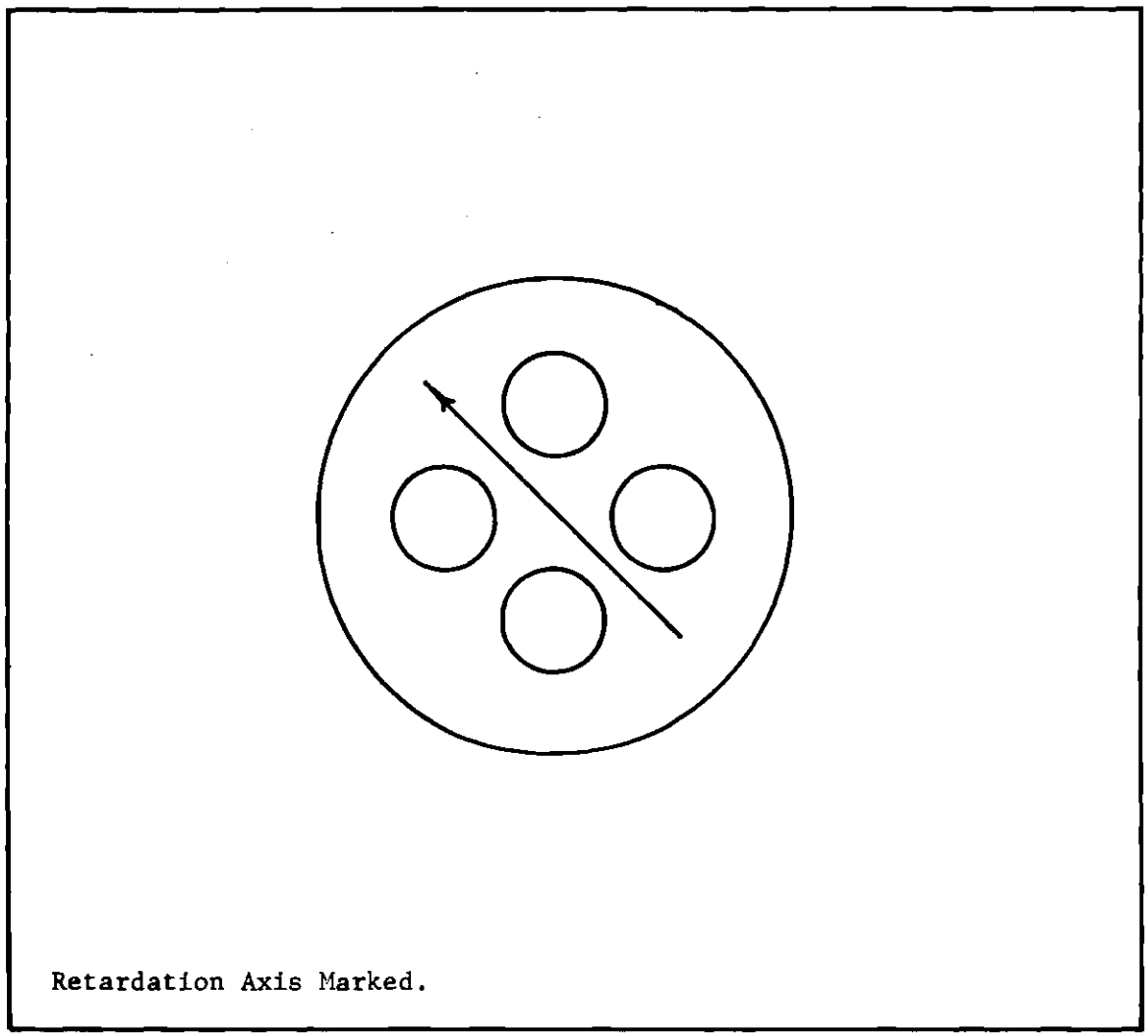

Fig. 33. Rotating $\lambda/4$ Plate.

The entrance slit of the spectrograph was 78 microns wide and the exit slit 32 microns. This provided a trapezoidal slit function, with a spectral half width of approximately .120 cm^{-1}.

Results--Phase Sensitive Detection

It was possible to measure, at least semi-quantitatively, the Faraday rotation and circular dichroism exhibited by some of the easily isolated features in the $^3\pi_1 \leftarrow {}^1\Sigma^+$ transition of ICℓ. The circular dichroism of the ICℓ features near 5852 Å, which were observed with the Ne source, is shown in Figure 34. The three peaks which appear in this Figure correspond to the three ICℓ lines studied previously.

Faraday rotation and circular dichroism in four vibrational bands of ICℓ were recorded. In each of the bands observed, it was impossible to clearly resolve the closely spaced features near the band head. The bands studied were the V'' = 0 → V' = 22,28 and V'' = 1 → V' = 12,13 systems. Away from the head of the band, the P and R lines of the V' = 22 band almost coincided. The spacing between adjacent P and R lines was somewhat greater in the V' = 28,12 systems, and the lines were almost equally spaced in the V' = 13 band. A reproduction of the data obtained for an adjacent P and R line in each band is shown in Figure 35, and it can be seen that the shape of the lines remains the same for all of the bands studied. It is obvious that these data are not noise free; the presence of this noise, made necessary by the low signal level, precluded the possibility of any fully quantitative measurements. The experimental data for a large portion of the V'' = 1 → V' = 12 band are shown in Figures 38 and 39, where they are compared with calculations based on the theory developed in this thesis.

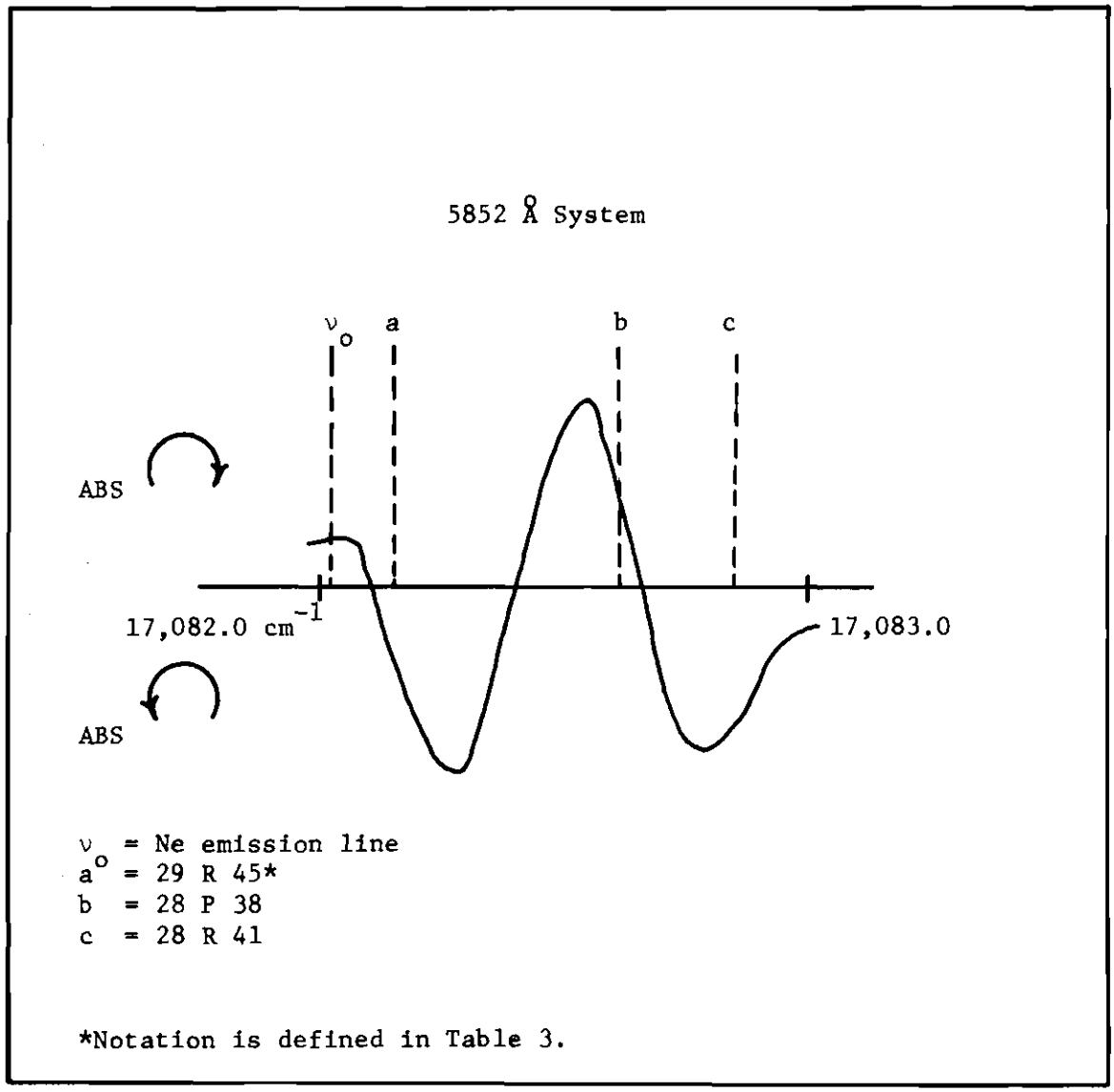

Fig. 34. Circular Dichroism in ICℓ Near 5852 Å in a D.C. Field of 2500 Gauss, Measured with Phase Sensitive Detection System.

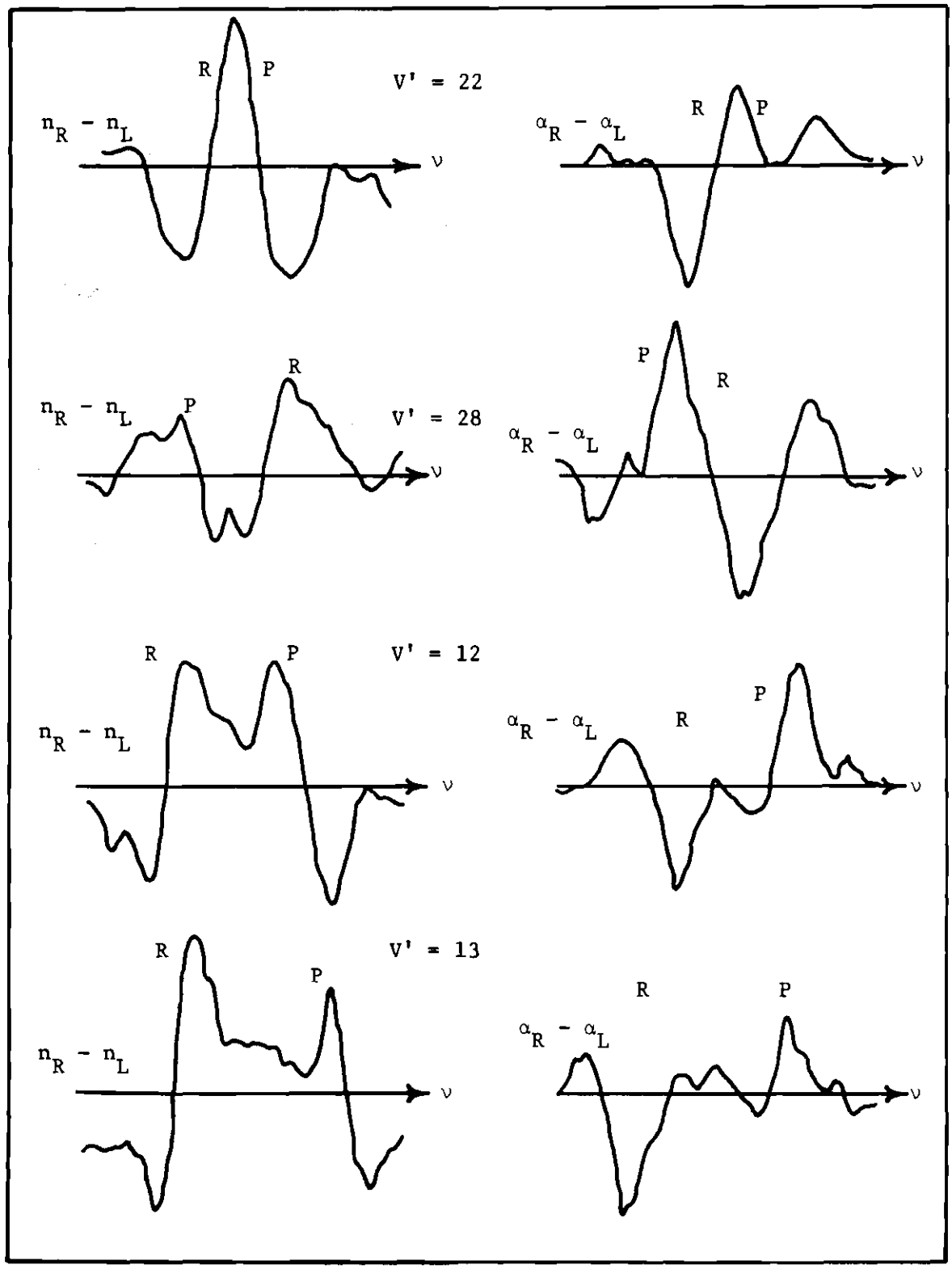

Fig. 35. P and R Type Transitions in Four Vibrational Bands of ICℓ in a Field of 2500 Gauss.

CHAPTER V

CONCLUSIONS--COMPARISON OF EXPERIMENT WITH THEORY

The data obtained using phase sensitive detection were used to test the theory developed in this thesis. The ICℓ transition under study has been designated a $^3\pi_1 \leftarrow {}^1\Sigma^+$ transition, which implies Hund's case (a) coupling. For heavy dihalide molecules, the coupling is believed to be case (c), but since this leaves some doubt regarding the magnitude of the magnetic moment along the internuclear axis the simpler case (a) approximation was used. A vector model of Hund's case (a) coupling using Herzberg's notation is shown in Figure 36. (55). In the computations a magnetic moment of one Bohr magneton along the internuclear axis was assumed. The magnetic field intensity was 2500 gauss. To compensate for the slit function, a half width of .200 cm^{-1} was used in the calculations. Since it was not possible to make quantitative measurements of the Faraday rotation and circular dichroism, it was not necessary to make quantitative calculations. The formulas were simplified by removing all of the multiplicative terms which were constant, or only slightly varying functions of the frequency. The matrix elements were calculated using symmetric rotor wave functions. The actual formulas used to calculate P, Q, and R type transitions are shown in the Appendix.

The three ICℓ features near 5852 Å, which were studied with the Ne source, are shown in Figure 37. The experimental data are compared with the calculated phenomena. In Figures 38 and 39 the experimental data are compared with calculations on the V" = 1 → V' = 12 band. A densitometer trace of the MRS of the same band is shown in Figure 40.

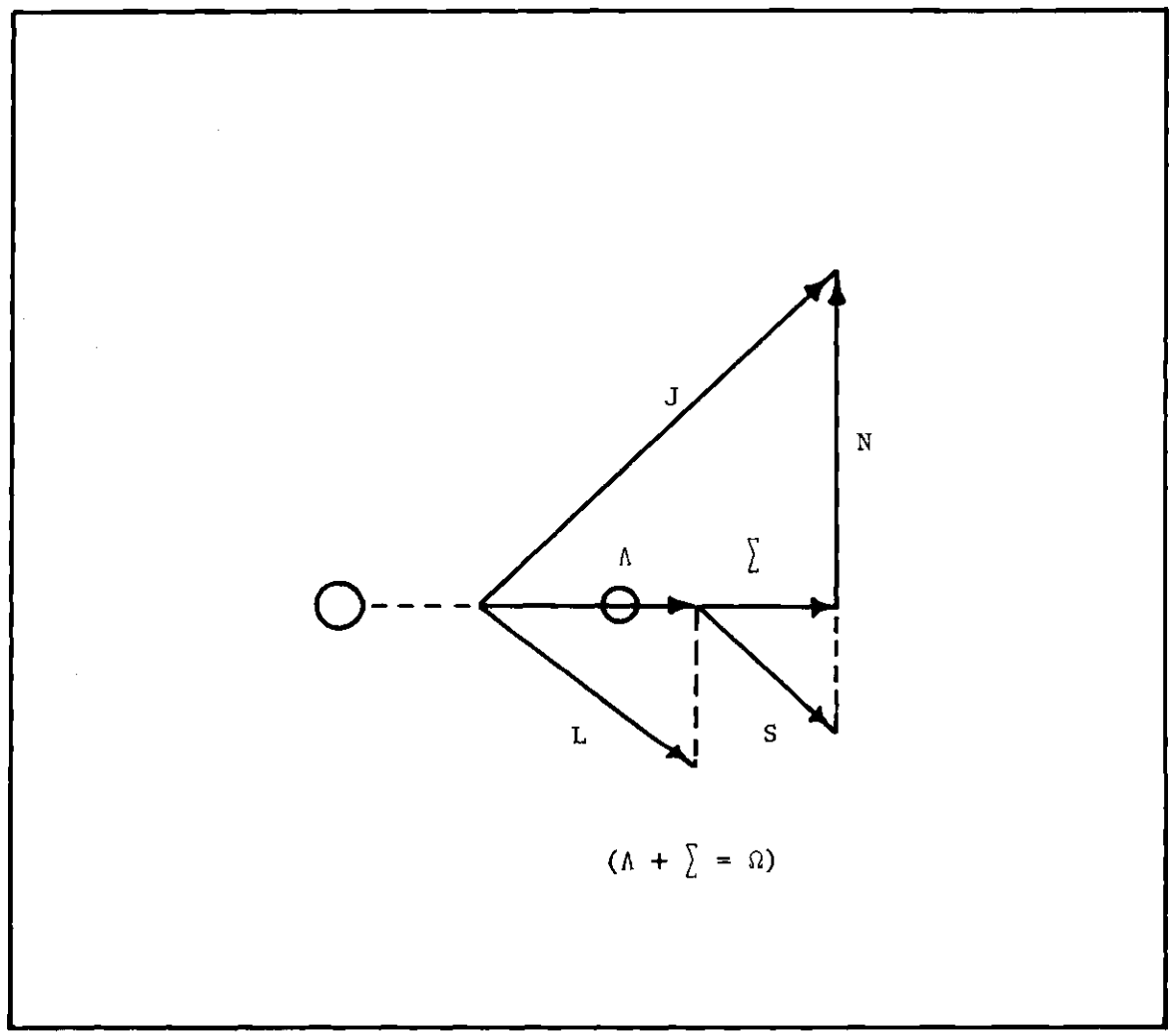

Fig. 36. Hund's Case (a) Coupling in a Diatomic Molecule.

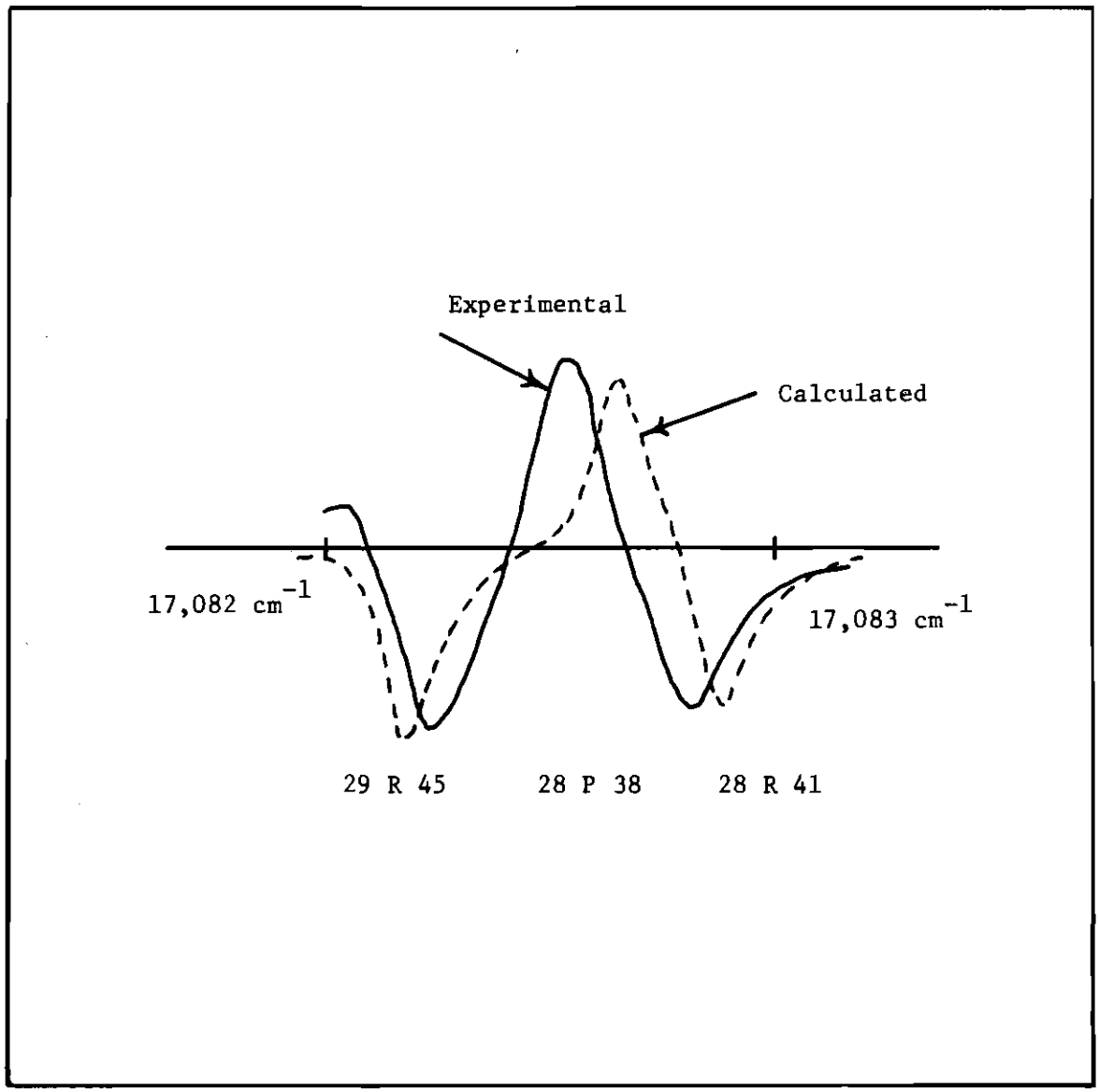

Fig. 37. Calculated and Experimental Data for ICℓ Lines Near 5852 Å.

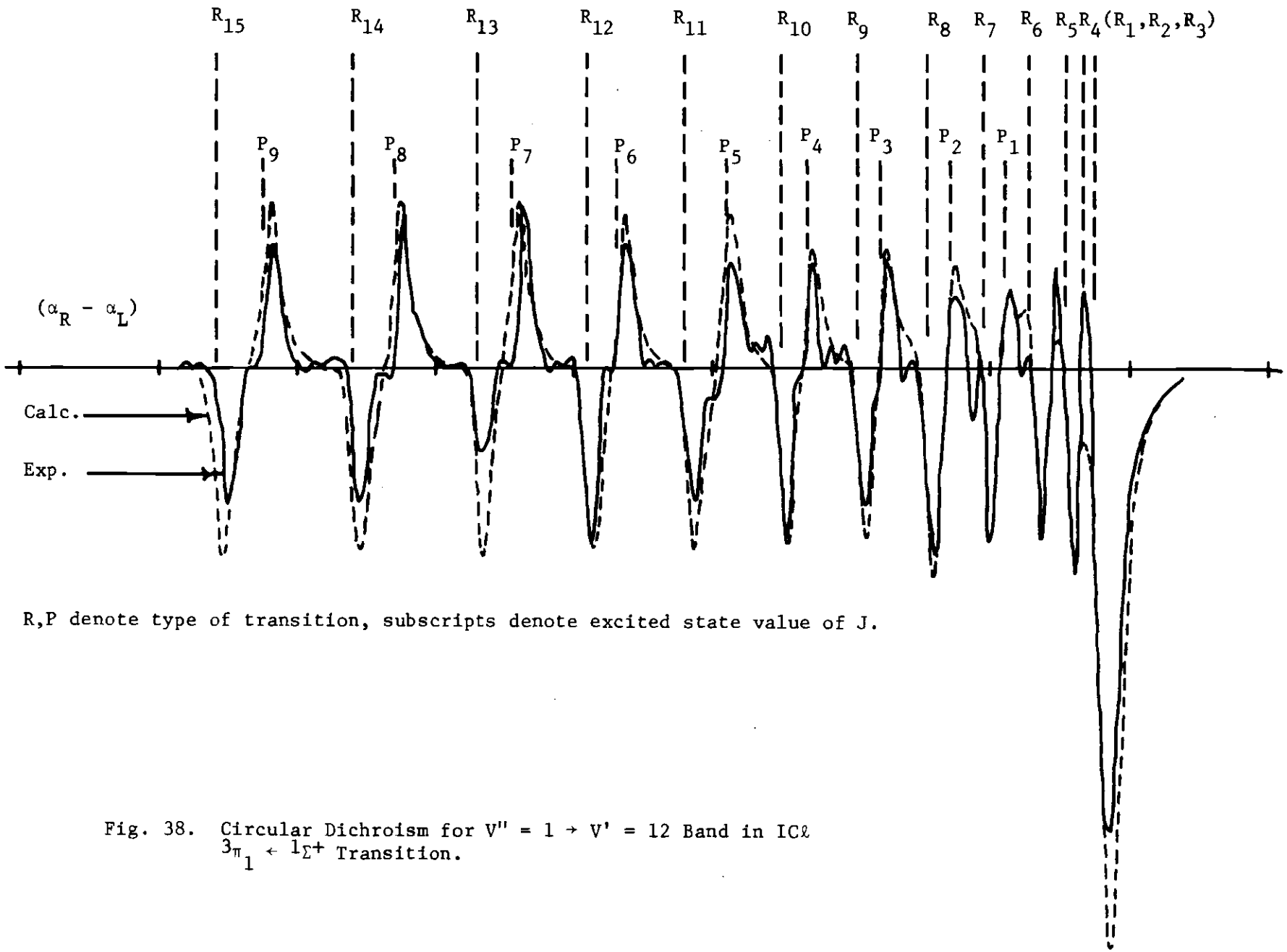

R,P denote type of transition, subscripts denote excited state value of J.

Fig. 38. Circular Dichroism for V'' = 1 → V' = 12 Band in ICℓ $^3\pi_1 \leftarrow {}^1\Sigma^+$ Transition.

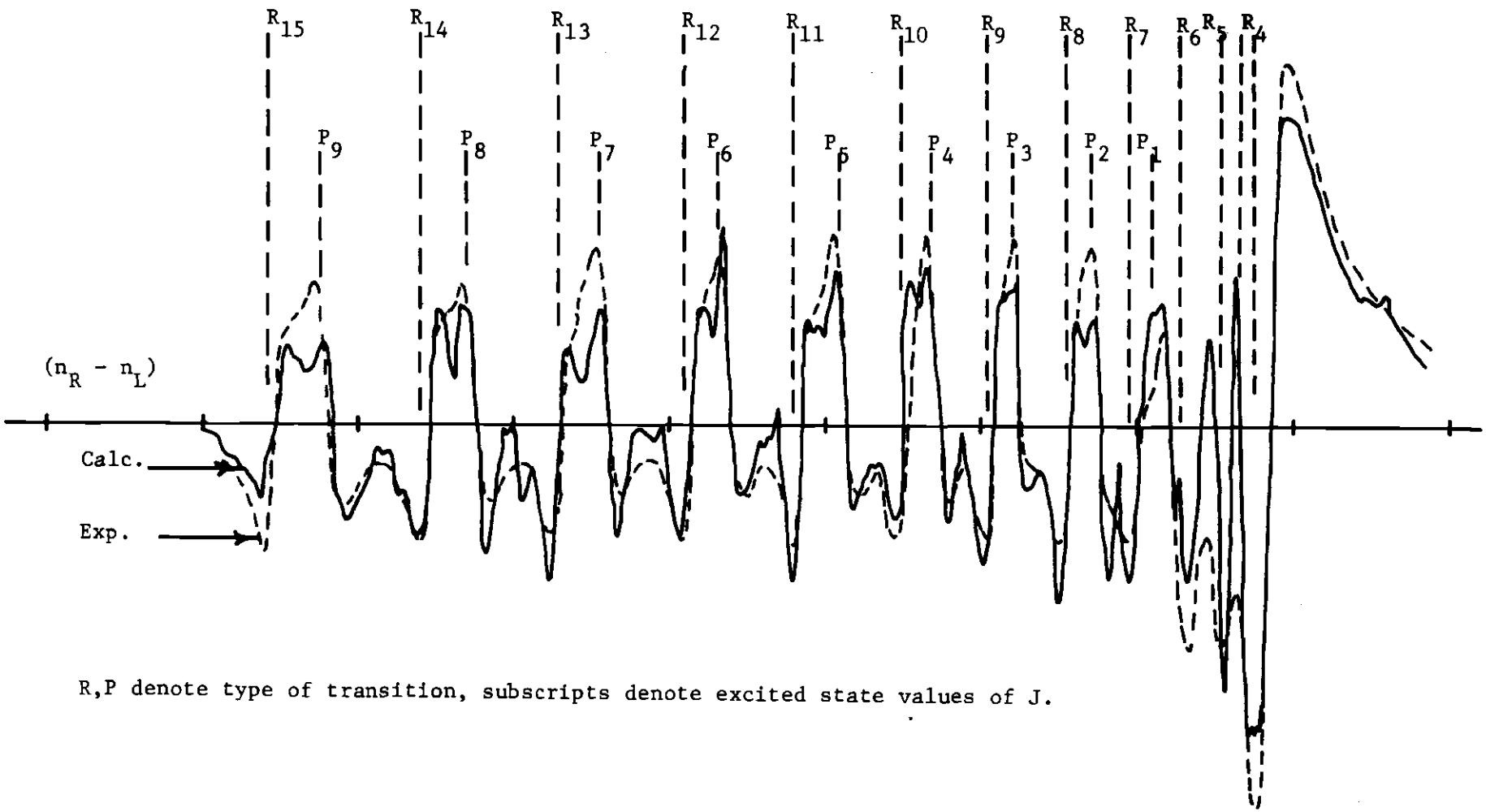

R,P denote type of transition, subscripts denote excited state values of J.

Fig. 39. Angle of Rotation for V" = 1 → V' = 12 Band in ICℓ $^3\pi_1 \leftarrow {}^1\Sigma^+$ Transition.

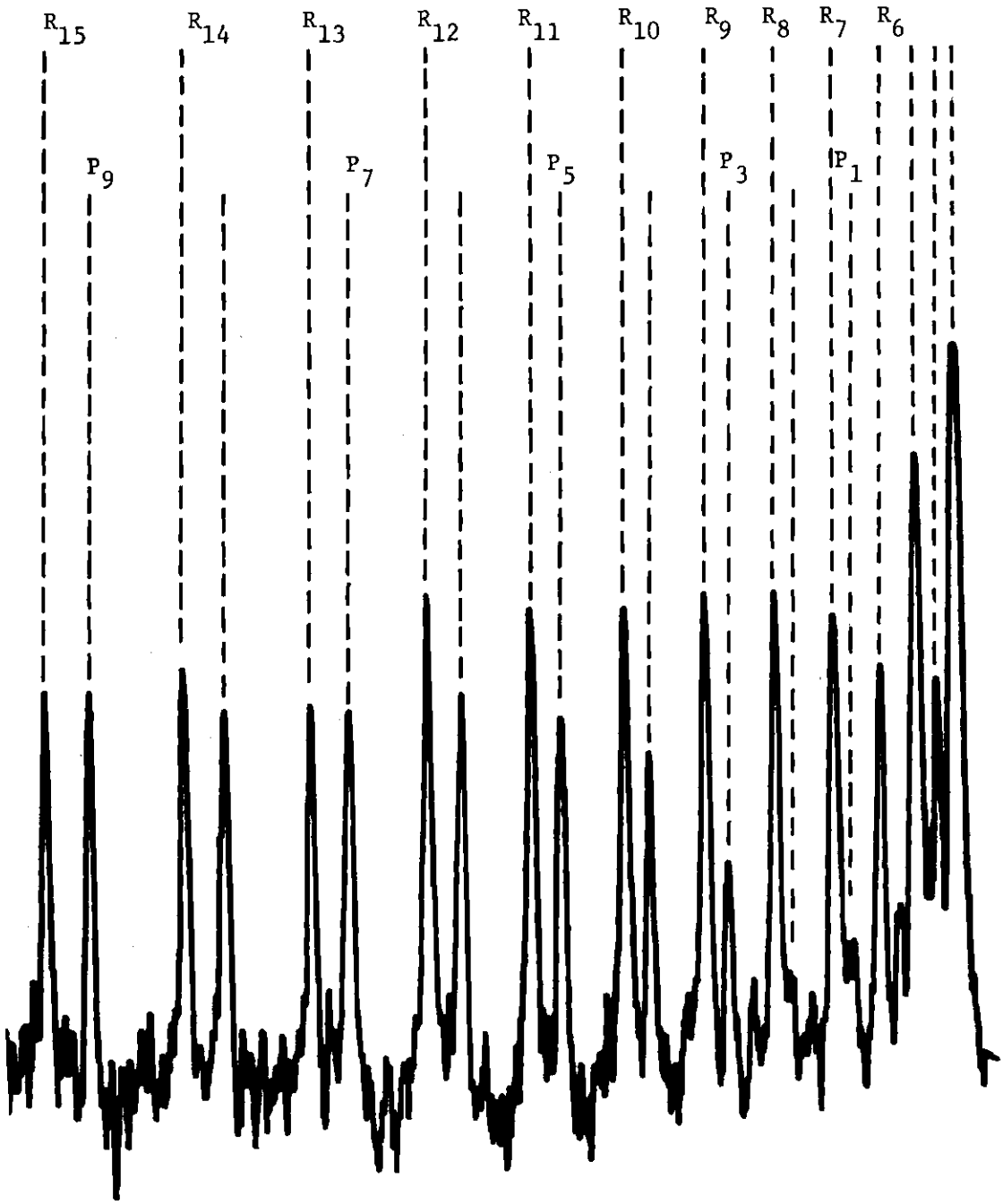

Fig. 40. Densitometer Trace of MRS of ICℓ V'' = 1 → V' = 12 Band in a Field of 2500 Gauss.

From the illustrations of the V' = 12 band, it is obvious that the experimental resolution was greater than that built into the calculations. This may be at least partially accounted for by the fact that a Lorentzian line was used in the calculations instead of the trapezoidal slit function. The broadening which occurred in the calculated features also accounted for the principal differences between the calculated and experimental data, especially near the band heat where much overlapping of features took place. The calculations could have been adjusted to fit the experimental data more closely by using a smaller line half width in the computations.

It was of special interest to observe the magnetic effects in the V'' = 0 → V' = 28 band. Hulthén found that excited state vibrational levels with V' $\geq$ 28 exhibited peculiar lambda doubling. In spite of the lambda doubling phenomenon, the magnetic effects measured in the V' = 28 band were consistent with the data collected for other bands. This indicates that the lambda doubling peculiarities must evolve from some cause which does not include a radical change in the coupling scheme of the ICℓ molecule.

It is of some importance to consider the possible effects of self-absorption on the measurement of Faraday rotation. The line width of importance in the Faraday phenomenon was controlled by the slit function, and hence had a half width of about .100 cm^{-1}. The absorption line width in the ICℓ sample may be approximated by the Doppler width, which is .015 cm^{-1}. Absorption experiments on the ICℓ sample indicated that the actual line half width was close to the Doppler approximation. If the absorption by lines with a half width of .015 cm^{-1} is taken into account when considering a phenomenon with a line width of .100 cm^{-1},

very little effect would be expected to occur. Only by broadening the absorption line width appreciably would the effect become noticeable.

When making photographic recordings of the magnetic rotation spectrum in ICℓ, an attempt was made to absorb the light passed by the analyzer with a second ICℓ sample placed in the optical path. Little effect was noticeable with the absorbing sample at room temperature, and only after heating the sample did absorption take place to any great extent. At 200° C, it was possible to almost completely absorb the MRS signal. The lack of any observed effect at room temperature was attributed to the fact that the magnetic rotation signal does not occur at the zero field line frequency, but rather on both sides of it. Only by broadening the lines in the absorption sample, which was not in a magnetic field, was it possible to absorb the MRS signal.

All of the discussions in this thesis have neglected anything which has a magnetic field dependence higher than first order. Since even the first order effects are in general quite small, it is not unreasonable to assume that higher order terms may be safely neglected. An attempt was made to experimentally determine the magnetic field dependence of the Faraday rotation and circular dichroism, by varying the magnetic field intensity. Measurements made on the $V'' = 1 \rightarrow V' = 12$ band indicated a first order dependence on the field intensity.

A possible manifestation of second order effects is the appearance of $\Delta J = \pm 2$ transitions. These will become allowed under the influence of the mixing of states caused by a magnetic field, but the transition intensity will depend on the magnetic field to the second order. An attempt was made to assign some unexplained lines appearing in the MRS

near the $V'' = 0 \rightarrow V' = 28$ band to such $\Delta J = \pm 2$ transitions, but without success.

It appears that the theory developed in this thesis, given the Hund's case (a) model of ICℓ, is adequate to explain the Faraday rotation and circular dichroism as they were observed. The data used to test the theory were fairly extensive, and it is not apparent whether or not the theory of magnetic rotation used by Carroll could explain the data. It is certain that Serber's work, based only on the "a" terms, would not explain the data satisfactorily. Carroll considered "b" terms in his calculations, but they were not exactly the same as those which appear in the formulas developed in this thesis. Although both Serber and Carroll claimed to explain the data available to them, these data were not very extensive, and did not provide an adequate test of their theories. In Figure 41 the shape of the Faraday rotation for a P and an R line are shown as computed by Serber, Carroll, and the formulas presented in this thesis. A damping function was applied to Serber's formulas to allow their application at the line origin.

The differences are obvious, and although Carroll's approximation does not compare unfavorably with that presented in this thesis, Serber's is quite different. It is apparent that only the limited amount of data available to him allowed his apparently successful explanation.

Q lines have received little previous attention in this thesis. The intensity of the Q lines, as they appear in Faraday rotation and circular dichroism, falls off rapidly away from the band origin, and only the first few are important. The shape of the first two Q lines in a vibrational band of the ICℓ molecule are shown in Figure 41. The first three Q lines were included in the calculations shown in Figures 38 and 39.

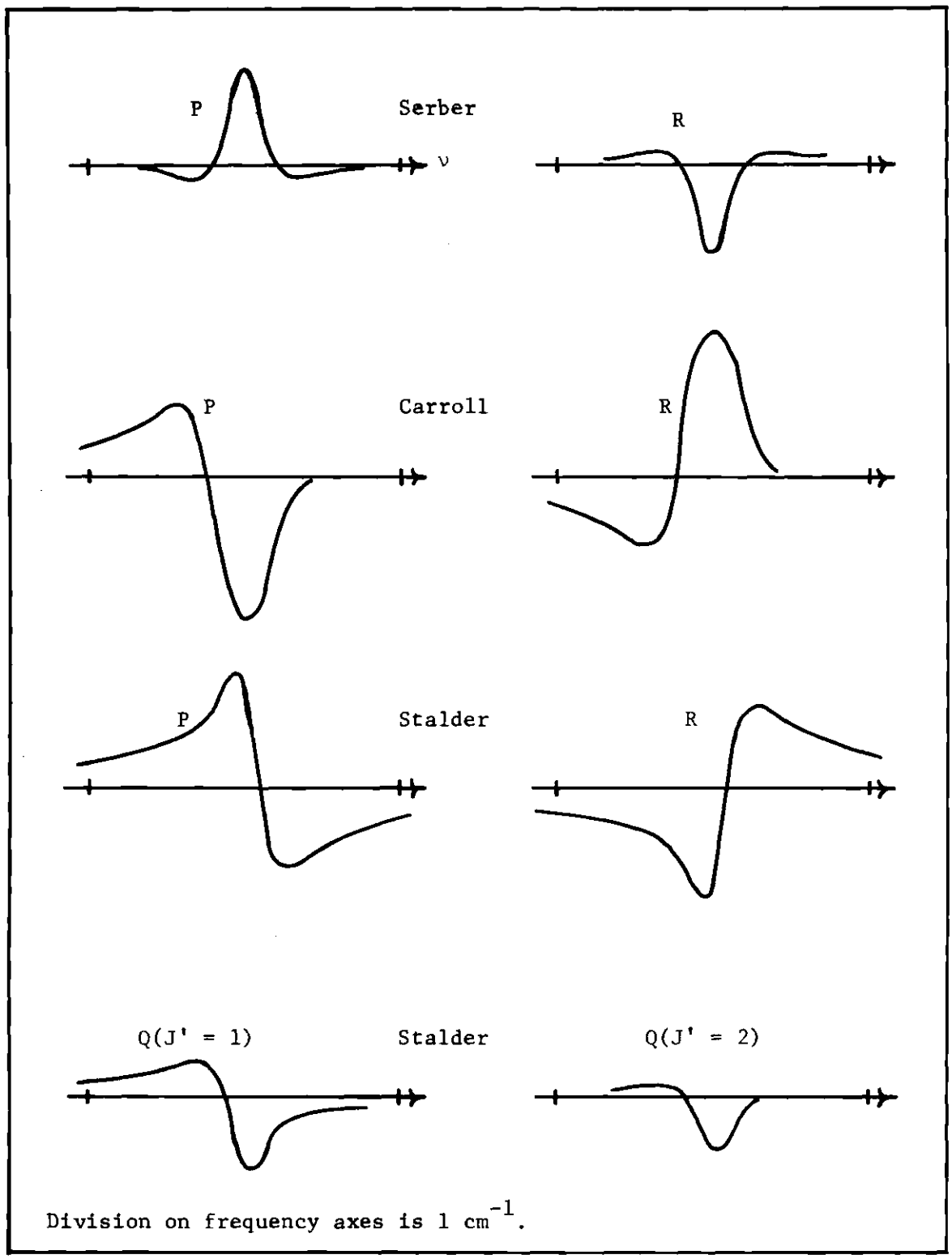

Fig. 41. Computed Value for Angle of Rotation.

APPENDIX

Formulas for Theoretical Calculations ($^3\pi_1 \leftarrow {}^1\Sigma^+$ in ICℓ)

R-Lines

$$(\phi,\theta) \propto \left\{ \sum_{M=-J}^{J} {}^{-} f(\nu) \frac{(J-M+1)(J-M+2)(J+2)}{(J+1)(2J+1)(2J+3)} - \sum_{M=-J}^{J} {}^{+} f(\nu) \frac{(J+M+1)(J+M+2)(J+2)}{(J+1)(2J+1)(2J+3)} \right.$$

$$-2 \sum_{M=-J+1}^{J} {}^{-} f(\nu) \left(\frac{.11675}{\Delta E_R}\right) \frac{(J-M+1)(J-M+2)(J+M)(J+2)}{(J+1)^2(2J+1)(2J+3)}$$

$$\left. -2 \sum_{M=-J}^{J-1} {}^{+} f(\nu) \left(\frac{.11675}{\Delta E_R}\right) \frac{(J+M+1)(J+M+2)(J-M)(J+2)}{(J+1)^2(2J+1)(2J+3)} \right\}$$

P-Lines

$$(\phi,\theta) \propto \left\{ \sum_{M=-J+2}^{J} {}^{-} f(\nu) \frac{(J+M)(J+M-1)(J-1)}{J(4J^2-1)} - \sum_{M=-J}^{J-2} {}^{+} f(\nu) \frac{(J-M)(J-M-1)(J-1)}{J(4J^2-1)} \right.$$

$$-2 \sum_{M=-J+2}^{J} {}^{-} f(\nu) \left(\frac{.11675}{\Delta E_P}\right) \frac{(J+M)(J+M-1)(J-M+1)(J-1)}{J^2(4J^2-1)}$$

$$\left. -2 \sum_{M=-J}^{J-2} {}^{+} f(\nu) \left(\frac{.11675}{\Delta E_P}\right) \frac{(J-M)(J-M-1)(J+M+1)(J-1)}{J^2(4J^2-1)} \right\}$$

Q-Lines

$$
\begin{aligned}
(\phi,\theta) \propto \Bigg\{ & \sum_{M=-J+1}^{J-} f(\nu)\,\frac{(J+M)(J-M+1)}{J(J+1)} - \sum_{M=-J}^{J-1+} f(\nu)\,\frac{(J-M)(J+M+1)}{J(J+1)} \\
& -2\sum_{M=-J+1}^{J-} f(\nu)\left(\frac{.11675}{\Delta E_P}\right)\frac{(J-M+1)(J-M+2)(J+M)(J+2)}{(J+1)^2(2J+1)(2J+3)} \\
& -2\sum_{M=-J}^{J-1+} f(\nu)\left(\frac{.11675}{\Delta E_P}\right)\frac{(J+M+1)(J+M+2)(J-M)(J+2)}{(J+1)^2(2J+1)(2J+3)} \\
& -2\sum_{M=-J+2}^{J-} f(\nu)\left(\frac{.11675}{\Delta E_R}\right)\frac{(J+M)(J+M-1)(J-M+1)(J-1)}{J^2(4J^2-1)} \\
& -2\sum_{M=-J}^{J-2+} f(\nu)\left(\frac{.11675}{\Delta E_R}\right)\frac{(J-M)(J-M-1)(J+M+1)(J-1)}{J^2(4J^2-1)} \Bigg\}
\end{aligned}
$$

To calculate ϕ, $f(\nu) = \dfrac{(\nu_M - \nu)}{(\nu_M - \nu)^2 + \Gamma^2}$, and to calculate θ, $f(\nu) = \dfrac{\Gamma}{(\nu_M - \nu)^2 + \Gamma^2}$.

The J and M values appearing in the formulas are those of the ground state. ν_M corresponds to the frequency, in cm^{-1}, of a Zeeman transition, and is given by the formula

$$\nu_M = \nu_o + \frac{M'}{J'(J'+1)}(.11675) \quad ,$$

where ν_o is the zero field transition frequency obtained from Hulthéns data (48,49).

The terms corresponding to intensity perturbations by the magnetic field include ΔE terms in the denominator. $\Delta E_R = E_{J',M'} - E_{J' - 1,M'}$ and $\Delta E_p = E_{J',M'} - E_{J' + 1,M'}$ where the E's refer to the energy of the excited state rotational levels in the magnetic field in cm^{-1}. These terms are given by the equation

$$E_{J',M'} = E^{o}_{J',M'} + \frac{M'}{J'(J' + 1)} (.11675) \quad ,$$

where $E^{o}_{J'M'}$ is the zero field term value for the excited state defined by J',M'. The + or - superscript on the Σ's corresponds to $\Delta M = +1$ and $\Delta M = -1$ absorption transitions. The value of Γ used in the calculations was .100 cm^{-1}, and the field intensity used to determine the magnetic effects was 2500 gauss.

BIBLIOGRAPHY*

1. W. H. Eberhardt, Wu-chieh Cheng, and H. Renner, J. Mol. Spect. 3, 664 (1959).

2. B. S. Snowden, Jr., and W. H. Eberhardt, J. Mol. Spect. 18, 372 (1965).

3. W. H. Eberhardt and H. Renner, J. Mol. Spect. 6, 483 (1961).

4. G. A. Mann and C. D. Hause, J. Chem. Phys. 33, 1117 (1960).

5. J. L. Aubel and C. D. Hause, J. Chem. Phys. 44, 2659 (1966).

6. P. Kusch and F. W. Loomis, Phys. Rev. 55, 850 (1939).

7. Robert W. Wood, Physical Optics Ch. 21, Macmillan Co., (1934).

8. Robert Serber, Phys. Rev. 41, 489 (1932).

9. Thomas Carroll, Phys. Rev. 52, 822 (1937).

10. A. D. Buckingham and P. J. Stephens, Annual Review of Physical Chemistry, Vol. 17, pp. 399-432. Annual Reviews, Inc., Palo Alto, Calif. (1966).

11. C. H. Townes and A. L. Schawlow, Microwave Spectroscopy, Ch. 13, McGraw-Hill, New York (1955).

12. Albert Moscowitz, Advances in Chemical Physics, Vol. IV, pp. 67, Interscience Publishers, New York (1962).

13. F. H. Crawford, Rev. Mod. Phys. 6, 90 (1934).

14. Henry Eyring, John Walter and George E. Kimball, Quantum Chemistry, Ch. 7, John Wiley and Sons, New York (1961).

15. H. A. Kramers, Kon. Acad. Wet. Amsterdam 33, 959 (1930).

16. P. J. Stephens, Inorganic Chemistry 4, 1690 (1965).

17. P. J. Stephens, J. Chem. Phys. 43, 4444 (1965).

18. M. L. Sage, J. Chem. Phys. 35, 969 (1961).

---

*Abbrevations herein follow the form used by Chemical Abstracts 55 (1961).

19. M. P. Groenewege, J. Mol. Phys. 5, 541 (1962).

20. G. Porter, Radiation Research, Supplement No. 2, p. 479.

21. L. I. Grossweiner, Scientific American 202, 134 (1960).

22. R. G. W. Norrish, American Scientist 50, 131 (1962).

23. David N. Bailey and David M. Hercules, Journal of Chemical Education 42, A83 (1965).

24. B. A. Thrust, Proc. Roy. Soc. A243, 555 (1958).

25. Royal Marshall and Norhan Davidson, J. Chem. Phys. 21, 659 (1953).

26. D. E. Paul and F. W. Dalby, J. Chem. Phys. 37, 592 (1962).

27. A. Shilman and R. A. Marcus, J. Chem. Phys. 39, 996 (1963).

28. F. W. Dalby, J. Chem. Phys. 41, 2297 (1964).

29. R. G. W. Norrish, Proc. Chem. Soc. (London), 247, September 1958.

30. R. G. W. Norrish and B. A. Thrush, Chem. Soc. (London) Quarterly Reviews 10, 149 (1956).

31. M. I. Christie and G. Porter, Proc. Roy. Soc. A212, 390 (1952).

32. B. A. Thrust and J. J. Zwolenik, Trans. Farad. Soc. 59, 582 (1963).

33. R. Stephen Berry, G. Neil Spokes and Martin Stiles, J. American Chem. Soc. 84, 3570 (1962).

34. Gilbert J. Mains, John L. Roebber and G. K. Rollefson, J. Phys. Chem. 59, 733 (1955).

35. Gisela K. Oster and R. A. Marcus, J. Chem. Phys. 27. 189 (1957).

36. P. L. Goodfriend and H. P. Woods, Texaco Experiment Incorporated, T. P. 230.

37. Stig Claesson and Gunnar Wettermark, Arkiv För Kemi 11, 561 (1957).

38. L. S. Nelson and N. A. Kuebler, J. Chem. Phys. 37, 47 (1962).

39. D. A. Ramsay, J. Chem. Phys. 20, 1920 (1952).

40. S. H. Bauer, G. Herzberg, and J. W. C. Johns, J. Mol. Spect. 13, 256 (1964).

41. G. Porter, Disc. Farad. Soc. 9, 60 (1950).

42. G. Porter, Proc. Roy. Soc. A200, 284 (1950).

43. J. H. Callomon and D. A. Ramsay, Canadian J. Phys. 35, 129 (1957).

44. Stig Claesson and Lars Lindqvist, Arkiv För Kemi 12, 1 (1957).

45. Stig Claesson and Lars Lindqvist, Arkiv För Kemi 11, 535 (1957).

46. H. J. Gerritsen and M. E. Heller, Applied Optics, Supplement on Chemical Lasers, 73 (1965).

47. E. Back, Ann. d Phyzik 76, 317 (1925).

48. Erik Hulthén, Nils Johansson, and Ulla Pilsäter, Arkiv För Fysik 14, 31 (1958).

49. E. Hulthén, N. Järlsäter, and L. Koffman, Arkiv För Fysik 18, 479 (1960).

50. W. H. Eberhardt, Unpublished Data on ICℓ.

51. C. E. Moore, Atomic Energy Levels, Circular Nat. Bur. of Standards No. 467 (1959).

52. Gerhard Herzberg, Atomic Spectra and Atomic Structure, pp. 96-119, Dover Publications, N. Y. (1944).

53. S. Tolansky, High Resolution Spectroscopy, Ch. 1, Pitman Publishing Corp. New York (1947).

54. Karl Lang, Acta Physica Austriaca 5, 376 (1951).

55. Gerhard Herzberg, Spectra of Diatomic Molecules, D. Van Nostrand Co., Inc., New York (1965).

VITA

Arnold Frederick Stalder was born on April 11, 1939, in Chicago, Illinois to Arnold and Margaret Caroline Stalder. He graduated from Round Lake Community High School in Round Lake, Illinois in June, 1957. He entered Georgia Institute of Technology in June, 1957, and received a Bachelor of Chemical Engineering (Co-op) Degree in June 1963. He entered graduate school in the School of Chemistry at Georgia Institute of Technology in September, 1962.

During his undergraduate years he was a member of Tau Beta Pi and Phi Kappa Phi honorary societies, and was elected to associate membership in Sigma Xi in 1965.